The 13th Symposium on Polar Science

15 – 18 November 2022

National Institute of Polar Research
Research Organization of Information and Systems

Session OA

Antarctic meteorites

Program and Abstracts

Convener
Naoya Imae (NIPR)

【OA】Antarctic meteorites

Scopes

This session is held to present recent research outcomes for Antarctic meteorites and micrometeorites. It will also be an opportunity for general and topical discussion sessions dealing with new data from non-Antarctic meteorites and extraterrestrial materials, and related experimental and theoretical works.

Convener : **Naoya Imae (NIPR)**

Real-time Oral presentations (09:55 – 12:00, 13:00 – 15:00: JST)

Date: Thu. 17 November

Chair: Akira Yamaguchi (NIPR)			
	9:55 - 10:00	Opening	Akira Yamaguchi (NIPR)
OAo1	**10:00 - 10:15**	A New Lunar Meteorite Naming Nomenclature	*Ryan Zeigler (NASA Johnson Space Center), Jessica Barnes (University of Arizona), Jon Friedrich (Fordham University), Carl Agee (University of New Mexico), Katherine Burgess (Naval Research Laboratories), Catherine Corrigan (Smithsonian Institution), Juliane Gross (NASA Johnson Space Center), Katherine Joy (University of Manchester), Francis McCubbin (NASA Johnson Space Center), Kevin RIghter (NASA Johnson Space Center)
OAo2	**10:15 - 10:30**	Pb–Pb dating of Yamato 86032	*Kengo Ito (The University of Tokyo), Magdalena Huyskens (University of California, Davis), Qing-Zhu Yin (University of California, Davis), Tsuyoshi Iizuka (The University of Tokyo)
OAo3	**10:30 - 10:45**	Iron redox systematics in martian mantle melts and identification of primary liquids	*Kevin Righter (NASA Johnson Space Center)
OAo4	**10:45 - 11:00**	Crystallization of poikilitic shergottites as deduced from textural and mineral compositional diversities of seven samples.	*Sojiro Yamazaki (University of Tokyo), Takashi Mikouchi (University of Tokyo), Chi Pui Tang (Macau University of Science and Technology)
OAo5	**11:00 - 11:15**	Origin of silica polymorphs in eucrites: Implications for the crystallization of eucritic magma and metamorphic history of Vestan crust	*Rei Kanemaru (JAXA/ISAS), Akira Yamaguchi (NIPR, SOKENDAI), Naoya Imae (NIPR, SOKENDAI), Aiko Nakato (JAXA/ISAS), Junko Isa (ChibaTech), Hirotsugu Nishido (OUS)
OAo6	**11:15 - 11:30**	Impact-induced (?) Cr-diffusion in the metallic phase in chondrites and achondrites	*Junko Isa (Chiba Institute of Technology)
OAo7	**11:30 - 11:45**	Petrography and Oxygen isotopic compositions of Ca-Al-rich inclusions from Asuka-9003 and 09535	*Nozomi Matsuda (UCLA), Ming-Chang Liu (LLNL), Kevin D. McKeegan (UCLA)
OAo8	**11:45 - 12:00**	Carbon and Sulfur Abundances in Carbonaceous Meteorites Revisited	*Tomoko Arai (Chiba Institute of Technology), Kenta Suzuki (Chiba Institute of Technology), Ryota Moriwaki (Chiba Institute of Technology), Takafumi Matsui (Chiba Institute of Technology)
Break			

Chair: Naoya Imae (NIPR)			
OAo9	**13:00 - 13:15**	LON 94101 Provides a Unique Record of C-Class Asteroid Regolith Diversity	*Michael Zolensky (NASA Johnson Space Center), Loan Le (Jacobs), Matt Colbert (Univ Texas), Jessie Maisano (Univ. Texas), Moe Matsuoka (4National Institute of Advanced Industrial Science and Technology), Roger Harrington (Jacobs), Kent Ross (Univ Texas El Paso)
OAo10	**13:15 - 13:30**	Mineralogical and petrological study of Aguas Zarcas CM2 chondrite	*Kenei Ogiya (The University of Tokyo), Toru Matsumoto (Kyoto University), Akira Miyake (Kyoto University), Takashi Mikouchi (The University of Tokyo)
OAo11	**13:30 - 13:45**	Anhydrous phases preserved in CI chondrites	*Taro Ando (Kyoto University), Takaaki Noguchi (Kyoto University), Akira Yamaguchi (NIPR), Shoichi Itoh (Kyoto University)
OAo12	**13:45 - 14:00**	Mineralogical investigation of olivine grains in CI chondrites Ivuna and Orgueil	*Takashi Mikouchi (The University of Tokyo), Hideto Yoshida (The University of Tokyo), Minami Masuda (The University of Tokyo), Michael E. Zolensky (NASA/JSC), Tomoki Nakamura (Tohoku University)
OAo13	**14:00 - 14:15**	Na-rich phase in Ryugu particle: Evidence for metasomatic agent in the parent asteroid?	*Akira Yamaguchi (NIPR), Phase2 Kochi curation team
OAo14	**14:15 - 14:30**	An artificial laboratory alteration of the Ryugu samples: Comparison with the Orgueil CI chondrite and implication to the long durational sample storage	*Naoya Imae (NIPR & SOKENDAI), Naotaka Tomioka (JAMSTEC), Motoo Ito (JAMSTEC), Akira Yamaguchi (NIPR & SOKENDAI), Makoto Kimura (NIPR), Masayuki Uesugi (JASRI/SPring-8), Naoki Shirai (TMU/Kanagawa University), Takuji Ohigashi (IMS/KEK), Ming-Chang Liu (UCLA/Lawrence Livermore National Laboratory), Richard C. Greenwood (The Open University), Kentaro Uesugi (JASRI/SPring-8), Aiko Nakato (ISAS, JAXA), Kasumi Yogata (ISAS, JAXA), Hayato Yuzawa (IMS), Yu Kodama (Marine Works Japan, Ltd./Toyo Corp.), Masahiro Yasutake (JASRI/SPring-8), Kaori Hirahara (Osaka University), Akihisa Takeuchi (JASRI/SPring-8), Ikuya Sakurai (Nagoya University), Ikuo Okada (Nagoya University), Yuzuru Karouji (ISAS, JAXA), Toru Yada (ISAS, JAXA), Masanao Abe (ISAS, JAXA), Tomohiro Usui (ISAS, JAXA)
OAo15	**14:30 - 14:45**	New analytical tool for extraterrestrial material curation: A great advantage for an in-situ analysis and quick survey of organics	*Motoo Ito (JAMSTEC), Rei Kanemaru (JAXA), Junko Isa (Chiba Tech), Akira Yamaguchi (NIPR), Masaaki Miyahara (Hiroshima University), Toru Yada (JAXA/ISAS), Yuuka Niwa (TiTech), Akira Ishikawa (TiTech), Takaomi D. Yokoyama (JEOL), Hideyuki Takahashi (JEOL), Masayuki Uesugi (JASRI/SPring-8), Tomohiro Usui (JAXA/ISAS)

OAo16	**14:45 - 15:00**	The relationship between Ryugu samples and CY and CI chondrites: Another twist in the tale.	*Richard Greenwood (The Open University), I.A Franchi, R. Findlay, J. A. Malley, M. Ito, A. Yamaguchi, M. Kimura, N. Tomioka, M. Uesugi, N. Imae, N. Shirai, T. Ohigashi, M-C. Liu, K. Uesugi, A. Nakato, K. Yogata, H. Yuzawa, Y. Kodama, A. Tsuchiyama, M. Yasutake, K. Hirahara, A. Takeuchi, I. Sakurai, I. Okada, Y. Karouji, T. Yada, M. Abe, T. Usui, S. Watanabe, Y. Tsuda, K.A. McCain, N. Matsuda, K.D. McKeegan, S. Nakzawa, T. Okada, T. Saiki, S. Tanaka, F. Terui, M. Yoshikawa, A. Miyazaki, M. Nishimura, S. Sekimoto

Poster presentations

* No Zoom-based presentations (OAp1-OAp9)

OAp1	News about the high pressure mineralogy in Tissint (olivine-phyric shergottite): (Ferro-) Periclase and nano-micro Diamonds	*Viktor H. Hoffmann (Faculty of Geosciences, University of Munich, Germany), Melanie Kaliwoda (MSC_SNSB Munich, Germany), Malte Junge (MSC_SNSB Munich, Germany), Felix Hentschel (MSC_SNSB Munich, Germany), Wolfgang W. Schmahl (MSC_SNSB Munich, Germany)
OAp2	Elucidation of aqueous alteration in the lava units with nakhlites NWA 10153 and NWA 6148	*Kakeru Kukihara (Hiroshima university), Masaaki Miyahara (Hiroshima university), Akira Yamaguchi (NIPR), Yoshio Takahashi (The University of Tokyo), Yasuo Takeichi (KEK), Naotaka Tomioka (JAMSTEC), Eiji Ohtani (Tohoku university)
OAp3	Lohawat howardite: trapped noble gases and nitrogen isotopic signature	*Ramakant Mahajan (Physical Research Laboratory, Ahmedabad, India)
OAp4	Chemical characteristics of ungrouped iron meteorites from Yamato Mountains	*Naoki Shirai (Kanagawa University), Akira Yamaguchi (NIPR)
OAp5	Compositional information for the bulk S-contents of metallic cores of iron meteorite parent bodies. Implications for the sulphur abundance of the metallic core of the Earth.	*Péter Futó (University of Debrecen)
OAp6	Trapped Ar, Kr, and Xe in ordinary chondrites	*Ramakant Mahajan (Physical Research Laboratory, Ahmedabad, India)
OAp7	Chemical compositional characteristics of CBb and CH chondrites.	*Yoshihiro Hidaka (Waseda University), Taisei Fujimura (Waseda University), Mitsuru Ebihara (Waseda University)
OAp8	Raman micro-spectroscopic study of carbonates on the surafce of Y-980115	*Hiroharu Yui (Tokyo University of Science), Hayato Tsuchiya (Tokyo University of Science), Shu-hei Urashima (Tokyo University of Science), Keisuke Narahara (Tokyo University of Science), Aruto Kashima (Tokyo University of Science), Naoya Imae (NIPR), Akira Yamaguchi (NIPR)
OAp9	Primordial abundance of chondrule in CI chondrite	*Makoto Kimura (NIPR), Akira Yamaguchi (NIPR), Motoo Ito (JAMSTEC), Naotaka Tomioka

A New Lunar Meteorite Naming Nomenclature

Ryan A. Zeigler[1], Jessica J. Barnes[2], Jon M. Friedrich[3], Carl B. Agee[4], Katherine D. Burgess[5], Catherine M. Corrigan[6], Juliane Gross[1,7], Katherine H. Joy[8], Francis M. McCubbin[1], and Kevin Righter[1].

[1] *NASA Johnson Space Center, Houston, TX 77058, USA.*

[2]*Lunar and Planetary Laboratory, University of Arizona, Tucson, AZ, 85721, USA*

[3]*Department of Chemistry, Fordham University, Bronx, NY 10458, USA*

[4]*Institute of Meteoritics, University of New Mexico, Albuquerque, New Mexico 87131, USA*

[5]*Materials Sci. and Tech. Div., Code 6366, Naval Research Laboratory, 4555 Overlook Ave., Washington, DC 20375, USA*

[6]*Nat. Museum of Nat. History, Smithsonian Institution, MRC 119, 10th and Constitution Ave., Washington DC, 20560, USA.*

[7]*Rutgers State University of New Jersey, Department of Earth & Planetary Sciences, Piscataway, NJ 08854, USA*

[8]*Dept. of Earth and Environmental Sciences, University of Manchester, Oxford Road, Manchester, M19 3PL, UK*

The Apollo missions collected 382 kg of rock (2196 individual samples) from six sample sites in the equatorial regions of the lunar nearside. The Apollo sample suite contains a wide variety of lunar rock and soil samples, collected with excellent local geologic context. However, the Apollo suite was collected over a relatively restricted geographic region of the Moon, and each of the sites are strongly influenced by a single geologic event, the Imbrium Impact. In contrast, there are currently 562 lunar meteorite stones (926.6 kg) listed in the Meteoritical Bulletin Database [1]. Detailed pairing relationships are difficult to demonstrate in all cases, particularly for the large number of brecciated feldspathic meteorites, but these 562 stones represent at least 144 lunar meteorite pairing groups [2] and come from at least 40-50 source craters on the Moon. The source craters for lunar meteorites are essentially randomly distributed across the lunar surface, which makes lunar meteorites the most representative suite of lunar samples and the best estimate of the global composition of the lunar crust [3].

Unlike the Apollo samples, which have a more-or-less coherent nomenclature across the entire collection, the classification of lunar meteorites in the Meteoritical Bulletin Database is less consistent and less detailed (Table 1). The lack of a consistent nomenclature for lunar meteorites inhibits selection of samples for more detailed follow-on studies and makes comparison of samples between the Apollo and lunar meteorite collections more difficult. This abstract represents a progress report of an ad hoc committee assembled by the lunar and meteorite subcommittees of ExMAG (Extraterrestrial Materials Analysis Group [5]). The goal of the effort is to provide a framework for classifiers to use for consistent naming of future lunar meteorites, and perhaps to retroactively reclassify existing lunar meteorites (though it would be a significant effort).

Table 1: Current Lunar Meteorite Classifications

Lunar Meteorite categories	Number
Lunar	98
Lunar (anorth)	78
Lunar (bas. breccia)	19
Lunar (bas/anor)	3
Lunar (bas/gab breccia)	2
Lunar (basalt)	23
Lunar (feldsp. breccia)	283
Lunar (frag. breccia)	21
Lunar (gabbro)	11
Lunar (melt breccia)	11
Lunar (norite)	1
Lunar (olivine gabbro)	1
Lunar (olivine gabbronorite)	1
Lunar (troct)	3
Lunar (troct. anorth.)	5
Lunar (troct. melt rock)	2

Figure 1 shows the current iteration of our naming scheme for lunar meteorites. We propose, barring special circumstances, that all future lunar meteorites should be classified into one of the following six classifications (the bottom row of blue boxes in Figure 1): (1) Lunar Meteorite – Basalt; (2) Lunar Meteorite – Plutonic; (3) Lunar Meteorite – Granulitic Breccia; (4) Lunar Meteorite – Impact-Melt Breccia; (5) Lunar Meteorite – Fragmental Breccia; and (6) Lunar Meteorite – Regolith Breccia. Classifying a meteorite into one of these categories requires a small number of electron microprobe analyses and textural information obtained from back-scattered electron and/or optical petrographic microscopy. This scheme does not change the type of analyses currently needed to classify a lunar meteorite. There are three steps to the proposed classification process:

Step 1 – Show that the meteorite is lunar based on the Fe:Mn ratio in mafic silicates and the Ca-rich nature of the plagioclase. It can also be done through oxygen isotope measurements (falling on the terrestrial fractionation line).

Step 2 – Determine if the lunar meteorite is igneous or non-igneous. Igneous lunar meteorites have textures consistent with igneous samples, they are unbrecciated, and lack clasts or abundant FeNi-rich metal. Conversely, non-igneous samples have sedimentary or metamorphic textures, contain clasts set in a fine-grained matrix, and commonly have FeNi metal grains with a composition similar to those seen in chondritic meteorites.

Step 3a – For igneous lunar meteorites, determine if it is a basalt (extrusive) or plutonic (intrusive) sample. Basaltic lunar meteorites have igneous textures and are dominated by zoned pyroxene grains and calcic plagioclase grains (An_{80-90}), with minor and variable amounts of ilmenite, olivine, and silica (as well as trace other phases). In contrast, plutonic samples tend to have unzoned mafic silicate phases (when present), are coarse grained, and they can have both igneous and cumulate textures.

Step 3b – Non-igneous samples, under the currently proposed plan, fall into one of 4 breccia groups based on the following criteria. Fragmental breccias are clast-rich and typically have a wide variety of clast compositions, with a matrix that is clastic or a combination of clastic and glassy. Regolith breccias have the same clast and matrix characteristics as fragmental breccias, but also contain specific components that only form at or above the lunar surface, such as impact glass spherules or agglutinates. Impact-melt breccias tend to clast poor (typically with a more limited variety of clast compositions), with a matrix that is crystalline and/or glassy, and often contains vesicles or vugs. Granulitic breccias are typically clast poor, with a crystalline matrix where the minerals show evidence of recrystallization (e.g., 120° triple junctions).

This classification scheme is designed to accommodate the vast majority of lunar rock samples, without being analysis intensive or requiring extensive experience with lunar samples in order to successfully classify a meteorite. The final publication will contain abundant images that demonstrate the distinguishing features and textures discussed above to further aid in this. These new, more detailed meteorite classifications, if used consistently, will greatly aid in selection of samples for more detailed follow-on studies. Moreover, the classification scheme will also include more detailed information about the subdivision of the six meteorite classifications into chemical (e.g., feldspathic or mafic regolith breccias) or lithologic (e.g., whether plutonic samples are anorthosites, norites, etc.) subcategories (the green and yellow boxes in Figure 1). This additional information would not be captured in the top-level meteorite classifications in the Meteoritical Bulletin, but could be included in the notes section for a meteorite within the Bulletin if it was known at the time of submission.

References [1] Meteoritical Bulletin Database [2] List of Lunar Meteorites. [3] Korotev et al. (2003), *GCA* Vol 67: 4895-4923. [4] Extraterrestrial Materials Analysis Group.

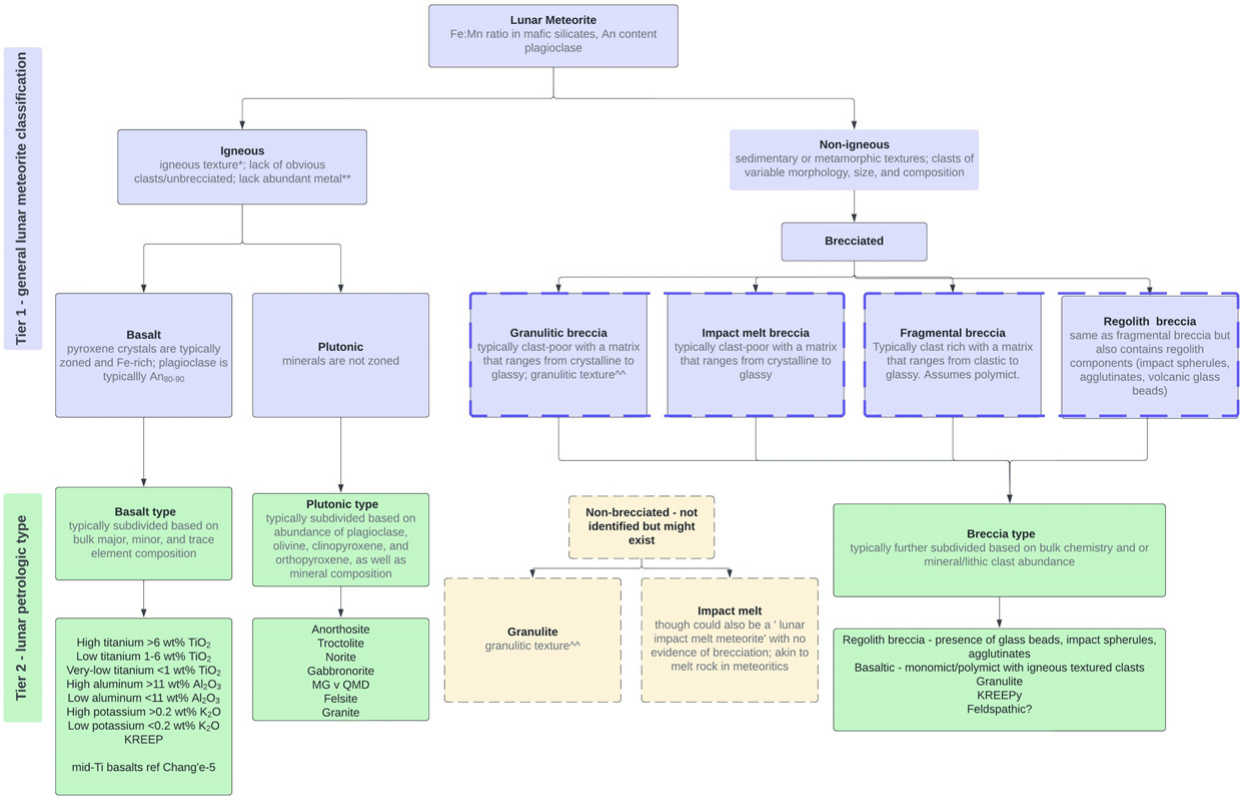

Figure 1: Schematic diagram showing proposed lunar meteorite classifications (in blue), as well as additional chemical and lithologic subdivisions (in green and yellow) to enable follow on studies.

Pb–Pb dating of Yamato 86032

Kengo Ito[1], Magdalena H Huyskens[2], Qing-Zhu Yin[2], Tsuyoshi Iizuka[1]
[1] *Department of Earth and Planetary Science, The University of Tokyo*
[2] *Department of Earth and Planetary Sciences, University of California at Davis*

Introduction:

The Moon exhibits significant differences between the nearside and farside hemispheres in elemental distributions[1], mare volcanic activity[2], and crustal thickness[3]. The origin of this dichotomy has been considered to be either:

1. lunar magma ocean (LMO) solidification[4] or
2. secondary process(es) (a large impact[5], mantle overturn[6]).

Based on recent observations of elemental distribution on the lunar surface, especially Mg# in mafic minerals of primitive crustal highland rocks, asymmetric crustal growth where crystallization progresses from the farside toward the nearside (direct link to 1.LMO solidification) is proposed as a model for the origin of the dichotomy[7].

If this model is correct, there should be a clear gap in the formation age between the lunar nearside and farside floatation crust. The pyroxene Pb–Pb age of the Ferroan Anorthosite (FAN) 60025 gives a precise age of 4359.2 ± 2.4 [Ma][8] for the nearside crust formation. On the other hand, no high-precision age constraints have been obtained for the formation of the lunar farside crust. In this study, we conducted high-precision pyroxene Pb–Pb dating of the Yamato 86032 meteorite, which is considered to have originated on the farside, to test the validity of the asymmetric crustal growth model and toward a more detailed understanding of LMO crystallization style.

Sample & experimental procedure:

Yamato 86032 (Y-86032) is a lunar anorthositic breccia found in 1986. The clasts are considered to be derived from the region far from the Procellarum KREEP Terrane (PKT) (possibly farside) because of the following unique features[9,10]:

1. The low bulk FeO (< 5wt.%), REEs, Th (<0.2 ppm), and U abundances,
2. The high Na contents in anorthite and high Mg# [=100×molar Mg/(Fe+Mg)] in mafic minerals (Magnesian anorthosite),
3. Anorthositic clasts in this meteorite retain old Ar–Ar ages compared to Apollo anorthosites.

Based on the Sm–Nd system, the formation age is estimated to be between 4.43-4.31 billion years ago[9,10].

A fragment of Y-86032 was crushed in ethanol using an agate mortar and pestle. Pyroxenes were concentrated by hand-picking under an optical microscope. We analyzed 3 pyroxene fractions from 2 different lithology (Y-86032, 138: 2 fractions, Y-86032, 144: 1 fraction) (Figure 1). Following Iizuka et al. (2014)[11], all sample fractions were leached four times in 1.5 mL of 0.5 M HNO_3 with ultrasonic agitation for 10 min, twice in 1.5 mL of hot 6 M HNO_3 for 1 h, and twice in 1.5 mL of hot 6 M HCl for 1h (Table 1). The acid residues were digested in a mixture of 25 M HF (25 drops) and 12 M HNO_3 (10 drops) at 120 °C for 2 overnights, followed by conversion to a soluble form by repeated evaporation with 12 M HNO_3 and 6 M HCl. Finally, the residues were evaporated and re-dissolved in 0.5 M HBr. The separation of Pb was performed using 0.05 ml of anion exchange resin AG1x8 200–400 mesh (Eichrom Technologies, U.S.A.). The Pb isotopes were measured using a Thermo Scientific TRITON plus at the University of California, Davis. Pb isotopic data were plotted using the Isoplot R software[12].

Table 1. Sequential acid leaching & digestion method.

	type of acid	duration	temperature
Wash 1 (W1)	0.5 M HNO_3	10 min × 4	25 ℃
Wash 2 (W2)	6 M HNO_3	1 hour × 2	110 ℃
Wash 3 (W3)	6 M HCl	1 hour × 2	110 ℃
Residue (R)	25 M HF + 12 M HNO_3	48 hours	120 ℃

Table 2. Amounts of Pb [unit: pg] eluted from each fraction.

	Px1	Px2	Px3
lithology	Y-86032, 138	Y-86032, 138	Y-86032, 144
Weight [mg]	1.13	2.71	1.19
Wash 1 (W1)	12.6	114.0	15.7
Wash 2 (W2)	27.9	205.4	14.7
Wash 3 (W3)	4.5	5.6	13.6
Residue (R)	19.1	21.1	26.8

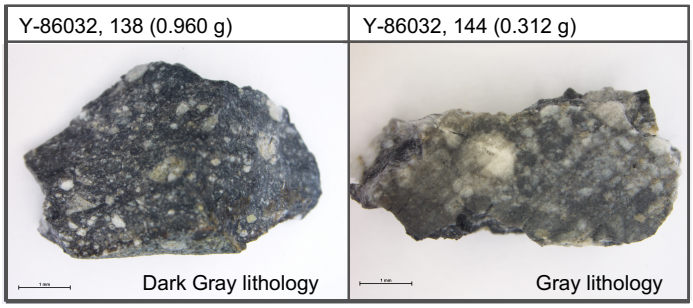

Figure 1. Optical images of Yamato 86032 used for this study.

Results & discussions:

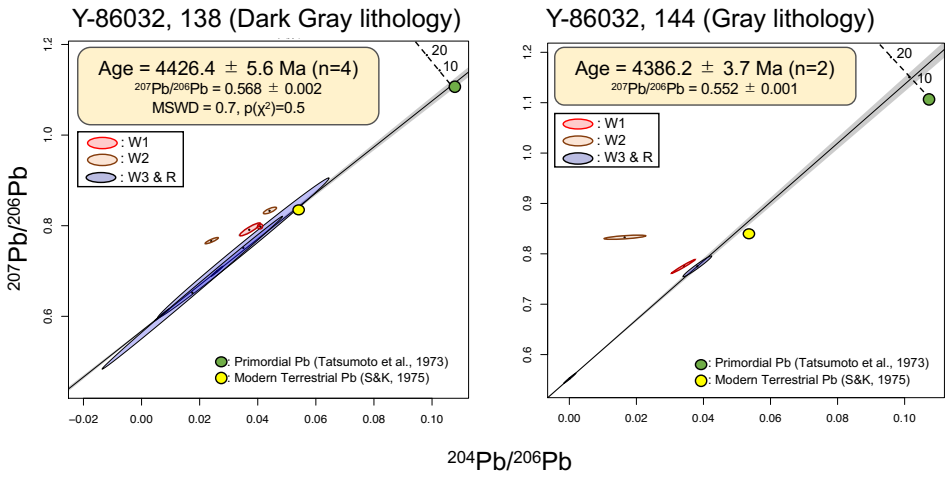

Figure 2. Inverse Pb–Pb isochrons of acid leachates & residues of Y-86032 pyroxene fractions. Data points used for isochrons are described as blue points (W3 & R). The yellow circle is modern day terrestrial Pb and the green circle is primordial Pb. The numbers in the figure represent the μ value ($^{238}U/^{204}Pb$) and each isochron pass through the initial Pb.

Pb concentrations in pyroxenes & Pb–Pb dating:

The Pb concentrations in pyroxenes estimated from the residue ranged from 7-22 ppb (Table 2). The high Pb amounts in W1 and W2 suggest that Pb from terrestrial contaminants and plagioclase in the meteorite have been dissolved from the pyroxene fractions. Because these washes are considered to have sufficiently removed common Pb, and 6 M HCl is considered to have caused the partial dissolution of pyroxene as in the previous study[8], both W3 and R are used for isochrons in this study.

Pyroxenes in two different fragments yielded different Pb-Pb dates: 4426.4 ± 5.6 [Ma] (n=4, MSWD = 0.7) from Y-86032, 138 (Dark Gray lithology), and 4386.2 ± 3.7 [Ma] (n = 2) from Y-86032, 144 (Gray lithology) , indicating that the pyroxene in each fragment has different formation timing.

Pb–Pb dates comparison to FAN60025:

The Pb–Pb dates of the Y-86032 are 27-67 [Ma] older than the Pb–Pb age of lunar nearside crust FAN60025, supporting the asymmetric crustal growth model that the lunar farside crust (or a region far enough from the PKT) is older than the nearside. There are two possible interpretations of the two different Pb–Pb dates obtained in this study. First, the Pb–Pb dates obtained here have a positive correlation with Mg# in mafic minerals and thus imply a cooling history of LMO. Mg# for each fragment in Y-86032 is higher than that of FAN nearside crust. The Mg# of olivine in FAN60025 and Y-86032 are compared here because it is difficult to determine the accurate estimation of Mg# in pyroxenes by their exsolution. The Mg# in FAN60025 olivine has a range of compositions (Fo_{42-66}: Fo#[＝100 × molar Mg/(Mg+Fe)])[13]. On the other hand, Mg# in Y-86032 olivine is Fo_{60-80} for those in the Dark Gray lithology, $Fo_{60.2-72.7}$ for those in the Gray lithology[10]. In this case, it is possible to consider that 4426 [Ma] of Y-86032 records the first stage of crust formation from the LMO, while 4359 [Ma] of FAN60025 records the last stage crystallization from the LMO. The second is that Y-86032 has experienced at least two shock metamorphisms[10] or thermal metamorphism because it contains some granulitic breccia[10], and the age obtained from Y-86032, 144 may record the timing of such metamorphisms.

This is the first report of a high-precision dating derived from a source other than the lunar central nearside crust. Further studies on the correlation between Mg# of mafic minerals in lunar pristine rocks and their high-precision formation ages are needed in the future.

References

[1] Jolliff et al. (2000). JGR: Planets, 105(E2), 4197-4216. [2] Head & Wilson. (1992). GCA, 56(6), 2155-2175.
[3] Wieczorek et al. (2013). Science, 339(6120), 671-675. [4] Loper & Werner. (2002). JGR: Planets, 107(E6), 13-1.
[5] Zhu et al. (2019). JGR: Planets, 124(8), 2117-2140. [6] Zhang et al. (2022). Nature Geoscience, 15(1), 37-41.
[7] Ohtake et al. (2012). Nature Geoscience, 5(6), 384-388. [8] Borg et al. (2011). Nature, 477(7362), 70-72.
[9] Nyquist et al. (2006). GCA, 70(24), 5990-6015. [10] Yamaguchi et al. (2010). GCA, 74(15), 4507-4530.
[11] Iizuka et al. (2014). GCA, 132, 259-273. [12] Vermeesch. (2018). Geoscience Frontiers, 9(5), 1479-1493.
[13] James et al. (1991). LPSC Proceedings (Vol. 21, pp. 63-87).

Iron redox systematics in martian mantle melts and identification of primary liquids

Kevin Righter[1]
[1]*Mailcode XI2, NASA Johnson Space Center, 2101 NASA Pkwy, Houston, TX 77058*

Many MgO-rich shergottites have olivine phenocrysts and a natural question to ask is if any of these represent primary melts from the martian mantle. To answer this requires knowledge of olivine liquid equilibrium in appropriate magma compositions. Because olivine-phyric shergottites represent either primary liquids or liquids that have been modified by fractionation or accumulation of olivine (or other phases), the equilibrium (and its K_d) 2MgO (liq) + Fe_2SiO_4 (olivine) = 2FeO (liq) + Mg_2SiO_4 (olivine), can be used to evaluate whether the olivine-bearing rocks represent liquids. Primary liquids are important to identify since they can allow estimation of compositions of martian magma source regions. If a liquid is primary, then the most magnesian olivine observed in a shergottite would be the first crystallizing olivine and in equilibrium with a liquid whose composition is the same as the bulk meteorite. Natural magmas contain iron in two oxidation states – Fe^{2+} and Fe^{3+} or FeO and Fe_2O_3. Because rocks and glass are typically analyzed for their bulk Fe content, which does not distinguish between FeO and Fe_2O_3, the Fe^{3+}/Fe^{2+} remains an unmeasured parameter for most shergottites, and igneous rocks in general. However, if the bulk composition, temperature, pressure, and fO_2 are known, the Fe^{3+}/Fe^{2+} ratio can be calculated based on experimental database (e.g. [1,2]). This approach has been applied to terrestrial and lunar lavas, as well as to Martian, and is one way to identify primitive melts from the mantles of such differentiated bodies (e.g. [3,4]). Relatively low FeO terrestrial magmas are known to have olivine/liquid K_d = 0.30 [5], whereas higher FeO martian magmas have higher olivine/liquid K_d = 0.34 to 0.39 [6,7]. The values of K_d are dependent on an understanding of redox systematics of martian liquids (high FeO) and knowledge of effect of pressure and depth range over which magma are generated. Recent studies have emphasized analytical approaches [2,8] or focused on alkali-free martian melts [7] which makes comparison difficult (and perhaps even meaningless) to more realistic alkali-bearing melts. Here we revisit olivine-melt equilibrium by applying our expression which was specifically developed for high FeO alkali-bearing martian melts. We also combine this with Matzen et al. 2022 data [7] for alkali-free melts to allow quantification of the effect of alkalis, and even low alkali melts. The expression for predicting Fe^{2+} and Fe^{3+} is $\ln(Fe^{3+}/Fe^{2+}) = a\ \ln fO_2 + b/T + cP/T + dX_{FeO} + eX_{Al2O3} + fX_{CaO} + gX_{Na2O} + hX_{K2O} + iX_{P2O5}$, where coefficients a through i are derived from multiple linear regression of the experimental data (**Figure 1**). This expression can also be used to calculate the change in redox state (or DFMQ) as a martian melt ascends to the surface (**Figure 2**).

Nearly 100 experimental results were compiled for olivine-liquid equilibrium in bulk compositions that are FeO > 15 wt% and limited to those >1200 °C, since we wish to apply the results to high temperature melting [9-20]. Use of the Kress and Carmichael (1991) [1] and O'Neill et al. (2018) [8] expressions developed primarily for lower FeO terrestrial liquids result in K_d = 0.36. Use of Righter et al. (2013) [4] and combined Righter-Matzen datasets [4,7] for higher FeO melts results in K_d in the range 0.37-0.39. If the K_d = 0.36, the shergottites Yamato 980459, NWA 2990, NWA 5789, Tissint, and EETA 79001 A, are all possible primary mantle melts, but the higher K_d = 0.37-0.39 would also allow LAR 06319/12011, NWA 6234 and 4468 to be primitive martian melts as well (**Figure 3**).

References

[1] Kress, V.C. and Carmichael, I.S.E. (1991) *Contrib. Mineral. Petrol. 108*, 82-92; [2[Jayasuriya, K.D., et al. (2004) *Amer. Mineral. 89*, 1597-1609; [3] Longhi, J., et al. (1978) *Geochim. Cosmochim. Acta 42*, 1545-1558; [4] Righter, K., et al. (2013) *Amer. Mineral. 98*, 616-628; [5] Roeder, P.L., & Emslie, R. (1970) *Contrib. Mineral. Petrol. 29*, 275-289; [6] Filiberto, J., & Dasgupta, R. (2011) *Earth Planet. Sci. Lett. 304*, 527-537; [7] Matzen, A.K., et al. (2021) *Amer. Mineral.*

19, 20; [8] O'Neill, H.St.C., et al. (2018) *Earth Planet. Sci. Lett. 504*, 152-162; [9] Agee, C.B., & Draper, D.S. (2004) *Earth Planet. Sci. Lett. 224*, 415-429; [10] Bertka, C.M., & Holloway, J.R. (1994) *Contrib. Mineral. Petrol. 115*, 313-322; [11] Musselwhite, D.S. et al. (2006) *Met. Planet. Sci. 41*, 1271-1290; [12] Filiberto, J., et al. (2010) *Geophys. Res. Lett. 37*(13); [13] Filiberto, J., et al. (2010) *Met. Planet. Sci. 45*, 1258-1270; [14] Blinova, A., & Herd, C.D. (2009) *Geochim. Cosmochim. Acta 73*, 3471-3492; [15] Filiberto, J., et al. (2009) *Amer. Mineral. 94*, 256-261; [16] Filiberto, J., et al. (2008) *Met. Planet. Sci. 43*, 1137-1146; [17] Monders, A.G., et al. (2007) *Met. Planet. Sci. 42*, 131-148; [18] Herd, C.D., et al. (2009) *Amer. Mineral. 94*, 244-255; [19] Nekvasil, H., et al. (2009) *Met. Planet. Sci. 44*, 853-869; [20] McCubbin, F.M., et al. (2008) *Jour. Geophys. Res.: Planets*, *113*(E11); [21] Martian meteorite compendium, https://curator.jsc.nasa.gov/antmet/mmc/index.cfm.

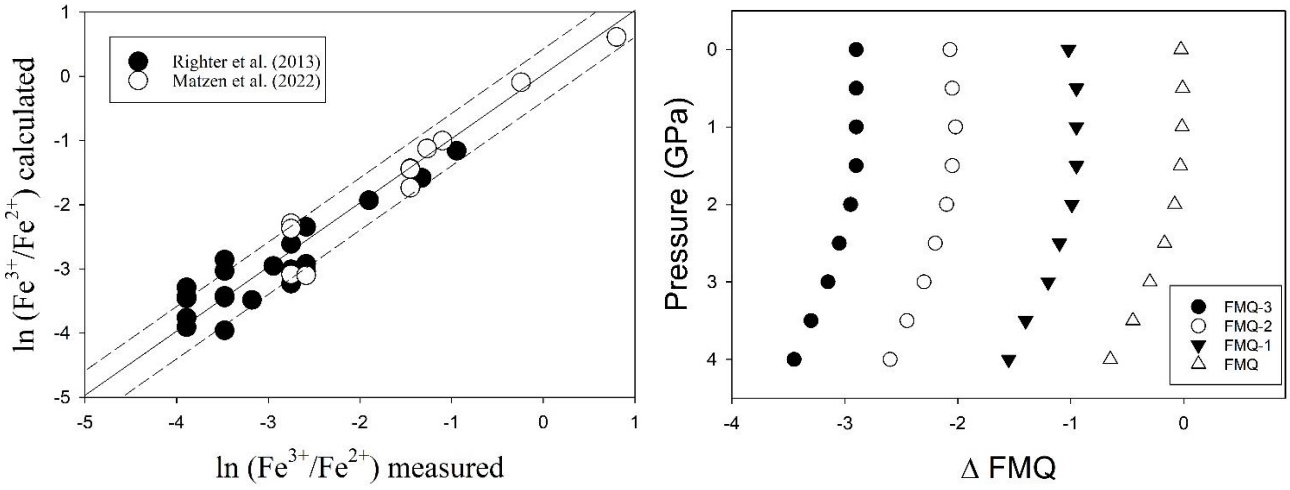

Figure 1: comparison of $\ln(Fe^{3+}/Fe^{2+})$ calculated versus measured with the combined Righter et al. (2013) and Matzen et al. (2022) datasets. Dashed lines are 1 sigma error on the regression.

Figure 2: Calculated oxidation of martian mantle liquids upon decompression and ascent. The change is small and less than one log fO_2 unit between FMQ-3 and FMQ, with much of the effect occurring at high pressures. Shallow decompression will lead to little or no change.

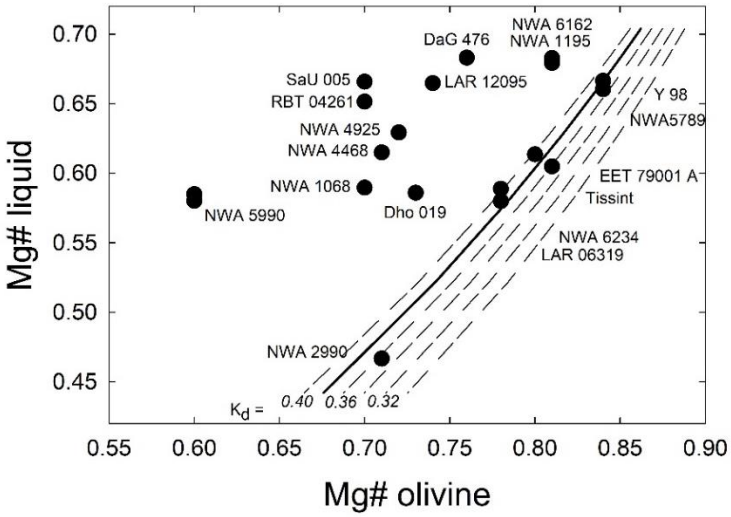

Figure 3: Mg# of olivine and liquids in equilibrium, calculated assuming specific values for the olivine-liquid (Mg-Fe) K_d (dashed lines). The value of K_d appropriate for martian liquids is higher than that for terrestrial compositions (0.30). Previous work has suggested values of 0.35-0.36, but application of our expression for Fe^{3+}/Fe^{2+} equilibrium results in K_d ~ 0.38 (heavy solid line). Several olivine-phyric shergottites fall along or near this line suggesting they could be liquid compositions: Yamato-980459, NWA 5789, EET 79001 (lithology A), Tissint, NWA 6234, LAR 06319, NWA 2990. Even LAR 06319 and NWA 6234 have high olivine modal % and adjustment to the Mg# liquid is necessary, these two compositions are still potential liquids. Data for meteorites from references in [21].

Crystallization of poikilitic shergottites as deduced from textural and mineral compositional diversities of seven samples.

S. Yamazaki[1], T. Mikouchi[2] and C. P. Tang[3]

[1]*Dept. Earth and Planet. Sci., University of Tokyo, Hongo, Tokyo 113-0033, Japan (yamazaki-sojiro615@g.ecc.u-tokyo.ac.jp)*

[2]*University Museum, University of Tokyo, Hongo, Tokyo 113-0033, Japan*

[3]*State Key Lab. of Lunar and Planet. Sci., Macau University of Science and Technology, Macau, China*

Introduction: Shergottites are young (mostly 160-570 Ma crystallization ages) igneous rocks of Martian magma, which comprise nearly 90% of Martian meteorites [e.g., 1]. Shergottites are generally classified into three subgroups based on their petrological characteristics: basaltic (diabasic), olivine-phyric and poikilitic, reflecting distinct crystallization processes of Martian magma. It is also known that shergottites originated from three distinct mantle reservoirs regardless of petrological grouping [e.g., 1-4]. Among three shergottite petrological groups, poikilitic shergottites are characterized by remarkable textures that well reflect their crystallization conditions. Poikilitic shergottites consist of a poikilitic region where pyroxene oikocrysts (usually reaching several mm in size) surround olivine chadacrysts and an interstitial non-poikilitic region where olivine, pyroxene and maskelynite (shock transformed plagioclase glass) are present. The poikilitic texture is considered to have formed in a magma reservoir at depth, while the non-poikilitic texture was formed by rapid cooling near the surface when oikocryst-bearing magma was transported to a shallower region [e.g., 3]. The recent discovery of many samples of poikilitic shergottites mostly from African deserts has revealed that there are significant petrological and compositional variations within this group. However, the factors to cause these differences as well as their final crystallization process near the surface are not well discussed. Therefore, in this study, we analyzed seven poikilitic shergottites, especially newly found samples, to compare their textures and mineral compositions. Using such data, we examine the magmatic crystallization process of poikilitic shergottites, especially crystallization of non-poikilitic regions, by applying crystal size distribution (CSD) analysis of non-poikilitic olivine crystals. We also calculated a heat transfer in the igneous body where oikocryst-bearing magma of poikilitic shergottites intruded near the Martian surface to estimate the size of the body and to discuss Martian crustal structures near the surface in general.

Samples and methods: We studied thin sections of NWA 14127, ALH 77005, NWA 4468, NWA 13366, NWA 13369, NWA 12241 and NWA 13227. Among them, NWA 14127, NWA 13227 and NWA 4468 are enriched samples and ALH 77005, NWA 12241, NWA13366 and NWA13369 are intermediate samples in terms of geochemical characteristics. Elemental maps were obtained using a JEOL JXA-8900 electron probe microanalyzer (EPMA) at the University of Tokyo (15 kV acceleration voltage and 80 nA beam current). The elemental maps were then used for quantitative analysis to decide the analysis points of olivine, pyroxene, maskelynite and spinel minerals in both poikilitic and non-poikilitic regions. For olivine, pyroxene and spinel, the quantitative analysis was set up at acceleration voltage of 15 kV and beam current of 12 nA and for maskelynite, acceleration voltage of 15 kV and beam current of 6 nA (beam diameter: 5 μm). To estimate the solidification time of the intrusive magma, CSD analysis was performed on olivine crystals in non-poikilitic region. We used ImageJ to measure the crystal size and number of olivine crystals. Here, the crystal growth rate of olivine was assumed to be ~3.1×10^{-8} mm/s [5].

Results: The seven poikilitic shergottites studied show variation in the abundance of poikilitic and non-poikilitic areas. The abundance of poikilitic regions is relatively higher for ALH 77005 and NWA 12241 at ~50 %, whereas the abundance of poikilitic regions for NWA13227 and NWA14127 are lower at only ~30%. It is also clear that there is a large textural variation in the proportion of maskelynite in non-poikilitic regions, with NWA 13227 and NWA 14127 accounting for ~40 %, whereas ALH 77005 and NWA 12241 accounting for ~10 %. The mineral compositions of the pyroxene oikocrysts of seven poikilitic shergottites do not show significant differences for the analyzed samples. The core is about $En_{69\pm8}Wo_{12\pm7}$ and the rim is about $En_{51\pm5}Wo_{35\pm5}$. As for mineral composition of olivine, NWA 13227 and NWA 14127 have larger compositional ranges ($Fo_{71\text{-}39}$) than those of other samples ($Fo_{82\text{-}58}$), suggesting that they may have been formed under the condition of faster cooling of magma. Regarding the maskelynite composition, NWA 13227, NWA 14127 and NWA 4468 have relatively large compositional ranges of $An_{65\text{-}35}Or_{0\text{-}10}$, suggesting faster cooling rate, whereas ALH 77005 and NWA 12241 have a narrower compositional range of $An_{65\text{-}45}Or_{1\text{-}3}$ that may have been formed at slow cooling rates. The CSD analysis result shows that the solidification time of seven poikilitic shergottites range from *ca*. 40 to 130 days. There is a negative correlation between the solidification time of the magma and the modal abundance of maskelynite in the non-poikilitic regions (Fig. 1). Because plagioclase crystallized after olivine and pyroxene, this may reflect the accumulation degree of olivine and pyroxene.

Discussion and Conclusion: Mineralogy of seven poikilitic shergottites has revealed that there is more variation in petrological texture and mineral compositions in this group than previously known [e.g., 4, 6]. Especially, the number of poikilitic shergottites with lesser amounts of poikilitic regions (such as NWA 14127 or NWA 13227) has increased. We consider that the

degree of crystal accumulation (pyroxene oikocryst and olivine) is an important factor that causes differences in petrological textures. In addition, a cooling rate of magma is related to the degree of crystal accumulation and makes differences in mineral compositions. Considering the differences in cooling rates and degrees of crystal accumulation, a model to consider a temperature gradient upon an intrusion of magma into a country rock was provided to assume the final crystallization of non-poikilitic areas of poikilitic shergottites near the Martian surface (Fig. 1). Assuming that such country rocks were universally present on Mars, samples with small degrees of accumulation and short solidification time, such as NWA13227 and NWA14127, would have been formed by rapid cooling of intrusive magma near the country rock. On the other hand, samples with a larger abundance of cumulus phases and a longer time of solidification, such as ALH 77005 and NWA 12241, are considered that they were formed under slower cooling condition near the center of the intrusive magma. The other samples formed at the intermediate regions of the intrusive body. To constrain the intrusive body size of poikilitic shergottites, we estimate the thermal evolution of the intruding magma from the thermal diffusion equation. Under the condition that thermal diffusion coefficient of both intrusive magma and country rock is 10^{-6} m^2/s, initial country rock temperature is 0 °C, initial intrusive magma temperature is 1200 °C and solidification temperature of the intrusive magma is 1000 °C, we calculated that the size of intrusion where the center area was solidified in ~127 days (ALH 77005 solidification time) was ~13 m (Fig. 2) [7]. Because we studied both enriched and intermediate poikilitic shergottites and obtained similar results for both geochemical groups, it is suggested that ~13 m size of intrusive bodies of poikilitic textures are universally present near the surface of Mars, regardless of the source magma from different mantle sources.

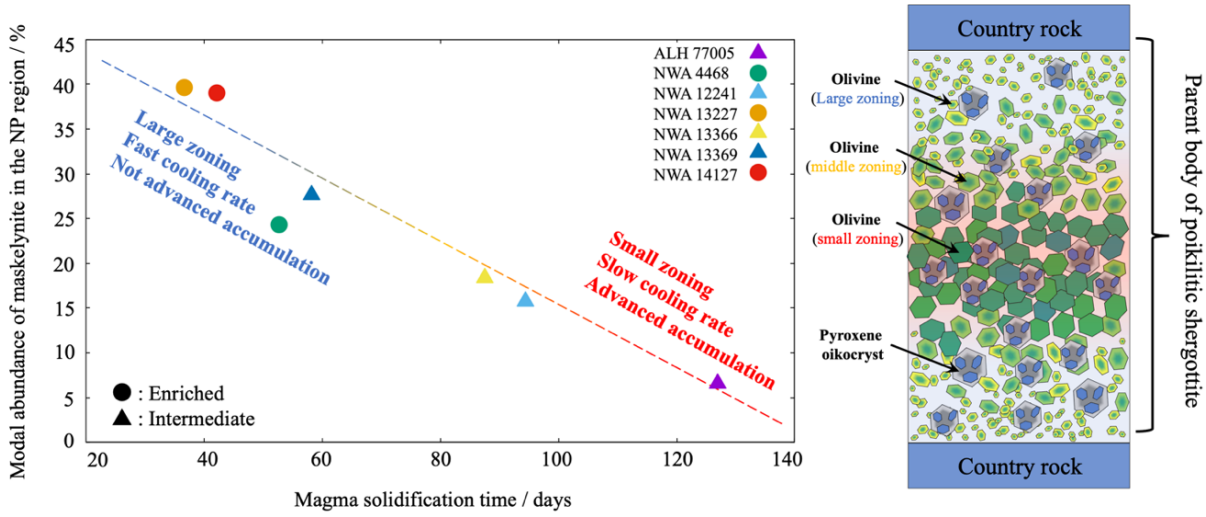

Fig. 1. Left. CSD analysis results showing a relationship between accumulation and crystallization time. Right. A schematic illustration showing a stratigraphy of an igneous body of poikilitic shergottites when they were solidified near the Martian surface to form non-poikilitic regions.

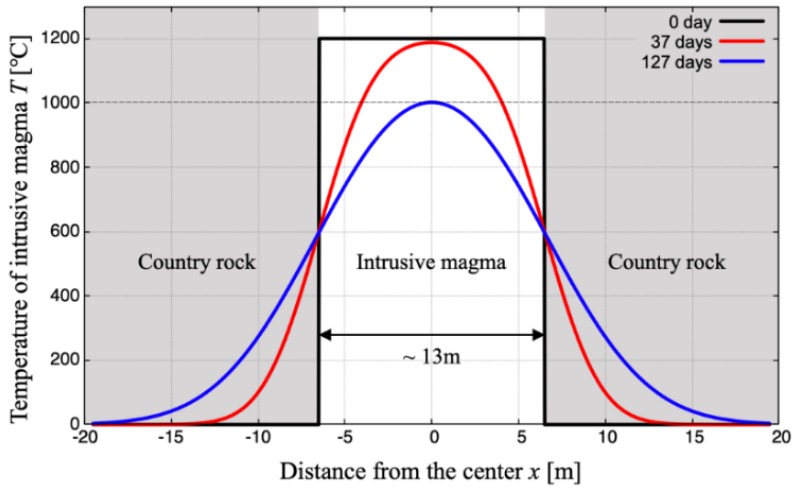

Fig. 2. Thermal evolution of intrusive magma assuming the formation of non-poikilitic regions of poikilitic shergottites. We assumed initial temperature of magma is 1200 ˚C and solidified at 1000 ˚C. The obtained result shows that the size of this body is ~13 m in size.

References

[1] Udry A. et al. (2019) *Jour. Geophys. Res. Planets*, *125*, e2020JE006523. [2] Howarth G. H. et al. (2014) *Meteorit. Planet. Sci.*, *49*, 1812-1830. [3] Howarth G. H. et al. (2017) *Meteorit. Planet. Sci.*, *52*, 391-409. [4] Rahib R. R. et al. (2019) *Geochim. Cosmochim. Acta*, *266*, 463-496. [5] Sarbadhikari A. B. et al. (2009) *Geochim. Cosmochim. Acta*, 73, 2190-2214. [6] Mikouchi T. and Kurihara T. (2008) *Polar Sci.*, *2*, 175-194. [7] Philpotts R. A. & Ague J. J. (2009) *Principles of Igneous and Metamorphic Petrology*: Cambridge University Press.

Origin of silica polymorphs in eucrites: Implications for the crystallization of eucritic magma and metamorphic history of Vestan crust

Rei Kanemaru[1], Akira Yamaguchi[2,3], Naoya Imae[2,3], Aiko Nakato[1], Junko Isa[4], Hirotsugu Nishoido[5]

[1]*ISAS, JAXA,* [2]*NIPR,* [2]*SOKENDAI,* [4]*PERC,* [5]*OUS*

1. Introduction

Meteorites contain various types of silica polymorphs, and their characteristics provide information about the thermal and shock history of parent bodies. Recently, Ono et al. [1] proposed that the occurrences of silica polymorphs in eucrites are related to the cooling rates determined by mineralogy and compositions of pyroxenes. They concluded that quartz in eucrites transformed from high-temperature polymorphs (i.e., tridymite, cristobalite) by soid-state transition. Tridymite in Y 980433 (cumulate eucrite) was observed after the isothermal heating experiment at 800°C for 96 hr. However, we point out that the following issues can be problematic. (1) Y 980433 originally contains quartz. The observed quartz after the heating experiment is indistinguishable from the original quartz. (2) Y 980433 is categorized to shock degree D [2]. A large amount of tridymite in Y 980433 converts to diaplectic glass (Fig. 1). In their study, we could not confirm the same sample area before and after the heating experiment. Therefore, it is unclear whether the transition from tridymite to quartz really occurred. In our study, we performed isothermal experiments of eucrites, and petrographic observations of the same sample area before and after heating. Moreover, we compare the results with the occurrence of silica polymorphs in several eucrites.

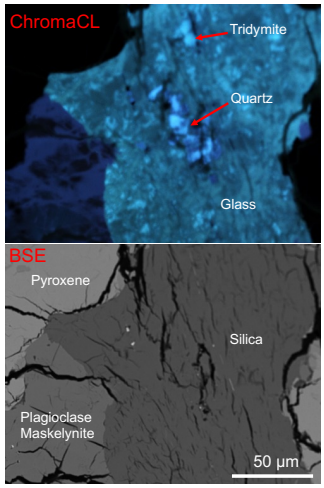

Fig. 1: ChoromaCL and BSE images of Y 980433.

2. Method and samples

We performed petrographic observations of polished slices using an optical microscope, a FE-SEM (JEOL JSM-7100) equipped with an EDS (Oxford AZtec Energy) and a false color-cathodoluminescence imager (Chroma CL, GATAN), an EPMA (JEOL JXA-8200), and a micro-Raman spectroscope (JASCO NRS-1000) from NIPR. The samples were coated with Os (~5 nm) for SEM observation and EPMA measurements. After petrographic observations, Os coating was removed using a lapping film (3 µm). We separated small chips (~2 mm) from polish slices. Isothermal experiments were performed using the same furnace used by Nakato et al. [3] at ISAS. The chip samples were placed in a stainless steel container, and that was evacuated down to approximately 1×10^{-7} torr using a turbo-molecular pump. We performed two sets of isothermal heating experiments (800ºC for100hr and 1000ºC for 100hr). After heating, the samples were cooled to room temperature in a vacuum.

3. Results and discussion

Heating experiments

We used two basaltic eucrites (Agoult, A-87272) as the starting materials for the isothermal heating experiments. These eucrites are classified into different petrologic types [4] and shock degrees [2] (Table 1). Most of the silica minerals in Agoult are MC tridymite. A-87272 contains a large amount of silica glass, minor MC-tridymite and quartz. The silica glass has a lathy shape and higher Al_2O_3 component (0.21 wt.%), which mineralogical features are comparable to tridymite in other eucrites. Hence, the silica glass in A 87272 is a diaplectic glass of tridymite formed by highly shock metamorphism. Our previous observations indicate that amorphization of tridymite is observed in shock degrees D and E eucrites.

Tridymite in Agoult and A-87272 did not convert to other phases after heating at 800 to 1000ºC for 100hr. Silica glass also did not convert to other phases after heating at 800 ºC for 100hr. On the other hand, a small amount of silica glass in A-87272 converts to quartz after heating at 1000 ºC for 100hr. The facts suggest that the tridymite in eucrites cannot convert into quartz after secondary heating events. Based on our observations, which are inconsistent with Ono et al. [1], we ruled out a formation of quartz from tridymite by the solid-state transition.

Silica minerals in eucrites

On the basis of our petrographic observations, silica minerals in eucrites are divided into the following four types: (Si-I~III, ungrouped). Si-I is characterized by abundant quartz and minor cristobalite (e.g., Stannern) (Fig. 2a). In the Si-I eucrites, the silica minerals occur mainly in association with large aggregates with opaques (troilite and ilmenite) and phosphate. Si-II is characterized by abundant quartz and tridymite (e.g., Y-75011) (Fig. 2b). In the Si-II eucrites, tridymite occurs as lathy coarse crystals or interstitially between pyroxene and plagioclase. In the tridymite, opaque minerals and phosphate are absent, as in the Si-I quartz. On the other hand, the occurrence of quartz is similar to those of Si-I eucrites. We observed a small abundance of

cristobalite in Si-II eucrites around quartz. Si-III is characterized by abundant tridymite (e.g., Agoult, Moama) (Fig. 2c). In the Si-III eucrites, tridymite occurs as coarse crystals or interstitially between pyroxene and plagioclase without opaques and phosphate, similar to the occurrence of tridymite in Si-II. The Si-ungrouped eucrites are characterized by abundant quartz and tridymite (a coarse-grained portion of Juvinas) but the quartz does not coexisted with opaque and phosphate (Fig. 2d). The quartz and tridymite are present in the same silica grain, which shows a sharp grain boundary.

Origin of silica polymorphs in eucrites

Ono et al. [1] proposed that the combination of silica minerals in eucrites has simply associated with the petrologic types. However, we could not find such relationships between Si-types and petrologic types [4] of eucrites. The fact indicates that the solid-state transition from high temperature polymorphs alone cannot explain the origin of silica minerals. On the basis of our isothermal experiments and petrographic observations, we proposed a new formation process of quartz in eucrites.

Tridymite is a stable phase at P/T condition at the solidus of eucritic magma. Therefore, all silica minerals in eucrite that crystallize in equilibrium conditions become tridymite (i.e., Si-III). On the other hand, it is also known that cristobalite can crystallize from experimentally quenched eucritic melts [1,5]. Ono et al. [1] indicated that the origin of quartz in eucrites is due to a solid-state transition from tridymite and cristobalite. However, we did not observe a phase transition of tridymite to quartz in our experiments. This suggestion is consistent with petrographic observations. The solid-state transition of tridymite to quartz could not explain the occurrence of opaques and phosphate in quartz at such a high frequency. Hence, we propose that quartz is formed from quenched residual melts (probably via silica glass) at disequilibrium conditions. In this case, we can well explain the occurrence of quartz coexisting with cristobalite, opaques, and phosphate (i.e., Si-I). Based on this discussion, Si-II is expected to be found that transitioned from an equilibrium state to a disequilibrium state during the crystallization process. The occurrence of silica minerals in Si-ungrouped eucrites cannot be explained by the crystallization process described above. In this study, we experimentally showed that silica glass transformed to quartz by secondary heating. Hence, quartz in Si-ungrouped formed from silica glass (diaplectic tridymite) by post-shock annealing. Actually, Juvinas is considered to have experienced shock partial melting. This fact is consistent with the amorphization of tridymite and the subsequent annealing.

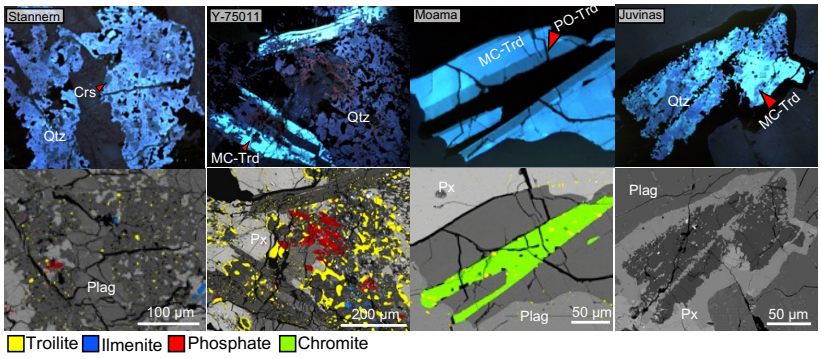

Fig. 2: ChoromaCL image and mineral map of eucrites. Stannern is Si-I eucrite which characterized by abundant quartz and minor cristobalite. Y-75011 is Si-II eucrite which characterized by abundant quartz and tridymite. Moama is Si-III eucrite which is characterized by abundant tridymite. Corse-grained portion of Juvinas is Si-ungrouped eucrite which is characterized by abundant quartz and tridymite (coarse-grained portion of Juvinas) but the quartz is not coexistence with opaque and phosphate. Qtz = quartz, Crs = cristobalite, MC-Trd = monoclinic tridymite, PO-Trd = pseudo-orthorhombic tridymite, Plag = plagioclase, Px = pyroxene.

Table 1. Classification of studied eucrites.

Sample	Petrologic type	Chemical type	Si-type
Y-75011	Basaltic/1	-	Si-II
NWA 049	Basaltic/2	Main group	Si-II
Millbillillie FG clast	Basaltic/4	Main group	Si-I
NWA 7188	Basaltic/4	Stannern group	Si-I
Y 983366	Basaltic/4	-	Si-I
Stannen	Basaltic/4	Stannern group	Si-I
Y-790266 CG clast	Basaltic/4	Stannern group	Si-I
Juvinas FG clast	Basaltic/4	Main group	Si-II
Juvinas CG clast	Basaltic/5	Main group	Si-ungrouped
Y-792510	Basaltic/5	Main group	Si-II
Millbillillie CG clast	Basaltic/5	Main group	Si-II
NWA 5356	Basaltic/5	-	Si-II
A-88174 FG clast	Basaltic/5	Stannern group	Si-III
EET 90020	Basaltic/5	Residual eucrite	Si-III
Agoult	Basaltic/5	Residual eucrite	Si-III
A-87272	Basaltic/7	Residual eucrite	-
Y-791195	Cumulate	-	Si-III
Moore County	Cumulate	-	Si-III
Moama	Cumulate	-	Si-III

CG = Coarse grained; FG = Fine grained

Most of silica minerals in A-87272 are silica glass

References

[1] Ono, H., Takenouchi, A., Mikouchi, T., Yamaguchi, A., Yasutake, M, Miyake A., Tsuchiyama, A., Association of silica phases as geothermobarometer for eucrites: Implication for two-stage thermal metamorphism in the eucritic crust, *MAPS*, 56, 6, 1086-1108, (2021). [2] Kanemaru, R., Imae, N., Yamaguchi, A., Takenouchi, A., Nishido, H., Estimation of shock degrees of eucrites using X-ray diffraction and petrographic methods, *Polar Science*, 26, 100605, (2020). [3] Nakato, A., Nakamura, T., Kitajima, F., Noguchi, T., Evaluation of dehydration mechanism during heating of hydrous asteroids based on mineralogical and chemical analysis of naturally and experimentally heated CM chondrites, *EPS*, 60, 855-864, (2008). [4] Takeda, H., and Graham, A. L., Degree of equilibration of eucritic pyroxenes and thermal metamorphism of the earliest planetary crust, *MAPS*, 26, 129-134, (1991). [5] Yamaguchi, A., Mikouchi, T., Ito, M., Shirai, N., Barrat. J.A., Messenger. S., Ebihara, M., Experimental evidence of fast transport of trace elements in planetary basaltic crusts by high temperature metamorphism, *EPSL*, 368, 101-109, (2013).

Impact-induced (?) Cr-diffusion in the metallic phase in chondrites and achondrites

J.Isa[1], K. Kurosawa[1], N. Sugiura[1], T. Niihara[2], T. Arai[1], and T. Matsui[1]
[1]*PERC, Chiba Institute of Technology, Chiba, Japan*
[2]*Department of Applied Science, Okayama University of Science, Okayama, Japan*

Shock-induced metamorphism recorded on meteorites has been extensively studied by petrographic observations and experimental studies since the dawn of the meteorite study, and yet they are still an important topic today. Recently, shock metamorphisms have been revisited and summarized by [1]. It is widely recognized that impacts can induce localized heating (up to melting); the impact heating has been considered one of the significant driving forces of the thermal metamorphism on the asteroids by some workers [e.g., 2]. Because of the wide range of the meteorite's mineral compositions, individual meteorite groups have various materials with the combinations of different shock impedances. Also, the individual meteorite groups likely came from different sizes of parent bodies and experienced various thermal histories. Therefore, observed "impact-induced" signatures in meteorites can broadly vary. Even only among equilibrated ordinary chondrites, numerous shock-related features are reported, and the most widely recognized features include shock metamorphism: undulose extinction, planar features, mosaicism, and planer deformation features in olivine; undulose extinction in low-Ca px, polysynthetic twin lamellae parallel to (100), mosaicism and planar deformation features in low-Ca clinopyroxene; undulose extinction, becomes partially isotropic, develops planner deformation features, and transform into maskelynite in plagioclase [3]. However, those silicate features are not robust against annealing conditions caused by heat induced by subsequent or during the shock events [4,5]. Rubin 2004 extensively investigated shock features across the ordinary chondrites, including minor features that had been reported as following shock features: silicate darkening [6,7], chromite veinlets [6], chromite-plagioclase assemblages [4], metal and sulfide veins [3], narrow silicate melt vein [8], large metal and/or sulfide nodules [9], polycrystalline troilite [10], irregularly shaped troilite grains within Fe-Ni metal [11], martensite and various type of plessite [12], rapidly solidified metal-sulfide intergrowths [13], metallic Cu grains [11], glassy melt pockets [14] and large regions of silicate melt [15]. Mobilization of metal-sulfide melts and subsequent secondary phase formation, such as the occurrence of metallic Cu grains, are sufficient indicators of the shock heating above the Fe-FeS eutectic (988 °C). They can be useful indicators. Such occurrence of secondary minerals, however, are not versatile shock indicators due to the high temperature requirement. For example, the temperature range of such features is higher than that of normal equilibrated temperatures recorded in the olivine-spinel thermometry in ordinary chondrites (H4: 600–700 °C [16]). It would be helpful to have chemical evidence that robustly recorded the shock features within or under the olivine-spinel equilibrium temperature to fully understand the shock records on the parent bodies; elemental mobilization within opaque minerals can be more utilized to understand the lower temperature phenomena. Kessel et al. 2004 [17], revisited the H chondrite's metamorphic temperature and f_{O2} conditions. They concluded that the low concentrations of Cr in the taenite grains are due to their lower closure temperatures relative to silicates. We found that their results imply a possible robust record of elemental mobilization at low temperatures recorded within the chromite/metal chemical composition. In our study, we revisited the phase compositions of chromite/metal, which are ubiquitously located in chondrites and achondrites. We investigated whether trace element distributions between chromite/metal can be used to indicate the parent bodies' shock features and/or thermal histories at a relatively lower temperature range.

Sample and Method:

We have primarily studied equilibrated ordinary chondrite NWA13458, H5 (Shock stage S2 defined based on shock metamorphic features in silicates) chondrite, and shock recovery experimental products of this chondrite. The shock recovery experiments were conducted with a two-stage light gas gun at Planetary Exploration Research Center (PERC) at Chiba Institute of Technology, Japan [18]. We used NWA13458 as targets and applied the experimental method [19] with three different heating conditions: ambient temperature, 350 °C, and 650 °C. Also, we compare the petrographic observations of our sample to the other meteorite groups, including mesosiderites, two primitive achondrites (Tafassasset, N3250), one Iron (Miles: IIE), and one chondrite (Forest Vale: H4).

We analyzed samples using the scanning electron microscope (SEM, JEOL JSM-6510LA) at PERC Chiba Institute of Technology. Energy dispersive X-ray spectroscopy (EDS) was used for the observation of trace elemental diffusion profiles in the different meteorite groups.

Preliminary Results:

We located chromite grains up to a few tens of microns in size next to Fe-metal (kamacite or taenite) grains. The texture of chromites is euhedral, subhedral, anhedral, and rounded. These selected chromite grains often occur adjacent to the silicate as well. Inside the kamacite grains, we found that Cr concentrations vary. As it was reported before in ordinary chondrite metal [17], in NWA13458, Cr concentrations in the middle of kamacite grains are very low. However, Cr diffusion profiles across the grains indicate that some of kamacite grains show a zoning profile; the Cr concentrations increased towards the edge of the chromite kamacite interface. The zoning profiles are not apparent in taenite that occurs next to chromite. The similar Cr diffusion profiles into metal from chromite grains are found in mesosiderites, two primitive achondrites (Tafassasset, N3250), one Iron (Miles: IIE), and one chondrite (Forest Vale: H4). Furthermore, zoning profiles are also common within chromite grains. A center of chromite (Cr-spinel) grain is more Mg-Al-rich, but the edge of the chromite becomes closer to the end member composition, $FeCr_2O_4$.

Discussion:

The Cr zoning profiles in metals are common in chondrites, primitive achondrites, and achondrites. These profiles are not associated with their cooling rates estimated by the Ni-diffusion profile, and some samples have different cooling histories: Miles and Forest Vale were shock-heated and then cooled rapidly to low temperatures. Mesosiderites were heated to solidus temperatures (~1200 °C) and subsequently cooled rapidly but cooled very slowly through ~500 °C. Therefore, it appears to be true that the Cr zoning is not simply caused by the same mechanisms with Ni diffusion in the FeNi metal. This separation appears to be puzzling because both elements' diffusion coefficients are relatively fast in FeNi metal (and $D_{Cr} > D_{Ni}$ [20]) if one thinks that both zonings are simply caused by self-diffusion. However, this Cr up-hill diffusion profile may seem natural to explain by the interdiffusion with considering the free energy of forming chromite. Kessel et al. 2004 reported low Cr concentrations in the Fe metal in H chondrites, which implies that the Cr concentration in FeNi metal was initially higher and lost by sub-solidus diffusion. It is natural to consider the Cr in the metal-formed chromite grains. Forming chromite requires oxygen provided through the oxide, and it can be controlled over the formation of chromite overgrowth and Cr diffusion profiles in the metal grains. We will further investigate the oxygen fugacity of the H chondrites after the closure temperature of the silicate and oxides. Also, we plan to investigate the possible effects on Cr diffusion in metals by understanding oxygen fugacity and local temperature changes caused by impact shock events.

References:

[1] Stöffler et al. (2018) MAPS 53(1), 5-49. [2] Rubin (1995) Icarus, 113(1), 156-167., [3] Stöffler et al. (1991) GCA *55*(12), 3845-3867. [4] Rubin (2003) GCA *67*(14), 2695-2709. [5] Rubin (2004) GCA *68*(3), 673-689. [6] Rubin 1992 GCA 56, 1705–1714. [7] Leroux et al., (1996) MAPS 31, 767–776. [8] Fredriksson et al. (1963) Space Res. 3, 974–983. [9] Rubin (1999) *J. Geophys. Res.* **104,** 30799–30804. [10] Bennett and McSween, (1996) MAPS **31,** 783–792. [11] Rubin (1994) *Meteoritics* **29,** 93–98. [12] Smith and Goldstein (1997) GCA **41,** 1061–1072. [13] Scott (1982) GCA **46,** 813– 823. [14] Dodd and Jarosewich (1979) EPSL **44,** 335–340. [15] Kring (1996) J. Geophys. Res. 101, 29353–29371. [16] McSween et al. (1988) In Meteorites and the early solar system, edited by Kerridge J. F. and Matthews M. S. Tucson: University of Arizona Press. pp. 102–113. [17] Kessel et al. 2004 MAPS *39*(8), 1287-1305. [18] Kurosawa et al. (2015) J. Geophys. Research-Planets, 120, 1237–1251. [19] Kurosawa et al. (2022) J. Geophys. Research-Planets, *127*, e2021JE007133. [20] Righter et al. (2005) GCA *69*(12), 3145-3158.

Petrography and Oxygen isotopic compositions of Ca-Al-rich inclusions from Asuka-9003 and 09535

Nozomi Matsuda[1], Ming-Chang Liu[2], and Kevin D. McKeegan[1]
[1]*Department of Earth, Planetary, and Space Sciences, University of California, Los Angeles, CA 90095, USA*
[2]*Lawrence Livermore National Laboratory, Livermore, CA, 94550, USA*

Introduction:

The current model explaining the whole-rock isotope dichotomy is the accretion of non-carbonaceous chondrites (NCs) and carbonaceous chondrites (CCs) parent asteroids inside and outside, respectively, of the early formed proto-Jupiter (Desch et al., 2018). It is observed that the largest, centimeter-sized Calcium-aluminum-rich inclusions (CAIs) are predominately found in CV and CK chondrites, with CAI sizes in all other chondrites being smaller (e.g., MacPherson et al., 2005). CAIs typically comprise 0.5–3 vol% in CCs that formed far from the Sun, but only < 0.1 vol% in enstatite and ordinary chondrites, collectively known as NCs, that formed closer to the Sun (Desch et al., 2018). Because CAIs are generally thought to have formed in the inner solar system, the fact that they were preferentially incorporated into CCs is puzzling.

Asuka (A)-9003 and A-09535 represent a new type of carbonaceous chondrite, designated CA (Kimura et al., 2021). These CA chondrites have unique features: they share similarly high chondrule/matrix ratios with ordinary chondrites but resemble CO and CV chondrites in terms of the abundances of refractory inclusions (4−6 vol%) and oxygen isotopic compositions (Kimura et al., 2021). With characteristic features of both NCs and CCs, the CA chondrites are in some sense transitional between materials that accreted in the inner solar system and those from the outer solar system. In addition, they could help shed light on complex histories of material transport before their accretion into the parent bodies. Here we present the results of petrological characterizations and oxygen isotopic compositions of CAIs in CA chondrites.

Methods:

CAIs studied were identified in polished thin sections of Asuka-9003 and 09535, on loan from the National Institute of Polar Research. The petrographic observation and chemical analysis were performed by scanning electron microscopy (SEM, Tescan Vega) equipped with an energy dispersive spectrometer (EDS) at UCLA. The oxygen isotope analysis was carried out on the UCLA CAMECA ims-1290 ion microprobe in multicollection mode.

Result and discussion:

CAIs in both A-9003 and A-09535 are typically fine-grained inclusions (FGIs). Based on mineralogy, the FGIs can be classified into four groups: (1) spinel-melilite-pyroxene inclusions, (2) spinel-hibonite-melilite inclusions, (3) spinel-hibonite-melilite-grossite inclusions, and (4) pyroxene-rich inclusions.

Spinel-melilite-pyroxene inclusions are irregularly-shaped. These inclusions have a spinel-rich core enclosed in melilite, both of which are rimmed by a complete or discontinuous layer of Ca-pyroxene. The inclusions contain fine-grained mixtures of Na-rich minerals which appear to be alteration products replacing melilite. Spinel-hibonite-melilite inclusions can be further divided into two types based on the morphologies. One has lath-shaped hibonite grains that are embedded in spinel and are subparallel to one another. Melilite occurs on the exterior of the inclusions. This morphology is similar to hibonite-spinel CAIs in the ALHA77307 (CO3.0) chondrite (Han et al., 2015). The other type is characterized by a layered structure of irregularly shaped nodules in the center composed of spinel that encloses hibonite and melilite. In some cases, melilite in the nodules has been partially converted into alteration products. Spinel-hibonite-melilite-grossite inclusions are either irregularly-shaped or round. These inclusions have similar mineralogy and textures to spinel-hibonite-melilite inclusions. MgO-rich and FeO-rich (Fe# (100 × molar Fe/(Mg + Fe) > 75) spinel are both present in this type of inclusions. FeO-rich spinel shows a porous texture, while MgO-rich spinel does not. This type of inclusion has been found in the Kainsaz (CO3.2) chondrite (e.g., Itoh et al., 2004). Pyroxene-rich inclusions are irregularly-shaped. They consist of Ca-rich pyroxene and often contain spinel, olivine, low-Ca pyroxene, melilite, and anorthite as accessory minerals. The first two groups of CAIs are much more abundant than the last two in both A-9003 and A-09535 samples. The observed mineralogic features in CA CAIs are similar to those in CAIs from both C (CO and CV) and O chondrites (e.g., Russel et al., 1998; MacPherson, 2014; Krot, 2019; Han et al., 2019).

Spinel-melilite-pyroxene inclusions and pyroxene-rich inclusions are up to ~600 μm in size, while spinel-hibonite-melilite inclusions and spinel-hibonite-melilite-grossite inclusions are relatively smaller (< 200 μm). The lack of millimeter- or centimeter-sized CAIs found in this study makes CA chondrites more similar to CO chondrites than to CV in terms of the CAI sizes (e.g., Russell et al., 1998; Itoh et al., 2004; Han et al., 2019)

Spinel and Ca-pyroxene in spinel-melilite-pyroxene inclusions have a narrow range of $\Delta^{17}O$ from −24 to −20‰. In comparison, melilite shows a large range of $\Delta^{17}O$ from −24 to −5‰. Spinel and hibonite in both spinel-hibonite-melilite and

spinel-hibonite-melilite-grossite inclusions have ^{16}O-rich compositions from −24 to −21‰ in Δ^{17}O. Melilite in these two types of CAIs has variable Δ^{17}O values, which range from −21 to −14‰. Hercynite and grossite are ^{16}O-poor compared to spinel, hibonite and melilite. Spinel, Ca-pyroxene, and hibonite in CA CAIs have ^{16}O-rich compositions similar to the isotopic composition of the Sun (McKeegan et al., 2011), suggesting that they still preserve the Δ^{17}O values of the nebular gas, and secondary processes either in the nebula or on their parent bodies did not affect these minerals. In contrast, melilite, grossite, and hercynite seem to have undergone isotope exchange with ^{16}O-poor components (e.g., matrix materials or water) during fluid-rock interactions, which have been invoked to explain the oxygen isotope compositions of CAI minerals from CO chondrites of type 3.1 and above (e.g., Brearley and Krot, 2013; Krot, 2019). This inference is supported by our petrologic observations which show that CA CAIs contain fine-grained nepheline, a product of fluid-assisted metasomatism on the parent bodies. From the petrological observations and oxygen isotope compositions, we conclude that CAIs from CA chondrites closely resemble those of CO chondrites. With CA chondrites having high chondrule/matrix ratios, CA chondrite-forming regions would need to be either a dust-poor or chondrule-rich environment like those in the inner solar system in which ordinary chondrites accreted but this reservoir should be in the CC region to best explain the CAI properties. Further studies of CA-chondrite components, including chondrules and matrix, are needed to shed more light on the origins of these unusual meteorites.

References

Brearley A. J., and Krot A. N., Metasomatism in the early Solar System: The record from chondritic meteorites. In Metasomatism and the Chemical Transformation of Rock, 659–791, 2013.

Desch S. J., Kalyaan A., and Alexander C. M. O., The effect of Jupiter's formation on the distribution of refractory elements and inclusions in meteorites, The Astrophysical Journal Supplement Series 238, 11–42, 2018.

Han J., Brearley A. J., and Keller L. P., Microstructural evidence for a disequilibrium condensation origin for hibonite-spinel inclusions in the ALHA77307 CO3.0 chondrite, Meteoritics & Planetary Science 50, 2121–2136, 2015.

Han J., Jacobsen B., Liu M-C., Brearley A. J., Matzel J. E., and Keller L. P., Origin of 16O-rich fine-grained Ca-Al-rich inclusions of different mineralogy and texture, Geochemistry 79, 125543, 2019.

Itoh S., Kojima H., and Yurimoto H., Petrography and oxygen isotopic compositions in refractory inclusions from CO chondrites, Geochimica et Cosmochimica Acta 68, 183–194, 2004.

Kimura M., Greenwood R. C., Komatsu M., Imae N., Yamaguchi A., and Sato R., Petrology and classification of A-9003, A09535, and Y-82094: A new type of carbonaceous chondrite, Meteoritics & Planetary Science 57, 302–316, 2021.

Krot A. N., Refractory inclusions in carbonaceous chondrites: Records of early solar system processes, Meteoritics & Planetary Science 54, 1647–1691, 2019.

MacPherson G. J., Simon S. B., Davis A. M., Grossman L., Krot A. N., Calcium-Aluminum-rich inclusions: major unsewered questions, Chondrites and the Protoplanetary Disk 341, 225–250, 2005.

MacPherson G. G., Calcium-aluminum-rich inclusions in chondritic meteorites. Meteorites, Comets and Planets: Treatise on Geochemistry, Second Edition, 139–179, 2014.

McKeegan K. D., Kallio A. P. A., Heber V. S., Jarzebinski G., Mao P. H., Coath C. D., Kunihiro T., Wiens R. C., Nordholt J. E., Moses Jr. R. W., and Burnett D. S., The oxygen isotopic composition of the Sun inferred from captured solar wind, Science 322, 1528–1532, 2011.

Russell S. S., Huss G. R., Fahey A. J., Greenwood R. C., Hutchison R., and Wasserburg G. J., An isotopic and petrologic study of calcium-aluminum-rich inclusions from CO3 meteorites, Geochimica et Cosmochimica Acta 62, 689–714, 1998.

Carbon and Sulfur Abundances in Carbonaceous Meteorites Revisited

T. Arai[1], K. Suzuki[2], R. Moriwaki[2], and T. Matsui[1,2]

[1]*Planetary Exploration Research Center, Chiba Institute of Technology, 2-17-1 Tsudanuma, Narashino, Chiba 275-0016, Japan (tomoko.arai@it-chiba.ac.jp)*

[2]*Institute for Geo-Cosmology, Chiba Institute of Technology, 2-17-1 Tsudanuma, Narashino, Chiba 275-0016, Japan*

Introduction: Cosmic dust and carbonaceous chondrites are of importance as major extraterrestrial source of carbon and organics, which possibly served as prebiotic seeds of life on the early Earth. One of science objectives of DESTINY+ is to characterize cosmic dust on the basis of physical and chemical properties directly measured prior to the atmospheric entry [1]. DESTINY+ is currently planned to be launched in 2024 and flyby Geminids-parent asteroid (3200) Phaethon in January, 2028 [1]. After the spacecraft is injected into a highly elliptical orbit around the Earth, it will gradually raise its orbit for about 2 years, to reach the Moon. Subsequently, it escapes from the Earth's gravity sphere through multiple lunar gravity assists, heading to Phaethon. Dust Analyzer (DDA) onboard DESTINY$^+$ will directly measure cosmic dust during the entire mission phases, including the Earth's spiral orbit, lunar swing-by, interplan-etary cruise, the Geminids dust stream and flyby of Phaethon [1]. DDA is an impact ionization time-of-flight mass spectrometer with integrated trajectory sensor, which will analyse micrometer and sub-micrometer-sized dust particles. The instrument will measure the parti-cle chemical composition (mass resolution $m/\Delta m \approx 100$-150), mass, electrical charge, impact velocity (about 10% accuracy), and impact direction (about 10° accuracy) [2]. Combined bulk chemistry and physical properties for measured dust particles are used to constrain the nature and origin of each dust particle. Carbon is a key element in DDA science, since it is directly linked with the mission objective. Carbon (C) and sulfur (S) abundances of meteorites are key elements to reflect secondary thermal and aqueous history and/or redox state of their parent bodies. Previous studies indicate that total abundances of carbon and sulfur varies substantially among multiple classes of carbonaceous chondrites and carbonaceous achondrite (ureilite) [3,4] A comprehensive study of bulk C and nitrogen (N) for multiple petrologic classes of carbonaceous chondrites conducted using a single analytical method shows that the elemental abundances broadly correlate with the degree of secondary thermal and aqueous alteration over the petrologic types [5]. The study also indicate that no systematic differences are present between meteorite falls and finds, implying that terrestrial alteration has a minor effect on bulk C and N abundances [5]. Motivation of this study is to demonstrate bulk-meteorite C and S abundance measurement with a different analytical method from previous studies, using an advanced C and S analyzer. Once the feasibility of measurement is confirmed, variations in C and S abundances among petrologic types of meteorites are discussed and compared with those from previous studies.

Samples & Methods: Bulk C and S abundances were measured for total six meteorite samples, including different petrologic types of carbonaceous chondrites, Murchison (CM2), Aguaz Zarcas (CM2), Allende (CV3), NWA 2086 (CV3) [6], NWA3133 (CV7), NWA 5515 (CK4) [7], NWA 765 (CK4/5) with two carbonaceous chondrites-related achondrites, NWA 6704 (CR chondrite-related achondrite) [8-11], Dhofar 1170 (ureilite) and Almahata Sitta (coarse-grained ureilite) [7, 12]. Aguas Zarcas, Allende, Almahata Sitta and Murchison are recorded falls and other six are finds. Considered the caution that variations in carbon abundances in multi-ple types of carbonaceous chondrites tend to be af-fected by intra-meteorite heterogeneities [5], the mass of a few hundred mg was used for measurement of each sample. C and S analyses were performed using Elementar inductar CS cube carbon and sulfur analyzer at Institute for Geo-Cosmology, Chiba Institute of Technology. The samples were pulverized using an agate mortar and pestle. The ceramic crucible was heated at 1100°C for 40 minutes using a muffle furnace to remove the adsorbed contaminants. Meteorite samples of 175–389 mg (Table 1) weighed and placed in the ceramic crucible, and about 2 g of tungsten/tin mixture and 0.5 g of pure iron were added as combustion improver. During the analysis, high-purity G1 grade oxygen (>99.99995%) was supplied at a rate of 450 mL/min to create a pure oxygen atmosphere, and the sample was introduced into a solid-state induction furnace where a voltage of 2000 W was applied to burn the sample. The carbon and sulfur in the sample were extracted as CO (partially CO_2) and SO_2, respectively. SO_2 was detected by the first non-dispersive infrared (NDIR) detector. In an oxidation tube (plati-num silica-gel, 550°C), CO and SO_2 oxidized to CO_2 and SO_3, respectively. SO_3 was collected in a trap (cellulose), and CO_2 was detected with the second NDIR detector. The carbon and sulfur content of the sample was calculated from the detected concentrations of CO_2 and SO_2 using the calibration coefficients for steel, which are set in the instrument, since the calibration coefficients for C chondrites are not known.

Results and Discussion:

Feasibility of bulk C & S analyses. Bulk C and S abundances for the six meteorites measured in this study are given in Table 1, and those for carbonaceous meteorites in the previous studies [5, 7] are listed in Table 2. Elemental abundances of both C and S in this study are broadly similar to those of previous studies for the same petrologic types with an exception of S

abundance of CK4 chondrites. While C abundance of Murchison in this study (2.043 wt%) is slightly lower than that from the previous study (2.70 wt%) [7], C abundance of Allende in this study (0.501 wt%) is higher than that in the previous study (0.27 wt%) [7]. S abundance of Murchison in this study (2.4266 wt%) is slightly lower than those of CM2 chondrites both from Antarctic and non-Antarctic meteorites in previous study (2.80 – 5.44 wt %) [5]. Note that S abundance of NWA 5515 CK4 chondrite (0.0545 wt %) in this study is significantly lower than those of CK4 chondrites both from Antarctic and non-Antarctic meteorites in the previous study (1.31 – 2.14 wt %). Except the S abundance in CK4 chondrite, the bulk-rock abundances for both C and S in this study comparable to those in previous studies indicate that analyses with the inductor C and S analyzer is feasible and valid.

Variation among petrologic types. Amongst carbonaceous chondrites measured, the CM2 chondrite displays the highest abundances, the CK4 chondrite shows the lowest and the CV3 falls in between both for C and S (Table 1). The bulk C and S abundances decrease with increasing thermal metamorphism, which is in line with previous studies [5]. For achondrites, CR-related achondrite NWA 6704 shows by far the lowest abundance both in C and S. The Almahata Sitta ureilite sample has the highest C abundance among all the samples measured with the S abundance comparable to that of CV3 NWA 2086. Further discussion on bulk C and S variations over petrologic types and on comparison with previous studies is pending analyses of additional samples by the analytical method used in this study.

References: [1] Arai T. et al., Phaethon. 52nd LPSC, Abstract #1896, 2021. [2] Krüger H. et al., 15th EPSC, abstract id. EPSC2021-871, 2021. [3] Gibson E. K. and Yanai K., Proc. Lunar Planet. Sci. Conf. 10th, 1045-1-51, 1979. [4] Gibson E. K. et al. (1984) LPS XV, 304-305. [5] Pearson V. K. et al., Meteoritics & Planet. Sci., 41, 1899-1918, 2006. [6] Meteoritical Bulletin, no. 89, MaPS 40, A201-A263, 2005. [7] Meteoritical Bulletin, no. 96, MaPS, 44, 1355-1397, 2009. [8] Sanborn, M. E. et al., Geochim. Cosmochim. Acta, 245, 577-596, 2019. [9] Le Corre L. et al., LPS XLV, Abstract #1311, 2014. [10] Irving A. J. et al., 74th Annual Meteoritical Society Meeting, Ab-stract#5231, 2011. [11] Fernandes V. A. et al., LPS XLIV, Abstract #1956, 2013. [12] Jenniskens P. et al., Nature, 458, 485-488, 2009.

Table 1. Bulk C and S abundances of meteorites in this study.

Sample	Type	Weight [mg]	C [wt%]	S [wt%]
Carbonaceous				
Murchison	CM2	275.6	2.043	2.4266
Aguas Zarcas	CM2	257.2	1.584	2.726
Allende	CV3	365.6	0.501	0.6521
NWA 2086	CV3	245.2	0.368	0.2806
NWA 3133	CV7	258.5	0.149	2.0104
NWA 5515	CK4	389.1	0.325	0.0545
NWA 765	CK4/5	236.8	0.119	1.6442
NWA 6704	CR achondrite	376.4	0.010	0.006
Almahata Sitta	Ureilite	175.0	4.896	0.2354
Dhofar 1170	Ureilite	121.4	3.582	0.9796

Table 2. Bulk C and S abundances of meteorites in previous studies [5, 7]. Data from [5] are colored in gray.

Sample	Type	C [wt%]	S [wt%]
Antarctic	CM2	1.324 (ALHA 77306), 1.514 (Y-74662)	3.490 (Y-74662), 3.863 (ALHA 77306)
non-Antarctic, Falls	CM2	2.16 (Nogoya) - 4.05 (Mighei)	2.80 - 5.44
		2.70 (Murchison)	not available
non-Antarctic, Finds	CM2	2.62 (Kivesvaara)	not available
non-Antarctic, Falls	CV3	0.27 (Allende) - 1.50 (Grosnaja)	not available
non-Antarctic, Finds	CV3	1.14 (Leoville)	not available
Antarctic	CK4	0.061 (Y-693)	1.604 (Y-693)
non-Antarctic, Falls	CK4	0.07 (Karoonda)	1.31 - 2.14
non-Antarctic, Finds	CK4	0.28 (Maralinga)	not available
Antarctic	Ureilite	3.022 (Y-74659)	0.518 (Y-74659)
non-Antarctic	Ureilite	2.07 - 4.10	0.179 - 0.58

LON 94101 Provides a Unique Record of C-Class Asteroid Regolith Diversity

Michael Zolensky[1], Loan Le[2], Matt Colbert[3], Jessie Maisano[3], Moe Matsuoka[4,5], Roger Harrington[2], Kent Ross[2,6].
[1]ARES, NASA Johnson Space Center, Houston, TX USA; [2]Jacobs Technology JETS, JSC, Houston, TX USA; [3]University of Texas High-Resolution X-ray CT Facility, University of Texas, Austin, TX USA; [4]National Institute of Advanced Industrial Science and Technology, Tsukuba, Japan; [5]Tohoku University, Sendai, Japan; [6]Univ. of Texas at El Paso, El Paso TX USA

Introduction: LON 94101 and its pairing mate LON 94102 are two of the largest CM finds, with a collective mass of 3.8kg. Over the years we noticed that every section of these meteorites appeared significantly different. These stones are highly brecciated and display an unprecedented range of CM lithologies [1-3, and numerous other papers]. They thus record direct information regarding the physical and petrologic characteristics of the CM parent asteroid(s) at the greatest scale observable from meteorites. Still unanswered questions are what the typical clast size was for each lithology, and what the full range of CM textures in LON 94101 could be. We were also interested in learning whether there were xenoliths in these breccias, these being apparently unknown for CM chondrites. Detailed characterization of an especially large sample is required to address these issues. This abstract reports results of the initial characterization of one large sample of LON 94101.

X-Ray Computed Tomography: We obtained a single 42g mass of LON 94101 from the Meteorite Working Group. LON 94101,4 is a relatively unweathered sample, simplifying measurements. The allocated stone measured 7 cm across in maximum dimension. In order to predetermine where to properly explore the stone we performed X-Ray Computed Tomography (XRCT) at the University of Texas High-Resolution X-ray CT Facility. We used the NSI scanner with a fine focus source, high power, 150kV, 0.25mA, no filter, Perkin Elmer detector. The beam-hardening correction = 0.25. Voxel size = 0.0352 mm. Total slices = 1846. Figure 1 shows a sample of the XRCT results.

XRCT imaging revealed over 20 distinct lithologies in the 42g stone, with individual lithologic clasts up to 2 cm each, and abundant, fine-grained, comminuted matrix powder between each clast. Inspection of the XRCT "slices" revealed the optimal place to slice through the stone, in order to maximize the variety of exposed materials (Figure 2). The stone was vacuum impregnated into a single block of epoxy and sawed slowly using no fluids to prevent compromising possible aqueous fluid inclusions. Figure 1 shows the plane where the stone was sliced.

Petrography, Spectroscopy and other Investigations: The two facing halves have now traveled different paths. One half (A) is described briefly here. The other half (B) was transferred to collaborators at the Open University (Ross Findlay, Ian Franchi, Richard Greenwood) where it has been undergoing petrographic and isotopic analysis, lithology by lithology. These latter investigations will be reported separately.

Slice A was polished (dry) and examined in a JEOL 7600 FEG SEM. It was in fact the largest sample ever examined in that instrument at JSC. We collected a BSE map, shown as Figure 3, and made petrographic investigations by EDS. Future electron microprobe measurements work will obviously require considerable subsampling. We transferred the still-intact sample to the Department of Earth Sciences, Tohoku University, for reflectance IR measurements of separate lithologies, using a Thermo Scientific Nicolet iN10 Fourier Transform Infrared Spectrometer. These results will be reported at the Symposium. Slice A reveals at least 18 distinct lithologies, ranging from CM2 to CM1, including C1 material lacking coarse-grained objects (i.e. no chondrules or chondrule pseudomorphs, etc.). These materials will be briefly described at the symposium.

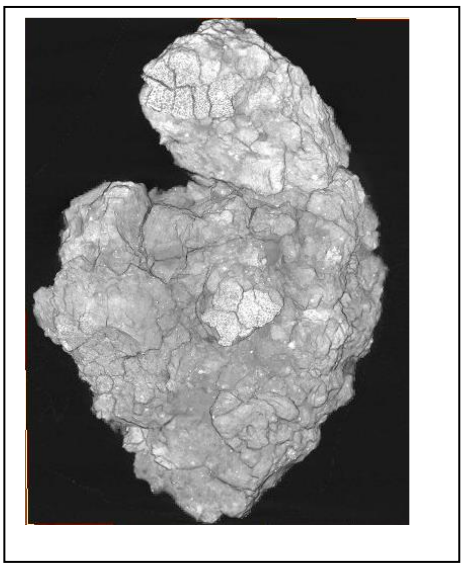

Figure 1 (left) Composite of XRCT imaging slices of LON 94101,4.
Figure 2 (right) Black plane indicates position of slice that bisected the sample into halves A and B.

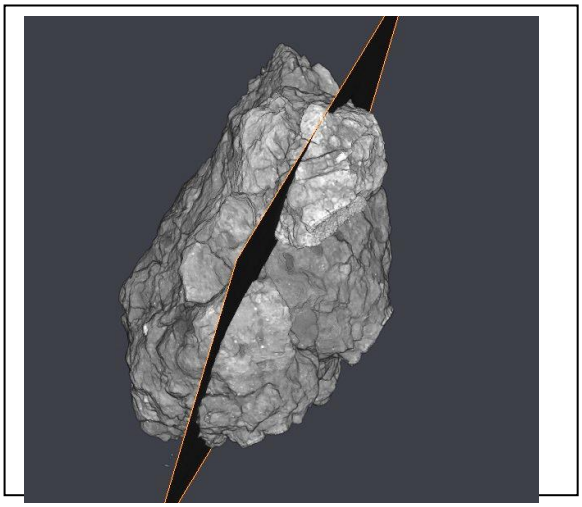

Conclusions: The work on this sample is still in progress but will reveal important details of CM C-class asteroid regolith properties to complement similar information from asteroid Bennu samples to be returned by the OSIRIS-REx spacecraft in 1 year. This work is only possible due to the deliberate collection and careful curation of meteorites from Antarctica.

Acknowledgements: We thank Prof. Michihiko Nakamura and Dr. Satoshi Okumura for assistance with the FTIR measurements, and the Meteorite Working Group for LON 94101,4. The NASA Cosmochemistry and Emerging Worlds Programs supported MZ.

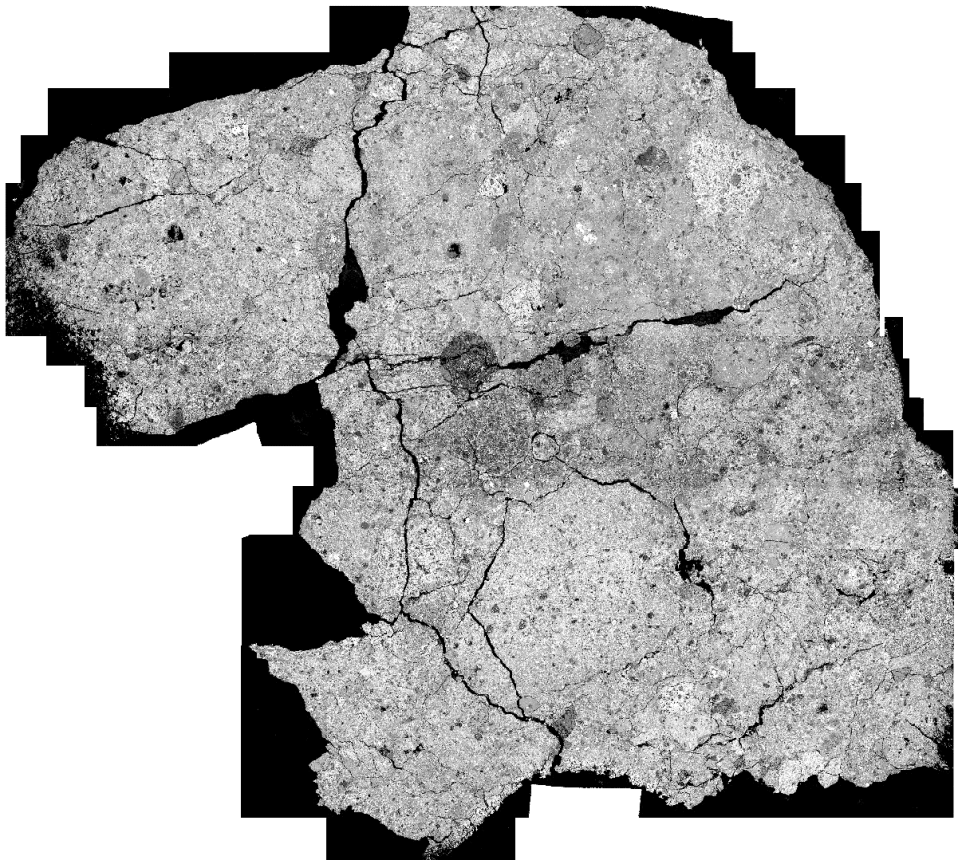

Figure 3. Backscattered Electron image of the face of slice A. Sample measures 7 cm across, diagonally.

References: [1] Lindgren et al. (2013) *MAPS* 48, 1-17**;** [2] Lentfort et al (2021) *MAPS* 56, 127-147; [3] Zolensky et al. (2021) *MAPS* 56, 49-55**.**

Mineralogical and petrological study of Aguas Zarcas CM2 chondrite

Kenei Ogiya[1], Toru Matsumoto[2], Akira Miyake[2] and Takashi Mikouchi[1]
[1]*University of Tokyo*
[2]*Kyoto University*

Introduction

Aguas Zarcas is a carbonaceous chondrite fell in Costa Rica on April 23, 2019. According to initial studies reported in the Meteoritical Bulletin, Aguas Zarcas is a brecciated CM2 chondrite. Another previous research showed that the meteorite was composed of several different lithologies, including unique metal-rich lithologies which are uncommon in CM chondrites, and they suggested that the Aguas Zarcas parent body was formed by impact with the CR chondrite parent body (Kerraouch et al., 2021). Kerraouch et al. (2021) describes such a metal-rich lithology called "Met-1" in detail, however, does not describe other lithologies, such as C1 lithology, in detail. Therefore, in this study, we performed detailed observation and analysis of the various lithologies in Aguas Zarcas and discussed further lithologic diversity of this meteorite.

Sample and analytical techniques

We prepared a dry-polished thick section (7 mm x 11 mm) from the Aguas Zarcas sample (10.32 g). It was first observed by optical microscopy in order to measure chondrule sizes. The average particle size, which is the average of the major and minor axes, was used as the size of the chondrule. The area and the length of the chondrules were measured on the image taken with optical microscopy using the ImageJ software. After using optical microscopy, observation by FE-SEM (JEOL JSM-7001F, Kyoto Univ.) and chemical composition analysis of the minerals by EDS attached to it were performed.

Results and discussion

The sample used in this study was found to contain four different lithologies, Clast-1 to -4, including lithologies that are not described either in the initial analysis or in Kerraouch et al. (2021) (Figure. 1). (1) Clast-1 lithology is a CM lithology, similar to the "Primary Accretionary Rocks" described by Metzler et al. (1992), which seemed to be a lithology that has not experienced brecciation (Figure. 1c). The petrologic subtype of this lithology was estimated to be 2.2 using the classification suggested by Lentfort et al. (2021) (Figure. 2). (2) Clast-2 lithology is a brecciated CM clast (Figure. 1c). (3) Clast-3 lithology is a metal-rich clast with a subtype of 2.2-2.8 and is considered to be a CM clast experienced relatively low degree of aqueous alteration (Figure. 1b). (4) Clast-4 lithology is also a metal-rich clast, but it is distinguished from Clast-3 by the almost complete absence of tochilinite-cronstedtite intergrowths (TCIs) (Figure. 1d). This may be similar to the most primitive CM lithology, which has experienced only a limited degree of aqueous alteration, as well as Asuka (A)12085, A12169, and A12236 described by Kimura et al. (2020).

Conclusion

Clast-1 is not described in Kerraouch et al. (2021), and this study shows that Aguas Zarcas contains a lithology that is previously unknown. Moreover, the CR chondrite-derived metal-rich lithologies described in the previous study and the Clast-3 and Clast-4 in this study have similar petrological and mineralogical characteristics. However, this study indicates that Clast-3 and Clast-4 may have experienced only a limited degree of aqueous alteration on the CM chondrite parent body, which has not been considered in previous studies. These results suggest that the Aguas Zarcas parent body contains a greater variety of lithologies showing different degrees of aqueous alteration than previously thought.

References

The Meteoritical Bulletin Database. https://www.lpi.usra.edu/meteor/metbull.php.

Kerraouch, I et al., The Polymict Carbonaceous Breccia Aguas Zarcas: A Potential Analog to Samples Being Returned by the OSIRIS-REx and Hayabusa2 Missions, Meteoritics & Planetary Science, 56(2), 277-310, 2021.

Metzler, K et al., Accretionary dust mantles in CM chondrites: Evidence for solar nebula processes, Geochimica et Cosmochimica Acta, 56. 2873-2897, 1992.

Lentfort, S et al., Classification of CM chondrite breccias—Implications for the evaluation of samples from the OSIRIS-REx and Hayabusa2 missions, Meteorics & Planetary Science, 56(1), 127-147, 2021.

Kimura, M. et al., The most primitive CM chondrites, Asuka 12085, 12169, and 12236, of subtypes 3.0–2.8: Their characteristic features and classification, Polar Science, 26, 100565, 2020.

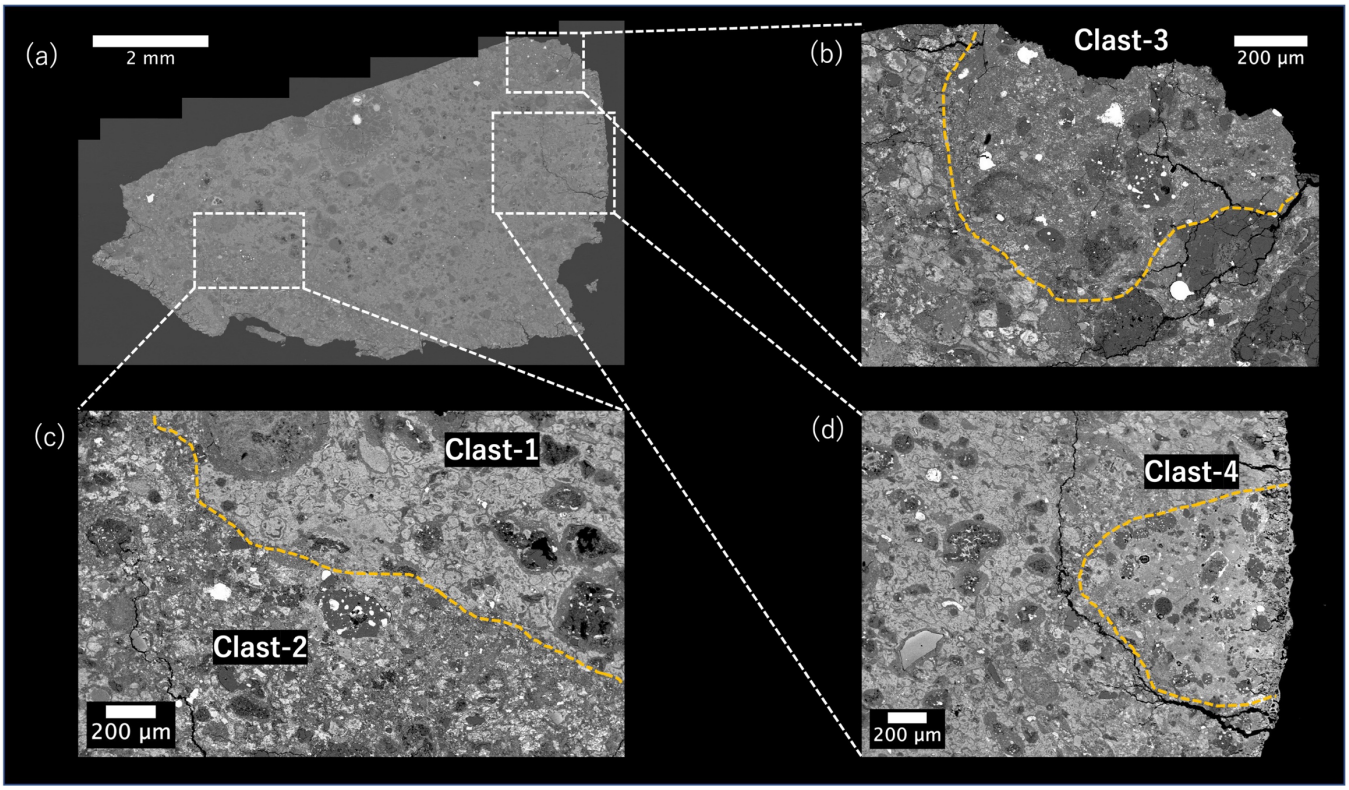

Figure. 1 Back-scattered electron (BSE) images of the Aguas Zarcas polished section studied, showing the presence of multiple lithologies. (a) Overall BSE image of the Aguas Zarcas sample. (b) Higher magnification BSE image, with the area surrounded by the dotted line indicating Clast-3 lithology. (c) Higher magnification BSE image, with the dotted line indicating the boundary between Clast-1 and Clast-2 lithologies. (d) Higher magnification BSE image, with the area surrounded by the dotted line indicating Clast-4 lithology.

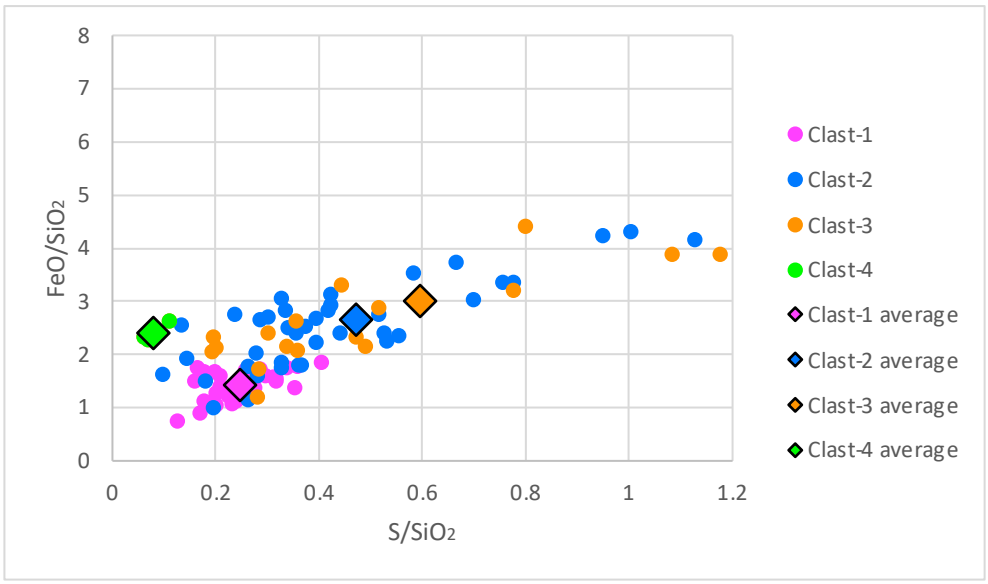

Figure 2. "FeO"/SiO_2 versus S/SiO_2 ratio for TCIs in each different lithology of the Aguas Zarcas sample analyzed in this study. Using the classification suggested by Lentfort et al. (2021), petrologic subtypes were determined from the ratios of "FeO"/SiO_2 for each lithology.

Anhydrous phases preserved in CI chondrites

T. Ando[1], T. Noguchi[1], A. Yamaguchi[2], and S. Itoh[1]
[1]*Kyoto Univ.*, [2]*NIPR*

Introduction: CI chondrites are considered to be the most chemically primitive rocks in the Solar System, because their bulk composition (except for volatiles) is similar to that of the solar photosphere [e.g. 1]. Ryugu is also known to be an asteroid composed of materials very similar to CI chondrites [e.g. 2-6]. The nature and origin of the precursor materials of the CI chondrites are however poorly understood because CI chondrites experienced pervasive aqueous alteration, as attested by their abundant secondary phases (i.e., phyllosilicates, magnetite, and carbonates) [e.g. 7]. Isolated anhydrous silicates, chondrules, and CAIs are rare in CI chondrites and Ryugu [6-12]. These phases and objects are a part of the precursors of CI chondrites and retain direct information about the material accreted on the CI parent body(ies). However, there has been no comprehensive study of these minor anhydrous phases in CI chondrites. It is important to understand the formation history of CI chondrites in order to compare with that of the Ryugu samples in more detail. Here, we report in-depth petrographic and mineralogical descriptions of anhydrous phases that survived heavy aqueous alteration of CI parent body(ies).

Samples and methods: We studied polished sections of the CI chondrite Ivuna and Orgueil in reflected light using an optical microscope and by conventional and field-emission scanning electron microscopes (SEM) at Kyoto University. Quantitative analysis of the chemical compositions of the anhydrous phases and matrix phyllosilicates was performed at NIPR using an electron microprobe.

Results and discussion: Both Ivuna and Orgueil meteorites contain a lithology with a high concentration of anhydrous minor phases represented by olivine. Therefore, we call the lithology “olivine-rich lithology”. Because most areas of these meteorites contain few olivine crystals, we call them “major lithology”. Phyllosilicate-rich matrix of the olivine-rich lithology is enriched in Fe, Na and K compared to the major lithology. Mode of olivine (<50 μm across) in the olivine-rich lithology is about 2%. Their forsterite mol% ranges from 62.3 to 99.5. The FeO vs. MnO and FeO vs. Cr_2O_3 diagrams seem to show two different trends, which may suggest two different origins of olivine in the CI chondrites. Pyroxene (<15 μm across) is less abundant than olivine. They are low-Ca pyroxenes and their En mol% is >95 and their Wo mol% is <5.8 but the majority has <1.2. We identified the first well-preserved porphyritic olivine chondrule in Ivuna. The mesostasis of the chondrule has been replaced by abundant magnetite. P-bearing (up to 0.96 wt.%) Fe, Ni-metal (~10 μm) is included in the phenocrystic olivine, and Fe-phosphide is present on the surface of the chondrule. We also identified refractory oxide minerals such as spinel, perovskite, and hibonite, strongly suggesting a link to CAIs. One Fe, Cr-sulfide (S: 40.2 wt.%, Cr: 34.0 wt.%, Fe: 15.0 wt.%, Zn: 3.5 wt.%) was observed in Ivuna. The chemical composition suggests that it is daubréelite or zolenskyite. These minerals are found in enstatite chondrites and form in highly reducing environments. Some pyrrhotite and pentlandite rarely contain Ir-Os-Pt alloys up to about 200 nm. Based on their chemical composition, their formation temperatures range from ~1900 to ~1600 K. Although CI chondrites are generally thought to have accreted in areas far from the sun [13], our results clearly show that materials formed in extremely high-temperature and/or very reducing environments also incorporated in CI chondrite parent body(ies).

References: [1] Anders, E. and Grevesse, N. (1989) Geochim. Cosmochim. Acta 53, 197-214. [2] Yada, T. et al. (2022) Nat. Astronom. 6, 214-220. [3] Yokoyama, T. et al. (2022) Science 10.1126/science.abn7850. [4] Nakamura, E. et al. (2022) Proc. Japan Acad. Ser. B, 98, 227-282. [5] Ito, M. et al. (2022) Nat. Astronom. [6] Nakamura, T. et al. (2022) Science 10.1126/science.abn8671. [7] Tomeoka, K. and Buseck, P. R. (1988) Geochim. Cosmochim. Acta 52, 1627-1640. [8] Frank, D. et al. (2014) Geochim. Cosmochim. Acta 142, 240-259. [9] Morin et al. (2022) Geochim. Cosmochim. Acta. 2022.06.17 [10] Liu, M.-C. et al. (2022) Nat. Astronom. [11]Frank, D. et al. (2011) 42nd LPSC #2785. [12]Nakashima, D. et al. (2022) Nat. Portfolio. [13]Desch, S. et al. (2018) The Astrophysical Journal Supplement Series, 238(1), 11.

Mineralogical investigation of olivine grains in CI chondrites Ivuna and Orgueil

T. Mikouchi[1], H. Yoshida[1], M. Masuda[1], M. E. Zolensky[2] and T. Nakamura[3]
[1]*University of Tokyo, Tokyo 113-0033, Japan (mikouchi@um.u-tokyo.ac.jp),* [2]*NASA Johnson Space Center, TX 77058, USA,*
[3]*Tohoku University, Sendai 980-8578, Japan*

Introduction: CI chondrites preserve the primitive chemical composition matching with the solar photosphere and thus provide important information about the evolution and dynamics of the protoplanetary disk in the early solar system. Recently, analysis of asteroid Ryugu samples returned by JAXA's Hayabusa2 spacecraft has revealed that they were nearly identical to CI chondrites in chemistry and mineralogy [e.g., 1-3], further strengthening the importance of these primitive solar system materials. Because all of these materials suffered extensive aqueous alteration in their parent body(s), there remains little anhydrous minerals that escaped such alterations. Olivine is one of such minerals, but its abundances in CI chondrites and Ryugu samples are both much less than 1 vol.%. Also, olivine grains with reasonably large size (>10 μm) suitable for oxygen isotope analysis to constrain their origins are limited because most olivine grains in these samples are usually smaller than 5 μm [e.g., 1-7]. Therefore, the origin of such small olivine grains in Ryugu samples and CI chondrites is uncertain. Since we have been successful to detect numerous small olivine grains in Ryugu samples [3,7], we applied the same technique to perform extensive search for olivine grains in CI chondrites (Ivuna and Orgueil) to compare with olivine mineralogy of Ryugu samples and to discuss their possible common origins.

Samples and Methods: In order to mimic the size of Ryugu samples analyzed [3], we prepared polished sections of 1-3 mm fragments of Ivuna and Orgueil and analyzed them using JEOL JXA-8530F FE-EPMA at Univ. of Tokyo. After olivine grains were found using Mg X-ray mapping, the quantitative analysis was performed at 12 kV accelerating voltage with 30 nA beam current (counting times at peaks: 30 sec). This analytical condition allowed us to obtain accurate mineral compositions even from ~1 μm olivine grain both for major and minor elements [7].

Results: As reported in previous studies [e.g., 8,9], both Ivuna and Orgueil exhibit obvious brecciated textures on mm to μm scale. Mg X-ray maps show heterogeneous distributions of olivine grains whose size is up to 50 μm and overall abundance is <<1 vol.%. Olivine is present only in brecciated clasts that show relatively weak degrees of aqueous alteration as we saw in Ryugu samples [3,10]. Phyllosilicates in such "less altered" clasts are slightly more Fe-rich compared to those in altered clasts. These less altered clasts contain Ca carbonates although they are absent in altered clasts. This observation is identical to Ryugu samples as the modeling calculation of progressive aqueous alteration of chondritic anhydrous minerals predicts that only Ca carbonates form when the water to rock ratio is low, resulting in less aqueous alteration [3,10]. Similarly we found a hydrous Mg,Na phosphate grain in Ivuna only in the less altered clast that is also found in Ryugu samples [3,11]. There are numerous tiny olivine grains more abundantly in Ivuna compared to Orgueil (Fig. 1). Accordingly, the abundance of olivine in Ivuna appears slightly higher than that of Orgueil, which is consistent with the previous study [e.g., 9]. Because CAI is only found in Ivuna among CI chondrites [12], it is also consistent with the presence of more abundant "less altered" clasts in Ivuna compared to Orgueil. The olivine compositions of Orgueil and Ivuna are nearly identical. The most Fe-rich olivine in the polished sections studied is Fo_{67}, but >90% grains are clustered at Fo_{99}. There is rare presence of LIME olivine whose MnO contents reach up to 2.2 wt% (Fig. 2). The CaO content is usually less than 0.1 wt%, while Cr_2O_3 has a wide range of 0-0.6 wt%. The Mn-Cr plot shows that there are two distinct compositional trends as seen in Ryugu samples [7] (Fig. 3). We tried to find a relationship between the morphology of olivine grains and their mineral compositions to consider their origins. However, most olivine grains are present as isolated small single crystals (always rimmed by submicron Fe-rich rims), and we could not find a clear relationship. Nevertheless, there are rare grains showing a characteristic mineralogy. For example, there is an aggregate of small olivine grains that have high Mn contents, suggestive of the LIME origin (Fig. 2). Another example is a composite grain of olivine and low-Ca pyroxene (Fig. 4). Combining the texture and high Cr content of olivine, this grain would be a fragment of chondrule.

Discussion and Conclusion: By applying the same analytical method which we employed for the analysis of Ryugu samples [3,5], we found small (<5 μm) olivine grains in CI chondrites Orgueil and Ivuna that have identical mineralogy to Ryugu olivines. Interestingly, we found two compositional trends in minor element contents, especially in Mn-Cr systematics (Fig. 3). It is hard to discuss their origins only from olivine textures because of very limited number of olivine grains showing characteristic morphology, but their distinct compositions provide some hint. The relatively Mn-rich and Cr-poor trend would be origins from amoeboid olivine aggregates (AOA). In fact LIME olivine grains are plotted along this trend, which is common in AOA olivines [e.g., 13]. In contrast, the other trend is relatively Cr-rich and Mn-poor and we interpret that such compositions are suggestive of the chondrule origin. The composite grain of olivine and low-Ca pyroxene (Fig. 4) is plotted on

this trend, and such mineralogy is common in chondrules. Similar observation has been known for Ryugu samples, further supporting their close genetic relationship [e.g., 1-3]. It seems that the abundance of AOA-like olivine is higher compared to chondrule-like olivine (Fig. 3) and the similar distinct population is found in Ryugu olivine [7]. Because the formation of the original Ryugu parent body is considered to have been considerably early (~2 Ma after CAI) [3], it would be natural to contain more AOA-like olivine grains than chondrule grains. However, it is closely related to dynamical transportation events of small components happened in the early solar system, and thus more accurate proportional estimate of AOA/chondrule populations will help better understanding such events.

References: [1] Yokoyama T. et al. (2022) Science 10.1126/science.abn7850. [2] Ito M. et al. (2022) Nature Astronomy, 10.1038/s41550-022-01745-5. [3] Nakamura T. et al. (2022) Science 10.1126/science.abn8671. [4] Liu M.-C. et al. (2022) Nature Astronomy, 10.1038/s41550-022-01762-4. [5] Piralla M. et al. (2020) Geochim. Cosmochim. Acta, 269, 451-464. [6] Morin G. L. F. et al. (2022) Geochim. Cosmochim. Acta, 332, 203-219. [7] Mikouchi T. et al. (2022) 85th Annual Meeting of The Meteoritical Society, #6180. [8] Morlok A. et al. (2006) Geochim. Cosmochim. Acta, 70, 5371-5394. [9] Alfing J. et al. (2019) Geochemistry, 79, 125532. [10] Mikouchi T. et al. (2022) Hayabusa Symposium 2022. [11] Ma C. et al. (2022) 85th Annual Meeting of The Meteoritical Society, #6134. [12] Frank D. et al. (2022) Meteoritics and Planet. Sci. (submitted). [13] Komatsu M. et al. (2015) Meteoritics and Planet. Sci., 50, 1271-1294.

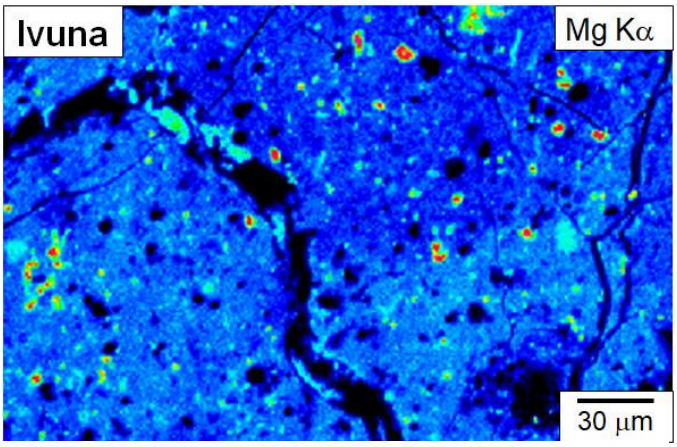

Fig. 1. Mg X-ray map of Ivuna CI chondrite. This clast contains numerous olivine grains smaller than 10 μm (shown in red~bright blue spots in the phyllosilicate (dark blue) matrix).

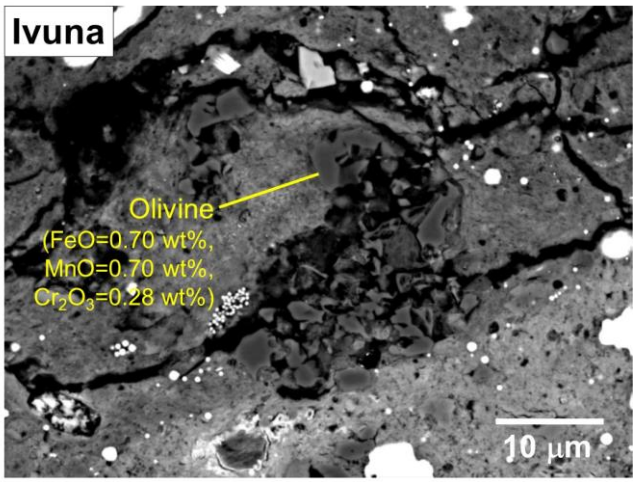

Fig. 2. Back-scattered electron (BSE) image of olivine in Ivuna. There is an aggregate of olivine grains in the center of the image. Most of these olivine grains have high Mn content (~0.7 wt%) similar to LIME olivine.

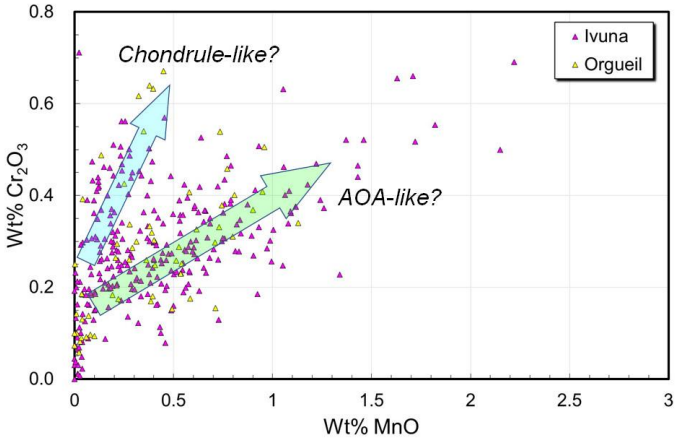

Fig. 3. Mn-Cr systematics of olivine in CI chondrites Ivuna and Orgueil. There are two compositional trends as found in Ryugu olivine [7], suggesting origins of either chondrule or AOA.

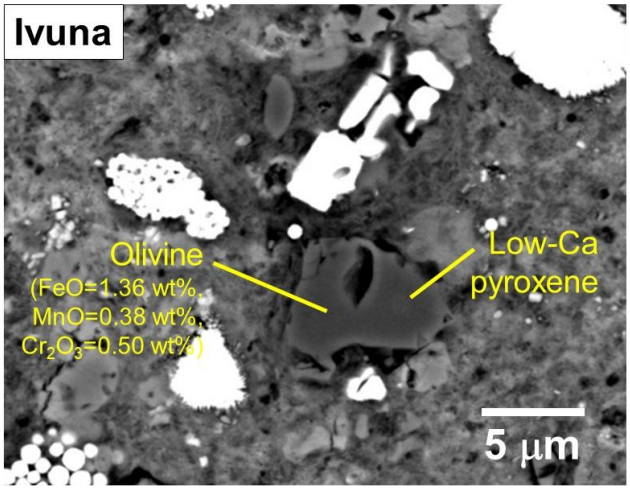

Fig. 4. BSE image of olivine in Ivuna. The olivine grain near the center of the image has a high Cr content. A small low-Ca pyroxene crystal is accompanied.

Na-rich phase in Ryugu particle: Evidence for metasomatic agent in the parent asteroid?

Akira Yamaguchi[1,16], Naotaka Tomioka[2], Motoo Ito[2], Makoto Kimura[1], Naoki Shirai[3,4], Richard C. Greenwood[5], Ming-Chang Liu[6,17], Kaitlyn A. McCain[6], Nozomi Matsuda[6], Masayuki Uesugi[7], Naoya Imae[1,16], Takuji Ohigashi[8,9], Kentaro Uesugi[7], Aiko Nakato[10], Kasumi Yogata[10], Hayato Yuzawa[8], Yu Kodama[11], Kaori Hirahara[12], Ikuya Sakurai[13], Ikuo Okada[13], Yuzuru Karouji[10], Satoru Nakazawa[10], Tatsuaki Okada[10], Takanao Saiki[10], Satoshi Tanaka[10], Fuyuto Terui[14], Makoto Yoshikawa[10], Akiko Miyazaki[10], Masahiro Nishimura[10], Toru Yada[10], Masanao Abe[10], Tomohiro Usui[10], Sei-ichiro Watanabe[15], Yuichi Tsuda[10,16]

[1]NIPR, [2]JAMSTEC, [3]Tokyo Metropolitan University, [4]Kanagawa University, [5]The Open University, [6]UCLA, [7]JASRI/SPring-8, [8]UVSOR Synchrotron Facility, Institute for Molecular Science, [9]KEK, [10]ISAS/JAXA, [11]Marine Works Japan, Ltd., [12]Osaka University, [13]Synchrotron Radiation Research Center, Nagoya University, [14]Kanagawa Institute of Technology, [15]Nagoya University, [16]SOKENDAI, [17]Lawrence Livermore National Laboratory

Introduction

Carbonaceous chondrites were derived from C-type asteroids. They represent remnants of primitive planetesimals that formed in the outer region of the early Solar System. These hydrated, organic-rich asteroids may have been responsible for the delivery of volatile components to the inner Solar System. Recent studies indicate that Ryugu particles are most similar to CI chondrites (e.g., Yokoyama et al. 2022; Ito et al. 2022). As a course of a consortium study by the Phase2 Kochi curation team, we found phases exceptionally rich in Na. Here, we discuss the origin of the Na-rich phases.

Analytical techniques

We found the Na-rich phases in a Ryugu particle, C0014. This particle was impregnated with epoxy resin, evacuated for ~30 min, and placed on a hot plate at ~50°C. All the procedures were done under purified nitrogen. The potted butt of the particle was polished by diamond lapping sheets (30-0.5 μm) without using any fluid under air. We minimized the exposure of this particle to air (<1 hour). We examined the polished section first using an FE-SEM (JEOL: JSM-7100F) equipped with an EDS (Oxford AZtec Energy) and then an EPMA (JEOL: JXA-8200) at NIPR. For crystallographic characterization, the section was processed using a FIB (FIB; Hitachi SMI-4050) at Kochi, JAMSTEC. The FIB section was examined by synchrotron X-ray diffraction at the beamline BL 20XU at SPring-8. The FIB section was further thinned by FIB and examined using a TEM (TEM; JEOL JEM-ARM200F) at Kochi, JAMSTEC.

Results and discussion

The polished section, C0014,1 (1.9 mm^2) is dominated by matrix and contains phyllosilicate clasts and various kinds of mineral grains. The section consists of phyllosilicates (85 vol%), magnetite (5 vol%), sulfide minerals (5 vol%), dolomite (3 vol%) and traces (<1 vol%) of pentlandite, cubanite, chromite, spinel, and apatite. The mineral mode and compositions are similar to that of the other particles we studied (Ito et al. 2022).

Na-rich phases occur as a Na-rich clast (Mg3) (41x32 μm) (Fig. 1) and tiny (<a few μm) Na-rich spots in the matrix. The Na-rich clast (Mg3) is subrounded and shows a feathery texture, similar to the low-Na phyllosilicates. This phyllosilicate clast (Mg3) is rich in Na_2O (~10-36 wt%) with the highest Na-spot (Na_2O 36.2 wt%) near the center. FE-SEM observations indicate that all the Mg3 clast we examined appear to be composed of phyllosilicate. Note that all phyllosilicate clasts in C0004 and other particles we examined contain less than 2 wt% Na_2O.

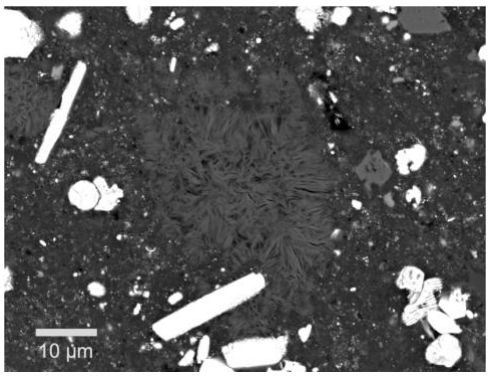

Fig. 1. BSE image of Na-rich clast (Mg3).

After detailed observations using an FE-SEM, we extracted a thick section from the Mg3 clast using a FIB and performed synchrotron X-ray diffraction (SXRD). A diffraction pattern from the section shows a reflection with d-spacing of 1.24 nm. The value is close to the basal layer spacing of saponite in the ambient condition. After the SXRD measurements, the FIB section was further processed into an ultrathin film, and TEM analyses were performed. The Na-rich clasts consist of interlayers with spacings of 0.7 nm and ~1.0 nm. The former likely corresponds to serpentine, and the latter corresponds to a saponite-like phase in which the interlayers have shrunk in the vacuum conditions in the TEM. The Na-rich spots observed in SEM could not be identified even under TEM.

Phyllosilicates that contain Na_2O>several wt% have been rarely found in chondritic meteorites. Ikeda (1991) and Kimura and Ikeda (1992) found Na-rich phyllosilicates ("sodian talc-rich clasts") in "CY" chondrites, Y-82162 and B-7904. However, Na_2O contents of these phyllosilicates are ~5-6 wt%, much lower than those of the Na-rich clast in C0014. Na-carbonate is suggested to occur on a C-type asteroid Ceres (De Sanctis et al. 2016). However, the presence of Na-carbonate is unlikely because we did not detect carbon by EDS. One may consider the presence of tiny non-silicate phases in the Mg3 phyllosilicate which are extremely rich in Na. Zolensky et al. (1999) found halite (NaCl) in the Monahans H chondrite. The lack of Cl (<0.02 wt%) rules out the presence of halite. Thus, the Na-rich phase is something hard to be identified by our analytical techniques and/or is extremely susceptible to short exposure to air. Among several candidates of metasomatic agents which were proposed on the basis of thermodynamic calculations (Zokotov 2012), we suggest that the Na-rich phases are sodium hydroxide (NaOH). NaOH is a deliquescent material and is easily decomposed during short exposure to the atmosphere. Although the origin of NaOH is unknown yet, we suggest that Na-rich fluid was introduced at the early stage of the evolution of the precursor body of Ryugu.

References

De Sanctis M.C. et al. (2016) Nature 536 https://doi:10.1038/nature18290
Ikeda Y. (1991) Proc. NIPR Symp. Antarct. Meteorites 4, 187-225
Ito M. et al. (2022) Nat. Astron. https://doi.org/10.1038/s41550-022-01745-5
Kimura M. and Ikeda Y. (1992) Proc. NIPR Symp. Antarct. Meteorites 5, 74-119
Yokoyama T. et al. (2022) Science. https://doi.org/10.1126/science.abn7
Zolensky M.K. Science 285, 1377-1379
Zolotov M.Y. (2012) Icarus 220, 713–729. http://dx.doi.org/10.1016/j.icarus.2012.05.036

An artificial laboratory alteration of the Ryugu samples: Comparison with the Orgueil CI chondrite and implication to the long durational sample storage

Naoya Imae[1,2], Naotaka Tomioka[3], Motoo Ito[3], Akira Yamaguchi[1,2], Makoto Kimura[1], Masayuki Uesugi[4], Naoki Shirai[5,13], Takuji Ohigashi[6,14], Ming-Chang Liu[7,15], Richard C. Greenwood[8], Kentaro Uesugi[4], Aiko Nakato[9], Kasumi Yogata[9], Hayato Yuzawa[6], Yu Kodama[10,*], Masahiro Yasutake[4], Kaori Hirahara[11], Akihisa Takeuchi[4], Ikuya Sakurai[12], Ikuo Okada[12], Yuzuru Karouji[9], Toru Yada[9], Masanao Abe[9], and Tomohiro Usui[9]

[1]NIPR, [2]SOKENDAI, [3]JAMSTEC, [4]JASRI/SPring-8, [5]TMU, [6]IMS, [7]UCLA, [8]The Open University, [9]ISAS, JAXA, [10]Marine Works Japan, Ltd., [*]Toyo Corp., [11]Osaka University, [12]Nagoya University, [13]Kanagawa University, [14]KEK, [15]Lawrence Livermore National Laboratory

Introduction: It has been revealed that the returned sample from the C-type asteroid Ryugu by Hayabusa2 corresponds to the CI chondrites (e.g., Ito et al., 2022; Nakamura T. et al., 2022). These grains have escaped from the Earth's atmospheric reaction at most, and the handling of the Ryugu particles in Phase 1 (Ph1) at JAXA and Phase 2 Kochi (Ph2K) curation was carried out in the glove boxes for Ryugu particles in purified nitrogen gas or vacuum under the condition of nearly entirely unexposed for terrestrial air. Initial investigation by the Ph2K team has focused on the unexposed air for the handling, sample transportation and analyses (Ito et al., 2022; Liu et al., 2022; Greenwood et al., 2022) avoiding potential affect to analytical results.

CIs have been known only in five worldwide *falls* and have not been recovered as *finds* at all. It has been recently reported that it occurs only from one micrometeorite (Dobrica et al., 2022). The limited numbers of CI meteorites and CI-like micrometeorites may be responsible to their susceptible nature on the Earth. The Orgueil CI chondrite can be more susceptible to terrestrial weathering than those of the other meteorites, and a significant amount of gypsum has rapidly formed after the fall (Gounelle and Zolensky, 2001).

In the present study, we examined the effects of the interaction of small Ryugu particles less than 0.5 mm with terrestrial air, that is, an artificial laboratory alteration under a controlled environment of humidity and temperature. We compared the results with that of the Orgueil CI chondrite as well as the Ryugu particles before laboratory alteration. The terrestrial alteration behavior of Ryugu particles is important for a clarification toward a direct linkage with Orgueil. It is also important for considering the long durational storage of the extraterrestrial materials, primarily reactive extraterrestrial materials on the Earth, such as the CI chondrites.

Experimental conditions: C0087 (~1 mg powder) and A0029 plus A0037 (~1 mg powder) were stored in a valve-opened desiccator in an air-conditioned laboratory room at NIPR and in a vacuumed desiccator by a diaphragm rotary pump at the Antarctic meteorite storage room, respectively, for more than five months after the initial X-ray diffraction measurements using Cu Kα (XRD; Rigaku SmartLab) (Ito et al. 2022). C0087 in a valve-opened desiccator was kept under the conditions of typical temperatures of 21–24 ºC and humidity of ~30% in January to February and 26–29ºC and 55–40% in March to June. A0029 plus A0037 in a vacuum desiccator was kept under the conditions of 22 ºC and ~50% (or less). XRD was used to find any detectable weathering products for these samples. XRD analytical conditions were described in Ito et al. (2022). We used a field emission scanning electron microscope (FE-SEM; JEOL JSM-7100F) with an energy dispersive X-ray spectrometer (EDS; Oxford AZtecEnergy X-Max^N 50) to search for micrometer-scale weathering products on their surface with the analytical conditions of 15 kV and ~1 nA with carbon coating. Grain surfaces of C0087 and A0029 plus A0037 for several grains (~0.1–0.3 mm in size) were placed on a carbon nanotube or a carbon adhesive tape. A polished section of C0087 grains was then observed.

Results: XRD: Main constituent mineral phases of the Ryugu grains are saponite, serpentine, magnetite, dolomite, and pyrrhotite (Ito et al., 2022). No significant changes were observed from initial XRD patterns, however, a very subtle peak appears at 2θ = ~12º (*d*-spacing of ~0.7 nm) (Fig. 1).

FE-SEM-EDS: Many tiny Ca-S oxides, 500 nm to 1 μm, have been identified on the peripheries of polished section of C0087 (Fig. 2) but not from A0029 plus A0037, since the EDS spectra of the grains commonly showed the peaks of calcium, sulfur, and oxygen. The observed Ca-S oxide occurs as isolate grains only on the grain surface (Fig. 2).

Discussion: A slightly increased peak at 2θ = ~12º from XRD may reflect the increased crystallinity of serpentine and/or saponite for C0087 and A0029 plus A0037 (Fig. 1). The presence of abundantly observed Ca-S oxide grains on the surface

for C0087 under the FE-SEM may suggest that it is an alteration product in the laboratory. The most plausible candidate for the Ca-S oxide phase could be gypsum. Further investigations (ultra-high magnification observations and their crystallography) of these phases by a transmission electron microscopy will be carried out. Nakamura T. et al. (2022) reported the small gypsum on calcite surface implying the alteration product on either Ryugu or the Earth. However, the occurrence quite differs from the present observation in C0087, which also suggest that the gypsum plausibly originated from the laboratory alteration. Sulfur-bearing species are mainly pyrrhotite in the Ryugu particles. Ca-bearing species are mainly dolomite, and a minor occurrence of apatite. Pyrrhotite and dolomite might have joined the terrestrial alteration as be observed from Orgueil. However, the alteration features from pyrrhotite and dolomite have not been clearly identified yet from Ryugu's artificial alteration products. The reaction mechanism to form gypsum on the grain surface is also not still clarified but could be due to fluid mobilizations of Ca and S ionswith H_2O derived from the air to form gypsum on the grain surface from the occurrence. On the other hand, Orgueil shows that finer grains and rims of euhedral coarser grains of pyrrhotites as well as dolomites have been altered, and significant gypsum has been observed on the surface of Orgueil (Fig. 2).

Summary: The degree of alterations of the Ryugu particles in the laboratory conditions was not severer than those of Orgueil (Fig. 2). This may be partly because of the limited periods and laboratory conditions for alteration.

Acknowledgements: The present study on the laboratory alteration of Ryugu was initially motivated in the Ph2K team via the discussion with Prof. A. Tsuchiyama in Ritsumeikan University and Chinese Academy of Sciences.

References: Dobrica E. et al. 2022. Geochimica et Cosmochimica Acta 317:286–305. Gounelle M. and Zolensky M. E. 2001. Meteoritics & Planetary Science 36, 1321–1329. Greenwood R. C. et al. 2022. Nature Astronomy (Accepted). Ito M. et al. 2020. Earth, Planets and Space 72, 133. https://doi.org/10.1186/s40623-020-01267-2. Ito M. et al. 2022. Nature Astronomy. https://doi.org/10.1038/s41550-022-01745-5. Liu M. -C. 2022. Nature Astronomy. https://doi.org/10.1038/s41550-022-01762-4. Nakamura T. et al. 2022. Science. 10.1126/science.abn8671. Uesugi M. et al. 2020. Review of Scientific Instruments 91, 035107. https://doi.org/10.1063/1.5122672.

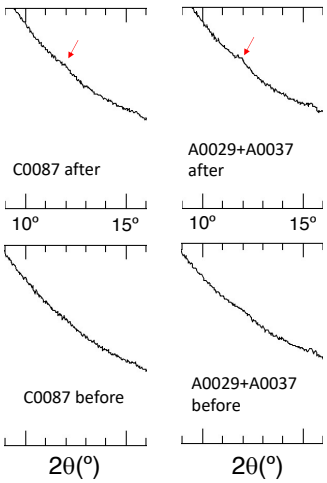

Figure 1. XRD pattern of 2θ = ~12°.

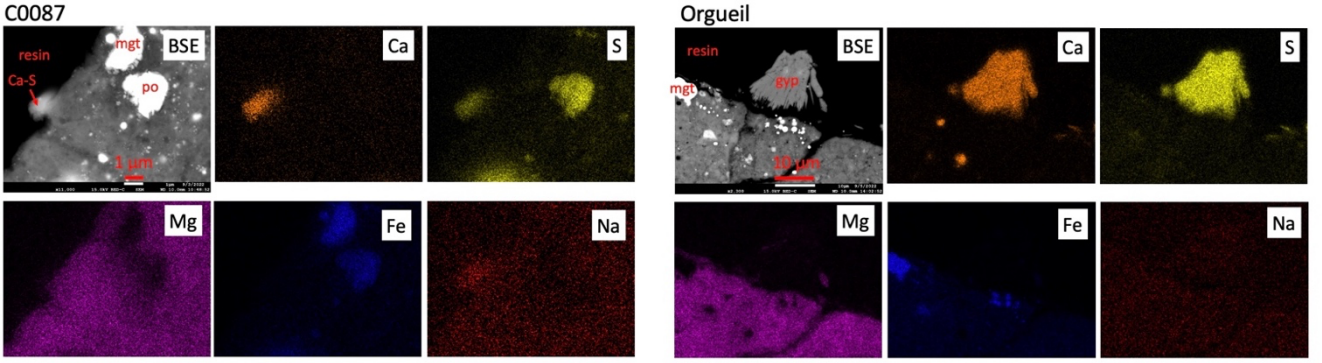

Figure 2. Back scattered electron (BSE) images and the elemental maps of Ca, S, Mg, Fe, and Na of a texture bearing the Ca-S oxide phase in C0087 and a texture bearing the gypsum in the Orgueil chondrite, which is shown as a red circle, respectively. Also note that minor Na is included for Ca-S oxide in C0087, but not for gypsum in Orgueil. mgt = magnetite. Ca-S = Ca-S oxide. po = pyrrhotite. gyp = gypsum. Gypsum in Orgueil was identified from μRaman and XRD.

New analytical tool for extraterrestrial material curation: A great advantage for an *in-situ* analysis and quick survey of organics

M. Ito[1], R. Kanemaru[2], J. Isa[3], A. Yamaguchi[4], M. Miyahara[5], T. Yada[2], Y. Niwa[6], A. Ishikawa[6], T. D. Yokoyama[7], H. Takahashi[7], M. Uesugi[8] and T. Usui[2].

[1]*JAMSTEC,* [2]*JAXA-ISAS,* [3]*Chiba Tech,* [4]*NIPR,* [5]*Hiroshima University,* [6]*TiTech,* [7]*JEOL Ltd.,* [8]*JASRI/SPring-8*

Introduction: Extraterrestrial organics in primitive meteorites, IDPs, returned samples from comets and asteroids (e.g., Brownlee et al., 2006; Yada et al., 2021) are one of the building blocks of the Solar System, and closely related with an origin of organics and life on Earth (e.g., Septon and Botta, 2005; Sandford et al., 2006). Now a day studies of organics in extraterrestrial materials are conducted by a combined and *in-situ* microanalysis such as NanoSIMS/SIMS for light element isotopes, STXM-XANES and AFM-IR for chemical functional groups, and TEM for textural observations (e.g., Garvie & Buseck, 2007; Floss et al., 2014; Kebukawa et al., 2019; Ito et al., 2022). Even a combined and *in-situ* microanalysis described above is a powerful tool to investigate nature of organics in extraterrestrial materials, analytical area is very limited of less than a few tens to few hundred μm in size. On the other hand, organics in primitive meteorites (i.e., carbonaceous chondrites) and returned samples from C-type asteroids contain a few weight percent of volume and are scattered all over a cm-mm sized sample with a μm scale.

A SXES (soft-X ray emission spectrometer) is a next generation analytical detector attached with SEM or EPMA system (Takahashi et al., 2016). Comparing with WDS (wavelength dispersive x-ray spectroscopy) detector, SXES can provides us (1) high spectral resolution (1.2 eV for FWHM of Zr Mζ) with energy ranges of 100 to 400 eV and 350 to 2300 eV, JS300N and JS2000 varied line spacing grating, respectively, allowing identify chemical shift (e.g., carbon functional group, Fe^{2+} and Fe^{3+}), (2) high detection sensitivity, (3) detection of multiple elements starting from lithium, and (4) low electron dose by both low accelerating voltage and beam current (Sakuda et al., 2010). The SXES-EPMA system could allow us to determine C and N abundances as well as phase identification and chemical bonding state (Takakura et al., 2022).

Here we present preliminary results of organics with different N/C and O/C ratios as standard materials, and C, N and O images of a C2-ung Tarda meteorite. We test the analytical capabilities of the SXES-EPMA system; (1) quick survey of organics in extraterrestrial materials, (2) an electron dose dependent, (3) analyzing a larger area (cm to mm in size), and (4) N/C and/or O/C ratios of organics for an initial characterization under a curation activity.

Experimental: We used the JEOL JXA-IHP200F FE-EPMA equipped with a SXES-ER detector (SS-94090EREP) at the JAXA curation with a defocused (50 μmϕ) and a focused beam of 10 nA and accelerating voltage of 5 keV for organic standards. BBOT [$C_{26}H_{26}N_2O_2S$], phenylalanine [$C_9H_{11}NO_2$], tryptophan [$C_{11}H_{12}N_2O_2$], Humic acid [C: 51, N:1.1, O:43], guanin [$C_5H_5N_5O$], thymine [$C_5H_6N_2O_2$] and cytosine [$C_4H_5N_3O$] were used for standard organic materials to optimize analytical conditions of spot and imaging analysis. Powdered organics are pressed into indium metal mount (1 cmϕ and 3 mm height), and then 20 nm of Au was coated on their surface.

Fig. 1 Typical SXES spectra of BBOT

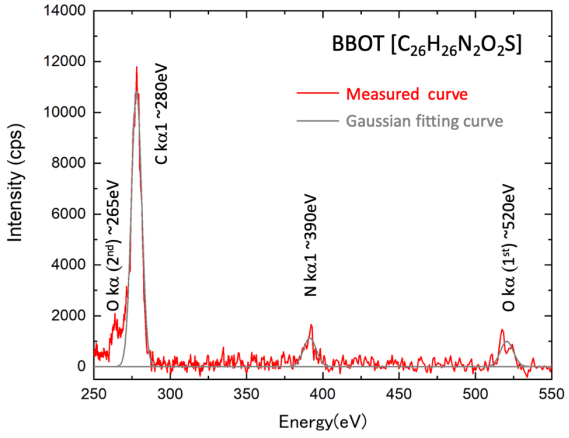

We prepared an epoxy-embedded polished thick section of Tarda (8 x 4 mm in size) with a 5 nm osmium coating on the surface. To acquire C, N and O elemental images of the Tarda, a 2 μm-focused electron beam of 30 nA with an accelerating voltage of 15 keV was used, irradiated over 64 × 48 μm^2 areas on the samples. Each analysis consisted of 3 scanned images of the same area, with individual images consisting of 80 × 60 pixels having a dwell time of 2 sec/pixel. The total acquisition time was approximately 12 hours (4 hours/1 scanned image) including dwell time and data fetching time from the detector to PC.

Results & Discussions: Figure 1 shows representative spectrum of BBOT ($C_{26}H_{26}N_2O_2S$) with N/C = 0.077 and O/C = 0.077. We observed clear peaks of $O_{k\alpha\,(2nd)}$ (~265 eV), $C_{k\alpha1}$ (~280 eV), $N_{k\alpha1}$ (~390 dpeV) and $O_{k\alpha\,(1st)}$ (~520 eV) with a spectral resolution of ~0.2 eV step. We, then, obtained the area of each peak by a Gaussian integral method. Figure 2 shows a calibration curve for N/C ratio (N/C ratio obtained by SXES analysis vs. N/C ratio of each standard). Note that we tried to obtain a calibration

curve for O/C ratio in organic standards with the same manner but no luck. Further investigation is neccesary to have a better calibration curves for O/C ratio in organics. We also plan to conduct phase identifications or chemical bond state of organics based on shapes of $C_{k\alpha 1}$ though analyses of known organics as a standard material with the SXES- EPMA system suggested by Takakura et al. (2022).

Fig. 2 Calibration curve for N/C ratio in organics

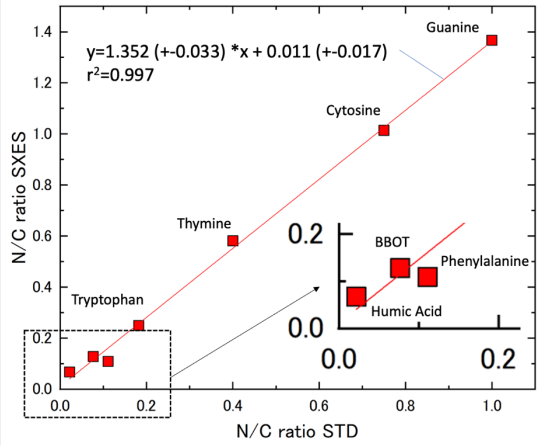

Tarda is classified as C2 ungroup meteorite that potentially derived from D-type asteroid (Marrocchi et al., 2021). Figure 3 shows images of epoxy-mounted Tarda; (a) $C_{k\alpha 1}$, (b) $N_{k\alpha 1}$, (c) $O_{k\alpha\ (1st)}$, (d) BSE, and (e) SXES spectra of N-rich organics, typical matrix and epoxy for comparison. We found micro-meter sized N-rich organics showing different characteristics in SXES spectra of the surrounding matrix and epoxy (Fig. 3e-1 to 3e-3; cf. spectra of epoxy was obtained by a broad beam-spot analysis mode). The SXES spectra of N-rich organics show different from that of epoxy and matrix (Fig. 3 e1-3). We observed that SXES spectrum shape changes and intensities are smaller with frames due to the electron irradiation damages during acquisition. We, therefore, used 1st frame dataset of C, N and O SXES images and spectrum extracted from these images. Although one can find a *region-of-interest* corresponding to organics by a combination of C, N and O images together with SXES spectra of the ROI, it is necessary to optimize analytical conditions of beam current, acquisition time, accelerating voltage to introduce less or not artificial chemical changes for organics.

Conclusions: This is "a first-attempt" for an *in-situ* investigations of organics in standards and Tarda carbonaceous chondrite utilizing the SXES-EPMA. It is, however, potentially useful for visualizing a spatially distributions of C and N, and N/C ratios of organics in extraterrestrial materials including returned samples from C-type asteroid Ryugu and Bennu. Newly installed EPMA/SEM with the JEOL SXES-EPMA system at JAXA curation will open a new window for better characterizations of extraterrestrial organics under a curation activity.

Acknowledgment: A technical support of SXES-EPMA operation by JEOL Ltd. (Mr. Domon) is highly appreciated.

References: Brownlee D. et al. (2006) *Science* 314, 1711–1716; Floss *et al.* (2014) *Geochim Cosmochim Acta* 139:1–25; Garvie & Buseck (2007) *Meteorit. Planet. Sci.* 42:2111–2117; Ito *et al.* (2022) *Nat. Astron.* 10.1038/s41550-022-01745-5; Kebukawa *et al.* (2019) *Scientific Reports* 9:3169; Marrocchi *et al.* (2021) *ApJL* 913:L9; Sakuda *et al.* (2016) *European Microscopy Congress 2016: Proc.*, 847–848; Sandford *et al.* (2006) *Science* 314:1720–1724; Sephton &Botta (2005) *Inter J Astrobiol* 4:269–276; Takahashi *et al.* (2016) *IOP Conf. Ser.: Mater. Sci. Eng.* 109:012017; Takakura *et al.* (2022) *Microsc. Microanal.* 28:1014; Yada, T. et al. (2021) *Nat. Astron.* 6, 214–220.

Fig. 3 SXES elemental and BSE images and spectra of Tarda

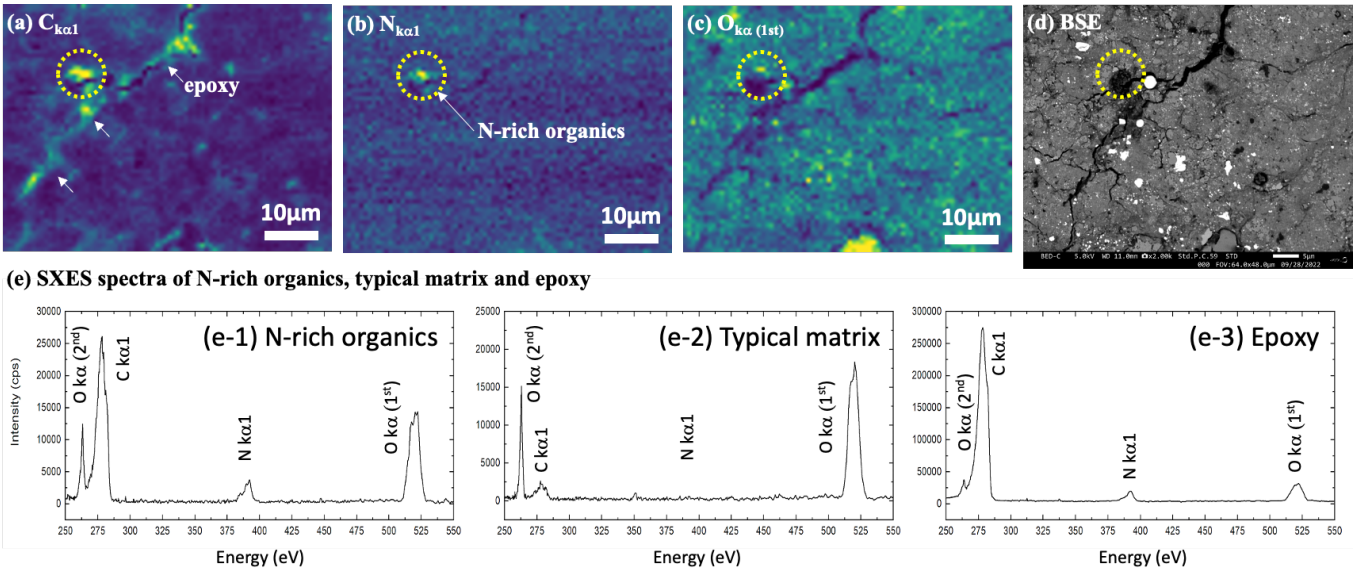

The relationship between Ryugu samples and CY and CI chondrites: Another twist in the tale.

R. C. Greenwood[1], I. A. Franchi[1], R. Findlay[1], J. A. Malley[1], M. Ito[2], A. Yamaguchi[3], M. Kimura[3], N. Tomioka[2], M. Uesugi[4], N. Imae[3], N. Shirai[5,17], T. Ohigashi[6,18], M-C. Liu[7], K. Uesugi[4], A. Nakato[8], K. Yogata[8], H. Yuzawa[6], Y. Kodama[19], A. Tsuchiyama[9], M. Yasutake[4], K. Hirahara[10], A. Takeuchi[4], I. Sakurai[11], I. Okada[11], Y. Karouji[12], T. Yada[8], M. Abe[8], T. Usui[8], S. Watanabe[13], Y. Tsuda[8,14] K. A. McCain[7], N. Matsuda[7], K. D. McKeegan[7], S. Nakzawa[8], T. Okada[8], T. Saiki[8], S. Tanaka[8], F. Terui[15], M. Yoshikawa[8], A. Miyazaki[8], M. Nishimura[8], S. Sekimoto[16], *[1]The Open University, Milton Keynes, MK7 6AA, UK. richard.c.greenwood@open.ac.uk [2]KOCHI JAMSTEC [3]NIPR, [4]JASRI/SPring-8, [5]TMU, [6]UVSOR IMS, [7]UCLA, [8]ISAS/JAXA, [9]Ritsumeikan Univ., [10]Osaka Univ., [11]NUSR., [12]JAXA, [13]Nagoya U., [14]SOKENDAI, [15]Kanagawa Institute of Technology, [16]Kyoto Univ., [17]Kanagawa Univ., [18]PF/KEK, [19]Toyo Corp.*

Between June 2018 and November 2019, the JAXA Hayabusa2 spacecraft made detailed observations and measurements of the C-type asteroid 162173 Ryugu. Two samples were collected and returned to Earth on 6th December 2020: a surface sample stored in Chamber A of the return capsule and a sub-surface sample in Chamber C. Near-IR orbital spectroscopic data indicated that Ryugu comprised material "similar to thermally and/or shock-metamorphosed carbonaceous chondrite meteorites" [1], with a possible match to the CY (Yamato-type) chondrites [2]. In contrast, initial studies at the JAXA ISAS facility suggested that the samples were "most similar to CI chondrites" [3]. As part of Phase2 Kochi curation studies [4], we have undertaken high precision oxygen isotope analysis of 4 Ryugu particles [5], with the aim of investigating their possible relationship to carbonaceous chondrites, in particular the CI and CY groups.

Seven sub-samples from four of the particles allocated to Kochi curation were analysed by laser fluorination [6]. Three particles were from Chamber C (C0014,21; C0068,21; C0087,2) and one from Chamber A (A0098, 2). CI chondrites Alais (n=2), Ivuna (n=2) and Orgueil (CI) (n=9), and CY chondrites B-7904 (n=1), Y-82162 (n=7) and Y-980115 (n=1) were analysed for comparison purposes. Sample transport, loading and analysis techniques employed ensured that the Ryugu particles were never exposed to atmospheric contamination [5]. All the samples in this study, with the exception of Y-82162, were run in "single shot" mode [7]. In most cases, due to the very small quantity of material involved, the amount of O_2 gas liberated during fluorination of the Ryugu particles was less than 140 µg, the approximate limit for bellows analysis on the MAT 253 mass spectrometer. In these cases analysis was undertaken using the MAT 253 cryogenic micro-volume. $\Delta^{17}O$ values were calculated as $\Delta^{17}O = \delta^{17}O - 0.52\delta^{18}O$ [5].

The weighted average of the Ryugu analyses (Fig. 1), both in terms of $\Delta^{17}O$ and $\delta^{18}O$, is close to CI average, but plots away from average value for the CY chondrite Y-82162 and our analysis of CY chondrite B-7904. Our new analysis of Y-980115 plots close to the CI chondrite Ivuna. However, while Y-980115 has been included in the CY group [2] it retains phyllosilicates and appears to have undergone variable heating [8]. Based on our new analysis, Y-980115 appears to have closer affinities to the CIs than the CYs. The data presented in Fig. 1 and 2 support the proposed relationship between Ryugu and the CI chondrites [3,4]. A possible match between Ryugu samples and CIs has also been suggested on the basis of bulk oxygen isotope data in two other recent studies [9.10].

Individual Ryugu analyses show a large range in $\delta^{18}O$ values, from 11.46‰ to 19.30‰ (Fig.1). This large range reflects intrinsic isotopic heterogeneity at the sampling scale involved [5], with detailed mineralogical studies [4,9,10] indicating a significant level of heterogeneity within individual Ryugu particles. In addition, SIMS analysis reveals that Ryugu mineral phases are isotopically heterogeneous, with magnetite and carbonates differing by more than 30‰ [11]. Calculations, using Ryugu modal data [4], yield bulk $\delta^{18}O$ values close to the range determined in this study [5]. There is a small resolvable difference between the average $\Delta^{17}O$ composition of the Ryugu particles and Orgueil, (0.66 ± 0.09‰ and $0.0.58 \pm 0.09$‰ respectively (2SD weighted)). Calculations indicate that this difference reflects the terrestrial contamination of Orgueil [5]. Orgueil is known to have undergone significant mineralogical alteration due to terrestrial contamination since its fall in 1864 [12]. Weathering in the terrestrial environment would pull the bulk analysis closer to the terrestrial fractionation line (TFL). This conclusion is consistent with evidence that interlayer water in Orgueil is of terrestrial origin [13], and that Orgueil contains ferrihydrite and sulphate [14], whereas Ryugu particles do not [4]. While Ryugu particles are the most uncontaminated CI-related material we have [5], they are not pristine and have been modified by a variety of processes in the regolith [15]. The evidence from Ryugu suggests that care needs to be taken when using CI meteorite data as Solar System proxy values e.g. [16].

Our new data has implications for the CY chondrites [2]. Instead of a single CY group our oxygen isotope data suggests that these meteorites may be derived from a minimum of two groups. Our data for Y-82162 is in agreement with that of [17] and shows a significant difference in $\Delta^{17}O$ compared to B-7904 (Fig.2). Y-86720 and Y-86789 are close in oxygen isotope composition to B-7904 [17] and can be considered to represent a sub-group. The $\Delta^{17}O$ difference between B-7904 sub-group

and Y-82162 would appear to preclude the possibility that both are derived from a single parent body. The fact that Y-980115, previously proposed to be a CY [2], plots away from both of the other CY clusters reinforces the likelihood that dehydrated and partially dehydrated carbonaceous chondrites are derived from multiple parent bodies. We are currently undertaking further oxygen isotope analysis to try and better define the relationship between unheated, hydrated carbonaceous chondrites and those groups that experienced varying levels of dehydration subsequent to aqueous alteration [2]. But it is already clear that the relationships between these various groups is complex and likely involves multiple parent bodies.

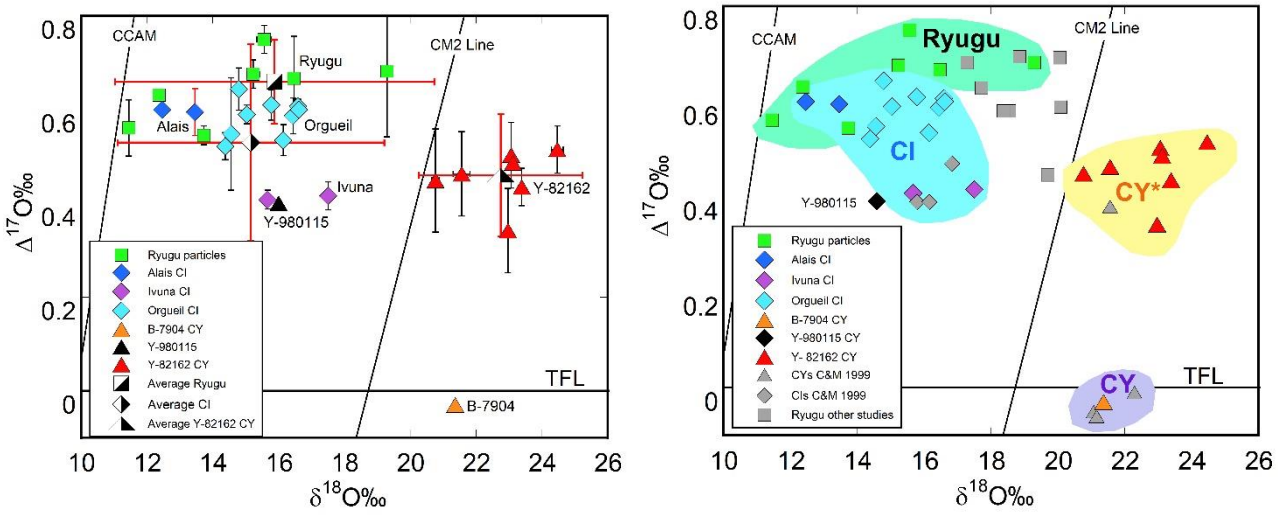

Figs. 1,2 Oxygen isotopic composition of Ryugu particles compared to CI and CY chondrites. Additional CY and CI data [17], additional Ryugu analysis [9,10].

References

[1] Kitazato K. et al. (2019) Science 364: 272-275. [2] King A. J. et al. (2019) Geochemistry 79: 125531. [3] Yada T. et al. (2021) Nat. Astron. https://doi.org/10.1038/s41550-021-01550-6 . [4] Ito M. et al. (2022) Nat. Astron. 6, 1163-1171. [5] Greenwood R. C. et al. (2022) Nat. Astron. (accepted). [6] Greenwood et al. (2017) Cheme Der Erde 77: 1-43. [7] Schrader D. L. et al. (2014) EPSL 407: 48-60. [8] Kikuchi et al. XXXX NIPR [9] Nakamura, E. et al. (2022) Proc. Jpn. Acad. Ser B 98, 227-282. [10] 10.Yokoyama, T. et al. (2022) Science 10.1126/Science.abn 7850. [11] McCain K.A./Matsuda N. et al. (2022) Nat. Astron. (in review). [12] Gounelle M. and Zolensky M. E. (2014) MAPS 49: 769-1794. [13] Baker L. (2002) MAPS 37: 977-985. [14] King A. J. et al. (2015) GCA 165: 148-160. [15] Tomioka N. et al. Nat. Astron. (in review). [16] Lodders K. (2003) Ap. J. 591: 1220-1247. [17] Clayton, M.K. & Mayeda, T. K. (1999) Geochim. Cosmochim. Acta 63, 2089 – 2104.

News about the high pressure mineralogy in Tissint (olivine-phyric shergottite): (Ferro-) Periclase and nano-micro Diamonds

V.H.Hoffmann[1], M. Kaliwoda[1,2], M. Junge[1,2], F.Hentschel[2], W.W. Schmahl[1,2]
[1]*Faculty of Geosciences, Department of Geo- and Environmental Sciences, University of Munich;*
[2]*Mineralogical State Collection Munich (MSM-SNSB), Munich, Germany.*

Introduction
The Tissint meteorite (fall 2011, S Morocco) was classified as a strongly shocked olivine-phyric shergottite. It is characterized by large olivine grains (up to mm-size) in a fine groundmass of pyroxene and plagioclase (maskelynite) as well as of a number of opaque phases (e.g. ilmenite, chromite, pyrrhotite) [1]. We have reported results of optical microscopy, studies by magnetic and mineralogical means, mainly focused on the phase composition and magnetic/shock signature [2,3]. In our poster we will present new results of detailed and systematic Micro Raman Spectroscopy experiments in order to investigate shock effects and shock introduced high pressure phases within melt veins/pockets in selected large olivine crystals. Peak shocks of 40-45 GPa have been reported earlier from Tissint as determined by Raman Spectroscopy [2,3, see also 11 and refs.]. However, locally much higher peak shocks might have occurred.

The main phases of Tissint Martian meteorite – an olivine-phyric shergottite – can be summarized as follows [1-5, references herein]:
- Olivine megacrysts, ~ Fo81, matrix olivines ~ Fo77
- Clinopyroxene (CPX)
- Plagioclase, all converted to maskelynite (not recrystallized)
- Magnetite (dominating magnetic phase)
- Fe-Ti-Cr oxides
- Fe-sulfides (pyrrhotite, significant Ni content)
- Phosphates (merrilite)

Samples and techniques
A polished section (PS) and several fragments of Tissint were used for our investigations. The preparation and polishing of the PS was done without using any diamond paste or powder, and the PS was not sputtered. Digital optical microscopy (Keyence VHX950F at MSM-SNSB, magnifications up to 2500) allowed to pre-select and pre-investigate in detail best suited olivine megacrystals with shock structures [12]. A Horiba XploRa One LASER Micro Raman microscope (at MSM-SNSB) was used for the 2/3D Raman experiments (mainly high resolution mappings with magnifications up to 1000x, 532 nm LASER).

Results and conclusions
A large number of shock produced phases has been detected and studied in detail, confirming our earlier peak shock determinations of 40-45 GPa. However, locally even higher peak shocks were probably present which produced the very complex phase composition within the melt veins / pockets. In general, this confirms the results of earlier studies by [4-10]. However, our high resolution Raman investigations allowed to study in more detail the 2D/3D distribution of the various shock produced phases. Outstanding and new findings are represented by:
(1) Various types of nano/micro diamonds, most likely CVD diamonds (details under investigation).
(2) Significant concentrations of phases of the (ferro-) periclase (Fe,Mg)O - (magnesio-) wuestite (Mg,Fe)O solid solution: common phases in the melt veins/pockets.
(3) We also found strong indications for the presence of C60 fullerenes within the melt veins / pockets.

The combination of digital optical microscopy (Keyence system) as a first step followed by high resolution LASER Micro Raman Spectroscopy has demonstrated to represent a significant improvement for investigating the phase composition and distribution within mineralogically complex systems [12].

The natural dissociation / conversion of the large olivines to magnesio-wuestite (and perowskite) due to high (impact) shock within olivine-phyric Martian meteorites was reported by [9, 10] and could be confirmed by our investigations. The presence of micro/nano diamonds in Martian meteorites was never observed before to our best knowledge.

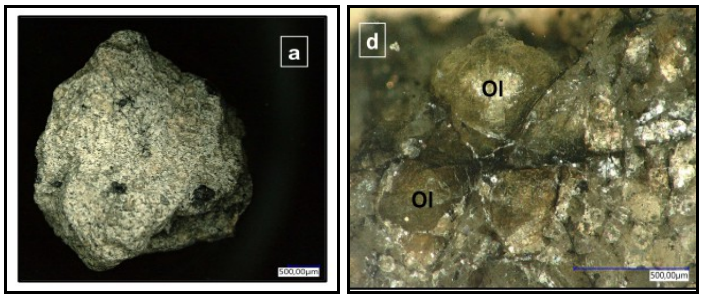

Figure 1: (a) Tissint fragment under study with melt-pockets. (d) Olivine mega-crysts (Ol), in transmitted light with melt veins. Olivines mostly show normal greenish colour.

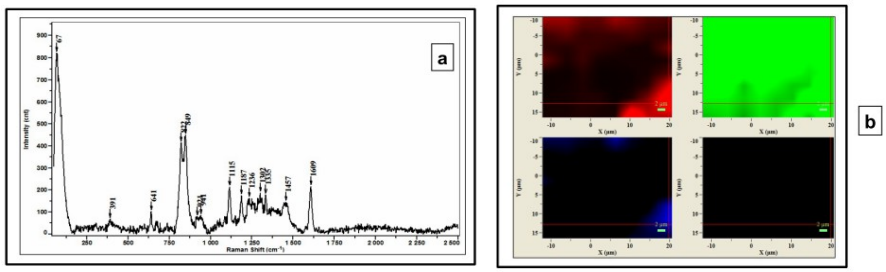

Figure 2: (a) A typical Raman spectrum of one of the investigated areas. Multiple carbon phases could be detected such as graphite (1609), various nano-micro diamonds (1302/1335) and amorphous carbon; and a (ferro-) periclase peak (67). (b) The 2D distribution of: green - olivine matrix; red - graphite; blue - diamond(s). The likely presence of C60 fullerenes is indicated by the (1457) peak.

References

[1] Meteor. Bull. Database, 04/2022;
[2] Hoffmann V., et al., 2012. Asteroids, Comets, Meteorites, #6344.
[3] Hoffmann V. et al., 2013. 35 th Symp. Antarct. Meteor., NIPR/Tokyo.
[4] Balta, J.B., et al., 2015. MAPS, 50(1), 63-85.
[5] Baziotis, I.P., et al., 2013. Nature Communications, 4, 1404.
[6] Chennaoui Aoudjehane, H. et al. , 2012. DOI: 10.1126/science.1224514.
[7] Ma, C., et al., 2016. Geochim. Cosmochim. Acta, 184, 240-256.
[8] Ma, C., et al., 2015. EPSL 422, 194-205.
[9] Miyahara, M., et al., 2012. PNAS 108/15, 5999–6003.
[10] Miyahara, M., et al., 2016. PEPI, 259, 18-28.
[11] Fritz J., et al., 2017. MAPS 52/6, 1216–1232.
[12] Hoffmann V., et al., 2022. Poster, IMA.

Elucidation of aqueous alteration in the lava units with nakhlites NWA 10153 and NWA 6148

Kakeru Kukihara[1], Masaaki Miyahara[1], Akira Yamaguchi[2], Yoshio Takahashi[3], Yasuo Takeichi[4], Naotaka Tomioka[5], and Eiji Ohtani[6]

[1]*Hiroshima university,* [2]*National Institute of Polar Research,* [3]*The University of Tokyo.,* [4]*High Energy Accelerator Research Organization,* [5]*Kochi Institute for Core Sample Research, JAMSTEC,* [6]*Tohoku university*

Introduction

The evidence for liquid water on the past Mars surface is found by the Mars explorations and research about Martian meteorites. Many kinds of phyllosilicate, carbonate, and sulfate minerals occur in Martian meteorite nakhlites [1]. The formation of these alteration minerals depends on temperature, water-rock ratio, dissolved ions species, and pH-Eh. Hence, alteration minerals in nakhlites provide a clue for elucidating ancient Martian surface conditions. Nakhlites are expected to originate from the nakhlite body formed by multiple lava flows on Mars [e.g., 2, 3]. Based on $^{40}Ar/^{39}Ar$ radioisotope ages, the nakhlites body composes of four lava units at least [4]. Alteration minerals occurring in each lava unit have been investigated enthusiastically [e.g., 2, 3]. It is likely that liquid water circulated in the nakhlite body. However, the vertical variation of aqueous alteration in the nakhlite body has not yet been elucidated in detail. NWA 6148 and NWA 10153 are members of nakhlites and their alteration minerals have not been investigated. Jambon et al. (2016) [3] suggest that NWA 6148 originates from the deeper part of the nakhlite body. NWA 10153 is hardly investigated and its position in the nakhlites body is not clear. In this research, we will investigate the petrological and mineralogical features of NWA 6148 and NWA 10153 to add new information about the alteration sequence in a vertical direction in the nakhlite body.

Methods and materials

NWA 6148 and NWA 10153 were embedded into epoxy resin and polished. For petrological and mineralogical descriptions, microtextural observation by an FE-SEM and chemical compositional analysis by an EMPA were conducted. We used an FIB system to prepare the ultra-thin foils of altered portions in the samples. The chemical species of iron, oxygen, carbon, and sulfur in the foils were analyzed by using the BL19A, PF-KEK. The microtextures, chemical compositions, and crystal structures of minerals in the foils were analyzed using an FE-TEM/STEM-EDS.

Results and discussion

NWA 6148 consists mainly of olivine, low-Ca pyroxene, and mesostasis. Plagioclase, K-feldspar, pyrrhotite, and Fe-Ti oxides occur in mesostasis. A quench texture was observed in mesostasis. NWA 6148 has a higher fraction of mesostasis (55.2 vol.%) than other nakhlites (7−24 vol.%) [2]. These features suggest that NWA 6148 does not originate from the deeper part of the nakhlite body; the high fraction of mesostasis is suggestive of a rapid cooling rate near the surface. The low-Ca pyroxene grains of NWA 6148 have Ca zoning. Such Ca zoning is found only in nakhlites NWA 5790 [3] and MIL 03346 [2]. The similarity in Ca zoning suggests that NWA 6148 belongs to the same lava unit as NWA 5790 or MIL 03346. Based on the volume ratio of mesostasis, the stratigraphic sequence is considered to be NWA 6148, NWA 5790 or NWA 6148, MIL 03346 from the top to the bottom of the lava unit. Distinguished alteration texture was not found in NWA 6148. Similarly, alteration minerals are not found in NWA 5790 [5]. On the other hand, iddingsite, one of the alteration textures, is identified in MIL 03346. Most of the alteration minerals in MIL 03346 are iron-rich hydroxy-silicates. Goethite, siderite, gypsum, or anhydrite are not observed in MIL 03346. The total amount of alteration minerals in MIL 03346 is only 0.24 vol% [6]. These features indicate that a part of the nakhlites body, where composes of NWA 6148, NWA 5790, and MIL 03346, would be less affected by aqueous alteration.

NWA 10153 consists mainly of olivine, low-Ca pyroxene, and mesostasis. Plagioclase, K-feldspar, pyrite, and Fe-Ti oxides occur in mesostasis. The compositions of olivine in NWA 10153 is more fayalitic (Fa=86.2±1.5mol%) compared to other nakhlites (Olivine in MIL 03346, NWA 817, and Y 000593 have similar major element compositions [2].). The volume amount of low-Ca pyroxene (~63.4 vol.%) is low compared to other nakhlites (69−84.2 vol.%) [7−9]. The low-Ca pyroxene grains of NWA 10153 have only Fe zoning. The Fe zoning is similar to those of Nakhla and Governador Valarades [10]. The lack of Ca zoning suggests that the lava unit including NWA 10153 is different from that including NWA 6148, NWA 5790, and MIL 03346. The compositions of olivine and the volume amount of low-Ca pyroxene of NWA 10153 do not match any other nakhlites. Accordingly, NWA 10153 may have originated from an unknown lava unit, which is supported by the fact that the initial Nd isotope composition of NWA 10153 is different from any other nakhlites [11].

Many alteration textures were observed around fayalitic olivine, plagioclase, and pyrite grains in NWA 10153. FIB-assisted XANES-TEM/STEM analysis reveals that the alteration textures of fayalitic olivine grains can be divided into four types: i) goethite-, ii) jarosite-, iii) saponite-, and iv) siderite-dominated types. We suggest the following alteration sequence:

first, a neutral to a basic fluid containing CO^{2-} reacted with fayalitic olivine, and most Fe and Mg ions were dissolved into the fluid. The fayalitic olivine was replaced with saponite and siderite precipitated simultaneously. Second, an acidic fluid dissolved pyrite, which reduced the pH of the fluid. Jarosite crystallized from the fluid with very low pH. Subsequently, with increasing the pH again due to the reaction between surrounding minerals and the fluid, goethite precipitated from the fluid finally. The change of alteration environment from neutral−basic to acidic conditions is consistent with those of nakhlites previously studied [12, 13].

We discuss the variation of aqueous alteration in the vertical direction of the nakhlites body based on the stratigraphy of nakhlite body inferred from $^{40}Ar/^{39}Ar$ isotope ages [4] and their assemblages of alteration minerals. Cohen et al. (2017) [4] suggest that the nakhlite body can be divided into four units: Unit I (Lafayette), Unit II (Y 000593 and NWA 5790), Unit III (MIL 03346 and Nakhla), and Unit IV (Y 000749) from the top to the bottom. The location of NWA 10153 in the nakhlites body has not been clarified. Considering the Ca zoning of low-Ca pyroxene, NWA 6148 is located within Unit II or III. Lafayette contains ferroan smectite, magnetite (or maghemite), and ferrihydrite as alteration minerals [14]. Y 000593 includes smectite, saponite, siderite, laihunite, gypsum, opal-A, jarosite, and goethite [15]. NWA 5790 does not contain alteration minerals [5]. The difference in the degree of alteration between Y 000593 and NWA 5790 indicates alteration is heterogeneous even in the same unit. In MIL 03346, iron-rich hydroxy silicates occur although their amount is very limited [6]. Iron-rich silicate (tentatively identified smectite), Ca-carbonate (probable calcite), and Ca-sulfate (possibly gypsum or bassanite) are observed in Nakhla [16]. Shiraishi et al. (2019) [13] identify laihunite, ferrihydrite, goethite, poorly-crystallized silica minerals, and a minor amount of iron sulfates in Y 000749.

Smectite is found in Lafayette (Unit I), Y 000593 (Unit II), Nakhla (Unit III). Smectite seems to occur throughout the nakhlite body. However, there are variations in the assemblage of alteration minerals in each lava unit: Magnetite (or maghemite) is found only in Unit I, Many kinds of alteration minerals are identified in Unit II, and Ca-carbonate is observed only in Unit III. It is unlikely that the same fluid circulated throughout the entire nakhlite body and induced these alterations. The alteration might occur in each lava unit of the nakhlite body.

References

[1] Treiman et al., 2005, Chemie der Erde Geochemistry 65, 203–270.
[2] Mikouchi et al., 2006, 37th LPSC, No.1865.
[3] Jambon et al., 2016, Geochimica et Cosmochimica Acta 190, 191–212.
[4] Cohen et al., 2017, Nature Communications, DOI: 10.1038/s41467-017-00513-8.
[5] Tomkinson et al., 2014, Meteoritics & Planetary Science 50, 287–304.
[6] Day et al., 2005, Meteoritics & Planetary Science 41, 581–606.
[7] Lentz et al., 1999, Meteoritics & Planetary Science 34, 919–932.
[8] Sautter et al., 2002, Earth Planetary Science Lett, 195, 223–238.
[9] Imae et al., 2003, Antarctic Meteorite Research 16, 13–33.
[10] Mikouchi et al., 2003, Antarctic Meteorite Research 16, 34–57.
[11] Righter et al., 2016, 47th LPSC, No. 2780.
[12] Nakamura et al., 2020, Japan Geoscience Union Meeting 2020 PPS10-P13.
[13] Shiraishi et al., 2019, The 10th Symposium on Polar Science Antarctic meteorites.
[14] Treiman et al., 1993, Meteoritics 28, 86–97.
[15] Suga et al., 2021, Minerals 11, 514.
[16] James et al., 1991, Meteoritics 26, Issue 2, 135–143.

Lohawat howardite: trapped noble gases and nitrogen isotopic signature

Ramakant R. Mahajan[1]
[1]*Physical Research Laboratory, Ahmedabad, 380009, Gujarat, India (email: ramakant@prl.res.in)*

Howardites, the members of HED (howardite, eucrite and diogenite) family, are the mechanical mixtures of eucritic and diogenitic material cemented by fine dust, with various constituents like melt spherules, remnants of impactor and enriched in solar noble gases (Cartwright et al., 2014). Asteroid Vesta is linked to HEDs as their parent body (McSween et al., 2019). Howardites provide an important clue about the processes occurred in past at the asteroidal surface, such as solar wind implantation, characterization of impactors, regolith processing. Noble gases are useful trace elements as isotopic anomalies are detected due to their scarcity in solid materials. In eucrites and diogenites, trapped solar gases are absent (for neon: Jaiswal et. al., 2022). Howardites are enriched with trapped noble gases (Cartwright et al., 2014; Mahajan et al., 2019). Noble gas studies in different howardites and their constituents comprises solar noble gases, which indicates that these constituents, before agglomeration, resided at the very top of the Vestan regolith.

Lohawat howardite is a texturally heterogeneous breccia having a variety of lithic fragments and minerals (Sisodia et al., 2001). The noble gases and nitrogen were extracted from a single chip weighing 577.38 mg and light noble gases were discussed earlier (Sisodia et al., 2001), while here, nitrogen and Kr-Xe from the same sample are discussed. The measured concentration and isotopic ratios for N, Kr, and Xe are presented in Table 1. The values in Table 1 are corrected for blanks, interferences and mass spectrometric corrections.

The concentration of trapped $^{84}Kr_t$ is (9.92 ± 1.4) x 10^{-11} cm^3STP/g, and that of $^{132}Xe_t$ is (4.84 ± 0.69) x 10^{-11} cm^3STP/g. The elemental ratio $^{84}Kr_t/^{132}Xe_t$ for Lohawat is 2.05 ± 0.41 and is in agreement with the aliquots studied earlier, 1.09 ± 0.23 and 1.96 ± 0.36, L1 and L2, respectively (Mahajan et al., 2019). The Kr and Xe isotopic ratios in stepwise extractions (Table 1) span in the region of Q-SW-HL-GCR in respective plots (not show here).

The trapped nitrogen composition, $\delta^{15}N_t$ is estimated by adopting the systematics given by Hashizume and Sugiura (1995) and Mahajan et al. (2019). The trapped nitrogen in this sample is, $\delta^{15}N_t$ = +18.4 ± 0.4 ‰. Trapped nitrogen values of ($\delta^{15}N_t$ in ‰) L1 = -41.7 ± 2.2 and L2 = -51.4 ± 0.7 were reported in bulk aliquots of Lohawat (Mahajan et al., 2019). This indicates that trapped nitrogen in Lohawat howardite is highly heterogeneous. Isotopic composition of trapped nitrogen in bulk samples of eucrites ranges from -52.9 ‰ to +22.4 ‰ (Miura and Sugiura, 1993; Mahajan et al., 2019). The observed $\delta^{15}N_t$ in eucrites can be explained as heterogeneous isotopic characteristics in subsurface / lower crust material of Vesta. The composition in Lohawat howardite can be explained as either is manifestation of fragments of various eucrites possessing variety of N isotopic signatures or alternatively with one eucrite type signature mixed with impactors possessing various N signature.

Table 1. Measured noble gases and nitrogen in Lohawat howardite

Isotope	Temperature 400ºC	Temperature 1000ºC	Temperature 1600ºC	Total
N (ppm)	0.43 ± 0.01	0.58 ± 0.03	0.12 ± 0.01	1.12 ± 0.06
$\delta^{15}N$	15.73 ± 1.55	100.23 ± 1.55	270.90 ± 2.73	85.49 ± 1.67
^{84}Kr cm^3STP/g, x 10^{-12}	4.96 ± 0.15	54.90 ± 0.05	55.64 ± 0.05	11.55 ± 3.78
$^{78}Kr/^{84}Kr$	0.0215 ± 0.0026	0.0471 ± 0.0007	0.0557 ± 0.009	0.0502 ± 0.0009
$^{80}Kr/^{84}Kr$	0.0348 ± 0.0136	0.1380 ± 0.0011	0.1602 ± 0.0011	0.1442 ± 0.0016
$^{82}Kr/^{84}Kr$	0.2327 ± 0.0005	0.3315 ± 0.0014	0.3699 ± 0.0008	0.3457 ± 0.0011
$^{83}Kr/^{84}Kr$	0.2297 ± 0.0002	0.3738 ± 0.0011	0.4307 ± 0.0008	0.3950 ± 0.0009
$^{86}Kr/^{84}Kr$	0.3084 ± 0.0006	0.3103 ± 0.0010	0.3019 ± 0.0013	0.3062 ± 0.0011
^{132}Xe cm^3STP/g, x 10^{-12}	2.50 ± 0.07	25.81 ± 0.02	22.02 ± 0.02	50.33 ± 0.16
$^{124}Xe/^{132}Xe$	0.0207 ± 0.0002	0.0228 ± 0.0002	0.0392 ± 0.0005	0.0298 ± 0.0004
$^{126}Xe/^{132}Xe$	0.0241 ± 0.0002	0.0374 ± 0.0006	0.0655 ± 0.0005	0.0490 ± 0.0005
$^{128}Xe/^{132}Xe$	0.0895 ± 0.0004	0.1204 ±0.0016	0.1530 ± 0.0009	0.1331 ± 0.0012
$^{129}Xe/^{132}Xe$	0.9275 ± 0.0032	1.1110 ± 0.0042	0.9627 ± 0.0072	1.0307 ± 0.0055
$^{130}Xe/^{132}Xe$	0.1658 ± 0.0003	0.1760 ± 0.0004	0.1811 ± 0.0025	0.1777 ± 0.0014
$^{131}Xe/^{132}Xe$	0.8239 ± 0.0008	0.8473 ± 0.0034	0.8854 ± 0.0053	0.8628 ± 0.0041
$^{134}Xe/^{132}Xe$	0.3721 ± 0.0008	0.4118 ± 0.0012	0.5036 ± 0.0012	0.4499 ± 0.0012
$^{136}Xe/^{132}Xe$	0.3254 ± 0.0014	0.3594 ± 0.0017	0.4642 ± 0.0021	0.4035 ± 0.0019

References

Cartwright, J. A., Ott, U. and Mittlefehldt D. W., The quest for regolithic howardites. Part 2: Surface origins highlighted by noble gases, Geochimica et Cosmochimica Acta, 140, 488-508, 2014.

Hashizume K. and Sugiura N., Nitrogen isotopes in bulk ordinary chondrites, Geochimica et Cosmochimica Acta, 59, 4057-4069.

Jaiswal S., Mahajan R. R., and Ngangom M., Neon in interior of the asteroid Vesta and comparison with the terrestrial planets, Journal of Asian Earth Sciences: X, 7, 100084, 2022.

Mahajan R. R., Sarbadhikari A. B., and Sisodia M. S., Noble gas, nitrogen composition and cosmic ray exposure history of two eucrites Vissannapeta, Piplia Kalan and one howardite Lohawat, Planetary and Space Science, 165, 23-30, 2019.

McSween H. Y. Jr., Raymond C. A., Stolper E. M., Mittlefehldt D. W., Baker M. B., Lunning N. G., Beck A. W., Hahn T. M., differentiation and magmatic history of Vesta: Constraints from HED meteorites and Dawn Spacecraft data, Geochemistry, 79, 135526.

Miura Y., and Sugiura N., Nitrogen isotopic compositions in three Antarctic and two non-Antarctic eucrites, Proc. NIPR Symp. Antarct. Meteorites, 6, 338-356, 1993

Sisodia M. S., Shukla A. D., Suthar K. M., Mahajan R. R., Murty S. V. S., Shukla P. N., Bhandari N., and Natarajan R., The Lohawat howardite: Mineralogy, chemistry and cosmogenic effects, Meteoritics & Planetary Science, 36, 1457-1466.

Chemical characteristics of ungrouped iron meteorites from Yamato Mountains

Naoki Shirai[1], Akira Yamaguchi[2]
[1]*Tokyo Metropolitan University,* [2]*National Institute of Polar Research*

Introduction

It was announced that Y-792345 (2.57 g), Y 000088 (4.25 g), Y 000090 (1.56 g) and Y 983934 (7.5 g) were classified into ungrouped iron meteorites [1]. According to the previous suggestion [2], it is likely that these ungrouped iron meteorites with less than 20 g of total mass are metal nodule of chondrites and achondrites. In this study, we determined elemental abundances for these iron meteorites as much as possible using LA-ICP-MS and EPMA, and the obtained results are compared with those of iron meteorites as well as those of metal fractions of chondrites and achondrites.

Experiments

Small metal fragments allocated from NIPR were mounted in epoxy and polished. LA-ICPMS analysis were carried out using a Thermo ElementXR coupled to CETAC LAS-213 at NIPR. Iron meteorites were ablated on line mode with spot size of 100 μm in diameter at a scan speedrate of 25-50 μm/s. All analyses were performed with 20Hz repetition rate and 100% power output. Under these conditions, ^{31}P, ^{53}Cr, ^{57}Fe, ^{59}Co, $^{60, 61, 62}$Ni, $^{63, 65}$Cu, $^{69, 71}$Ga, $^{73, 74}$Ge, ^{75}As, ^{95}Mo, $^{101, 102}$Ru, ^{103}Rh, $^{105, 106}$Pd, $^{182, 183, 184}$W, $^{185, 187}$Re, $^{189, 190}$Os, $^{191, 193}$Ir, $^{194, 195}$Pt and ^{197}Au were monitored in low resolution (R = 300). For quantification, North Chile (IIAB), Hoba (IVB) and NIST SRM663 are used as reference samples. EPMA, JEOL JXA-8200 at NIPR was used for the determination of Si, Fe, Co and Ni. The accelerating voltage was 15 keV and the operating beam current of 30 nA and defocused beam (100 μm in diameter) were used.

Results and Discussion

Y 983934, Y 000088 and Y 000090: The most noticeable chemical features of three ungrouped iron meteorites (Y 983934, Y 000088 and Y 000090) are significantly low Co abundances (3230 ppm for Y 983934, 2960 ppm for Y 000088, 2860 ppm for Y 000090) and higher Si abundances (2330 ppm for Y 983934, 1850 ppm for Y 000088, 1220 ppm for Y 000090). These chemical features are similar to those of metal fraction of enstatite chondrites and achondrites, and some ungrouped iron meteorites (Horse Creek and LEW 85368). CI-normalized elemental abundances for siderophile and chalcophile elements for Y 983934 are flat, and are similar to those of metal fractions of enstatite chondrites, indicating that Y 983934 is metal nodule of enstatite chondrite. Y 000088 and Y 000090 are significantly depleted in Re, Os, Ir, Mo, Ru and Pt compared with metal fractions of enstatite chondrite, while moderately and volatile siderophile elements are not fractionated among these elements. These chemical features can be seen in enstatite achondrites [3]. Fractionation of these refractory siderophile elements are explained by partial melting of enstatite chondrites. Thus, Y 000088 and Y 000090 are considered to be metal fraction of enstatite achondrites.
Silicon abundances of Y 000088 and Y 000090 are lower than that of Horse Creek, while these three iron meteorites have similar Ga and Ge abundances to each other, implying that these three iron meteorites are related. If so, fractionation trend seen in magmatic iron meteorites can be seen in these three iron meteorites. Although Y 000088 and Y 000090 have lower Ir, Re and W than those of those of Horse Creek, Au abundances for these three iron meteorites are almost similar to each other. Thus, it was excluded that Y 000088 and Y 000090, and Horse Creek are genetically related.

Y 792345: Compare with other iron meteorites, Y-792345 has a lower P abundance (11.1 ppm). Its abundance is similar to those for metal fractions of ordinary chondrites. Although CI-normalized elemental abundances for moderately and volatile siderophile elements of Y-792345 are similar to those of bulk metal of H ordinary chondrites, significant depletions of highly siderophile elements can be seen in Y 792345 compared with bulk metal of H ordinary chondrites. Chemical characteristics observed in Y 792345 can be seen in large metal nodule of ordinary chondrites and some iron meteorites such as ALH 84233 and LEW 88023 [2,4]. Slight difference can be seen in opposite fractionation of Re/Os and Ru/Pt ratios. In terms of its chemical composition, it is concluded that Y 792345 represent as metal fraction of H ordinary chondrite.

References

[1] Meteorite Newsletter (2021) vol. 28. [2] Wasson J. T. (2000) Lunar Planet. Inst. Contrib. 977 Workshop on Extraterrestrial Materials from Cold and Hot desert, 76-78. [3] van Acken D. et al. (2012) Geochimica et Cosmochimcia Acta 83, 272-291. [4] Widom E. et al. (1986) Geochimica et Cosmochimcia Acta 50, 1989-1995.

Compositional information for the bulk S-contents of metallic cores of iron meteorite parent bodies. Implications for the sulphur abundance of the metallic core of the Earth.

P. Futó[1], A. Gucsik[2]

[1]*University of Debrecen, Cosmochemical Research Group, Department of Mineralogy and Geology, Debrecen, Egyetem tér 1. H-4032, Hungary (dvision@citromail.hu)*

[2]*Institute of Low Temperature Science, Hokkaido University; Kita-19, Nishi-8, Kita-ku, Sapporo, 060-0819, Japan.*

It is known that central metallic cores are common in the differentiated planetary bodies of the Solar System. Iron meteorite samples provide an unique opportunity to study the composition of the metallic cores of asteroid – sized parent bodies, which had been disrupted by collision of roughly similar sized objects. Moreover, the iron meteorite parent asteroids are the earliest accreted planetary bodies, thus they preserve the original elementary composition of the early Solar System.
The isotopic signatures in iron meteorites suggest that they had been formed in two distinct formation reservoirs, which are proposed to be separated by Jupiter: thus inner (ISS) and outer Solar System (OSS) formation regions can be distinguished (Kruier et al. 1994). The two types of the parent asteroidal cores formed in carbonaceous (CC) (OSS) and noncarbonaceous (NC) (ISS) reservoirs in the early Solar System. In the outer Solar System, the parent asteroids of CC – type irons have formed in more oxidized formation conditions than the parent asteroidal bodies of NC – type iron meteorites, resulting in less Fe and higher Ni and Co concentrations in the metallic core (Chabot 2018). Zhang et al. (2022) found that CC – type iron cores have lower S, higher Ni content than NC – cores.

An abundance analysis have been performed for lighter elements by applying a simple modeling approach to obtain results, which may helps to understand the compositions of the terrestrial planetary cores in the Solar System.
Assuming the abundances of several elements in materials that made up the cores of Earth and other terrestrial planets are similar to determined meteoritic compositions, we aim to estimate the bulk S - content in the Earth's core having implications for the S – budgets in the metallic cores of the inner Solar system planets. The differentiated planetesimals have formed from chondritic materials therefore we also consider the chondritic bulk compositions. This study is based on the magmatic / non – magmatic iron meteorite, CI – chondrite and cosmochemically estimated abundances. One part of abundance data used in this study are listed in Table 1. and are taken from the literature.

	IID; IVB CC - irons[1]	Canyon Diablo[2]	IIAB NC - iron[3]	Planetary materials	CI - chondrites[4]	1. Earth's core[5]	2. Earth's core[6]
S (wt%)	0.5±0.5; 0.5±0.5	1	17±1.5		5.40	1.7	2.3

Table 1. Sulphur abundance data of several planetary materials. [1] Zhang et al. (2022); [2] Buchwald (1975); [3] Chabot (2004); [4] McDonough and Sun (1995); [5] Dreibus and Palme (1996); [6] Allegre et al. (1995).

The modeled S elemental abundance of the Earth's core are thought to be approximately higher than the S content of the most CC – iron asteroidal cores, however it is essentially lower than the relevant values of CI – chondrites. Based on cosmochemical and geochemical considerations and the analysis of the early formation of the terrestrial planetary bodies in the Solar system,we proposed that the metallic core made mostly of Fe 80 – 85 wt% - Ni 5 – 10 % alloyed with ~ 10 % lighter elements. In terms of our study, S is suggested to be the third most abundant light element of the core. The S content in the bulk core of the Earth is between 1.7 – 4 %, O – 3 – 5 % and Si – 2 – 4 % by weight. Among the chondritic type meteorites, the Earth's core is closer to CM chondrites (3.3 wt %, Wasson and Kallemeyn, 1988) rather than CI chondrites for bulk S content.

The geochemical models assume strong devolatilization of sulphur during Earth's core formation. The present – day core concentration of S is lower than the CI chondritic S – abundance, but its estimated value is similar to that of the CM - chondrites. Note that the different effects can modify the bulk S, P and other lighter element contents after the accretion of planetary bodies.These effects are expected to have been caused by processes during the core formation and the early planetary evolution. Accordinghly, a small amount of the core S content is delivered by a giant impactor during the early evolution of Earth.

References

Allegre, C. J., Poirier J-P., Humler E., Hofmann A. W. The chemical composition of the Earth, Earth and Planetary Science Letters, 134, 515 – 526, 1995.

Buchwald W. F., Handbook of Iron Meteorites, University California Press, 1418 pp., 1975.
Chabot N. L., Sulfur contents of the parental metallic cores of magmatic iron meteorites. Geochimica et Cosmochimica Acta, 68, 3607 – 3618, 2004.
Chabot N. L., Understanding iron meteorites and early Solar System metallic cores of asteroid parent bodies, European Planetary Science Congress Abstracts, EPSC 2018-108, 2018.
Dreibus G., Palme H., Cosmochemical constraints on the sulfur content in the Earth's core. Geochimica et Cosmochimica Acta, 60, 1125 – 1130, 1996.
Kruier T. S., Burkhardt C., Budde G., Kleine T. Age of Jupiter inferred from the distinct genetics and formation times of meteorites, Proceedings of the National Academy of Sciences, 114, 6712 – 6716, 1994.
McDonough W. F.; Sun S.s., The Composition of the Earth. Chemical Geology, 120, 223 – 253,1995.
Wasson, J. T., Kallemeyn G. W., Compositions of chondrites. Philosophical Transactions of the Royal Society A 325, 535–544, 1988,
Zhang B., Chabot N. L., Rubin A. E., Compositions of carbonaceous-type asteroidal cores in the early solar system, Science Advances, 8, eabo5781, 2022.

Trapped Ar, Kr, and Xe in ordinary chondrites

Ramakant R. Mahajan[1]

[1]*Physical Research Laboratory, Ahmedabad, Gujarat, 380009, India (email: ramakant@prl.res.in)*

Ordinary chondrites (OCs) make up about 85% of the meteorites fall on Earth. Their importance arises from the fact that some of them are the least altered samples of nebular agglomerates. This kind of material also thought to be one of the ingredients to the rocky planets. The ordinary chondrites show a wide range of oxidation state compared to highly reduced enstatite chondrites and most oxidized carbonaceous chondrites. The OCs are divided into three subgroups referred to as the H, L, and LL chondrites, on the basis of their total Fe-content, high, low and low-low (metallic-Fe content), respectively (Weisberg et al. 2006). An important question is whether meteorite of the same subgroup (H or L or LL) could have been derived from the same parent asteroid. Noble gases are being studied in bulk samples in this context.

Trapped noble gases in chondrites could be of different origin; (1) dissolved gases during accretion or formation of various constituents such as chondrules, CAIs, or matrix, or (2) gases implanted such as solar wind. Phase-Q is considered as one of the main carriers of noble gases in meteorites. Phase-Q lost the noble gases in varying degrees by thermal metamorphism in meteorite parent bodies. The metamorphism also changes elemental composition of Q gases. Therefore, phase-Q component cannot be utilized for the purpose of using as representative for noble gas inventory in the bulk samples (Busemann et al. 2000; Matsuda et al. 2010). Abundances of trapped noble gases in chondrites are important proxies to understand the depletions patter and characterization of volatile reservoirs. Solar type neon is present in many ordinary chondrites and is summarized in Kumar et al. (2021). The purpose of the present work is to determine the range and average of concentrations of trapped Ar, Kr and Xe in subgroups of ordinary chondrites. Trapped noble gases from bulk measurements of these meteorites therefore, not only provides a quantitative approach, but also has genetic relevance.

The ranges among individual subgroup of OCs also provides insights on an asteroid-wide scale for heterogeneity, if they derived from single parent asteroid. The investigations reported here has concentrated on whole-rock samples and melting extraction data set, rather than acid-resistant residues or other specific methods, in an attempt to calculate the overall noble gas inventory of the OCs. Here only those samples are considered where $^{36}Ar_t$, $^{84}Kr_t$ and $^{132}Xe_t$ and isotopic ratios were measured in same aliquot and data of neon isotopic ratios are available in the literature. The concentrations of trapped noble gases are summarized in Table 1. The full list of references for the meteorite data set is beyond the prescribe limit of the abstract, is made available with the author.

Table 1. Trapped gas concentration, cm^3STP/g. Q: meteorites having Q-phase type neon isotopic composition, SW: meteorites having solar wind neon isotopic composition.

OC	Number of meteorites	$^{36}Ar_t$			$^{84}Kr_t$			$^{132}Xe_t$		
		Min (10^{-9})	Max (10^{-8})	Average (10^{-8})	Min (10^{-11})	Max (10^{-10})	Average (10^{-10})	Min (10^{-11})	Max (10^{-10})	Average (10^{-10})
H-Q	38	2.66	19.9	1.71	4.77	8.03	1.73	4.08	7.97	2.05
H-SW	7	7.87	32.7	14.3	13.2	17.2	9.24	15.6	15.8	6.66
L-Q	43	1.19	8.67	1.50	2.60	8.27	1.45	1.88	16.8	1.59
L-SW	3	63.2	33.7	21.3	50.3	22.5	11.7	72.2	22.2	12.5
LL-Q	16	1.39	57.0	1.84	1.84	31.3	5.11	2.73	31.9	4.46

It is observed that the concentrations of trapped $^{36}Ar_t$, $^{84}Kr_t$ and $^{132}Xe_t$ in H, L, and LL chondrites shows wide range. The range is different for those showing phase-Q type and SW type neon isotopic compositions. Higher concentrations are clearly observed in those meteorites showing SW type neon compared to that of phase-Q type isotopic signature.

References

Busemann H., Heinrich B. and Wieler R., Primordial noble gases in "phase Q" in carbonaceous and ordinary chondrites studied by closed-system stepped etching, Meteoritics & Planetary Science, 35, 949-973, 2000.

Kumar A., Mahajan R. R. and Sarbadhikari A. B., Neon isotopic study in ordinary chondrites, 52nd Lunar and Planetary Science Conference, 1421.pdf, 2021.

Matsuda J., Tsukamoto H., Miyakawa C. and Amari S., Noble gas study of the Saratov L4 chondrite, Meteoritics & Planetary Science, 45, 361-372, 2010

Weisberg M. K., McCoy, T. J., and Krot A. N., Systematics and evaluation of meteoritic classification, In Meteorites and the Early Solar System II. (Eds. D. S. Lauretta and H. Y. McSween Jr.), p. 19-52, 2006.

Chemical compositional characteristics of CBb and CH chondrites

Y. Hidaka[1], T. Fujimura[1] and M. Ebihara[1]
[1]*Department of Earth Sciences, Waseda University, Tokyo 169-8050, Japan.*

Introduction: CB and CH chondrites are metal-rich chondrite groups [1, 2] and their oxygen isotopic compositions show a close relationship to CR chondrites [3]. The petrogensis of CB chondrites came to be considered as the condensation from impact-induced vapor plume [4, 5]. According to the similarity of oxygen isotopic composition between CB and CH chondrites, the parent bodies of these chondrites might exist close to each other. Then, how impact processes affected the origin and the evolution of CH chondrites? What was the difference between CB and CH chondrites? Impact-induced vaporization should cause volatility loss of elements, so chemical compositions and isotopic compositions must become powerful tool to discuss these issues.

Bulk chemical compositions of CB and CH chondrites have been scarcely reported and have been poorly discussed. Here, we report and characterize the results of our bulk chemical analyses for one CB and 4 CH chondrites and discuss their formation processes.

Samples & methods: Bulk chemical compositions of 1 CBb chondrite (MacAlpine Hills (MAC) 02675) and 4 CH chondrites (Asuka 881020, Asuka 881451, Patuxent Range (PAT) 91546 and Pecora Escarpment (PCA) 91467) have been determined by PGA, INAA, ICP-AES and ICP-MS. A chip sample weighing 130-440 mg of each meteorite was crushed into small chips and fine grains. Small fractions weighing ~40 mg of each meteorite were used for INAA, ICP-AES and ICP-MS, respectively. To evaluate the sample heterogeneity, 3 fractions of MAC 02675 and 2 fractions of PAT 91546 and PCA 91467 were subjected to INAA. Remaining chip samples weighing 150-400 mg of each meteorite were used for PGA.

The elements analyzed by INAA are Na, Mg, Al, Ca, Sc, V, Cr, Mn, Fe, Co, Ni, Zn, Se, Sm, Ir and Au, and by ICP-AES are Na, Mg, Al, P, Ca, Ti, V, Cr, Mn, Fe, Co, Ni, Zn, Sr and Ba, and by ICP-MS are Ga, Ge, As, Mo, Ru, Rh, Pd, Sn, Sb, W, Re, Ir, Pt and La, Ce, Pr, Nd, Sm, Eu, Gd, Tb, Dy, Ho, Er, Tm, Yb, Lu, Th and U, and by PGA are Na, Mg, Al, Si, S, Cl, Ca, Ti, Cr, Mn, Fe, Co and Ni.

Results: The Mg-, CI-normalized and Ni-, CI-normalized chemical compositions of CBb and CH chondrites are shown in Fig. 1. In Fig. 1a, refractory lithophile element (V to Al) to Mg ratios in CBb chondrite (CI x ~1.5) are slightly fractionated and significantly higher than those of CH chondrites (CI x ~1). In moderately volatile elements, Si//Mg, Cr/Mg, Mn/Mg and P/Mg ratios in CBb chondrite (0.61, 2.5, 0.27 and 3.6) are clearly different from those of CH chondrites (0.96, 1.1, 0.45 and 0.96). In volatile elements, although the Na/Mg ratio in CBb chondrite (0.26) is comparable with those of CH chondrites (0.24), the S/Mg and Zn/Mg ratios are higher in CBb chondrite (0.19 and 0.17) than those in CH chondrites (0.11 and 0.11).

In Fig. 1b, refractory siderophile elements to Ni ratios, except for W/Ni, are nearly identical between CBb and CH chondrites, but as volatility increases, CBb and CH chondrites show obviously different chemical compositional characteristics. Moderately volatile elements and volatile elements are more severely depleted in CBb chondrites than CH chondrites and the ratios of Cr/Au, As/P and Ga/S are clearly different in CBb chondrite (0.95, 0.52 and 1.0) from those of CH chondrites (0.72, 1.3 and 3.9). In addition to these differences, W/Ni ratio is clearly depleted in CBb chondrite (0.67) but is not depleted in CH chondrites (1.1) and the Re/W ratios are also different in CBb chondrite (1.9) from those of CH chondrites (1.2).

The CI-normalized and Mg-, CI-normalized REE abundances of CBb and CH chondrites are shown in Fig. 2. In Fig. 2a, REE abundances of CBb chondrite (CI x ~0.6-0.8) and CH chondrites (CI x ~1.1-1.4) are lower and higher than CI chondrites, respectively, and are slightly fractionated from CI chondrite composition. The La/Yb ratios of CBb chondrite is 1.2 and those of CH chondrites are 0.94. In Fig. 2b, CBb chondrite shows enrichment of REE abundances compared to CH chondrites in Mg-normalized values.

Discussions: We could find the several characteristic points of bulk chemical compositions in CBb and CH chondrites. The first is the differences of partitioning behaviors of P, Mn and Cr (Figs. 1a and 1b). The Cr-bearing troilite and daubréelite have been reported in CB chondrites [2], but not in CH chondrites, so Cr behaved as chalcophile elements only in CB chondrites. These data suggest that CB chondrites were more reduced than CH chondrites and in such highly reduced conditions, Mn and P might be partitioned into sulfides and metals, respectively. However, Mg# (molar Mg/[Fe+Mg] x100) in olivine and pyroxene are similar in CB chondrites (96-99 [2, 6]) and in CH chondrites (94-99 [7, 8]), so the redox states recorded in silicate minerals in CB and CH chondrites should not be so different. Therefore, in this timing, we are not sure what was a key role for changing partitioning behaviors of P, Mn and Cr between CB and CH chondrites.

The second is depletion patterns of volatile and moderately volatile elements (Figs. 1a and 1b). In both CBb and CH chondrites, the refractory lithophile and siderophile element patterns are not fractionated, but clear depletions can be seen on

more volatile elements than Na in lithophile elements and more volatile elements than Cr or Au in siderophile elements. In lithophile elements, CBb and CH chondrites show similar degree of depletion, but in siderophile elements, CBb chondrite shows more severe depletion than those of CH chondrites. In addition, there are some remarkable points present, such as Si-Mg fractionation and W depletion in CBb chondrite. For Si-Mg fractionation, it is known that chondrule and matrix show complementarily low and high Si/Mg ratios [9], and CBb chondrites are lack in matrix [2]. Therefore, one simple explanation is that the precursor materials of CBb chondrites were quickly isolated from gas reservoir before Si-rich matrix fractions condensed. In this case, very small and local gas reservoir should be required, such as impact vapor plume. For the W depletion, it is suggested that oxidizing conditions during evaporation process is required, such as impact vaporization process [5]. We guess that the chemical compositional trend of CBb and CH chondrites can be interpreted as the results of fractional condensation from chondritic gas reservoir.

The third is slightly fractionated REE patterns (Figs. 2a and 2b). CBb chondrite shows LREE-enriched and CH chondrites show HREE-enriched REE patterns. In Mg-normalized data, REE abundances are higher in CBb chondrite relative to CH chondrites and seem to be complementary between CBb and CH chondrites. It can be interpreted as the results of differentiation and/or evaporation as follows: CBb chondrites were melt and/or vapor components and CH chondrites were residues.

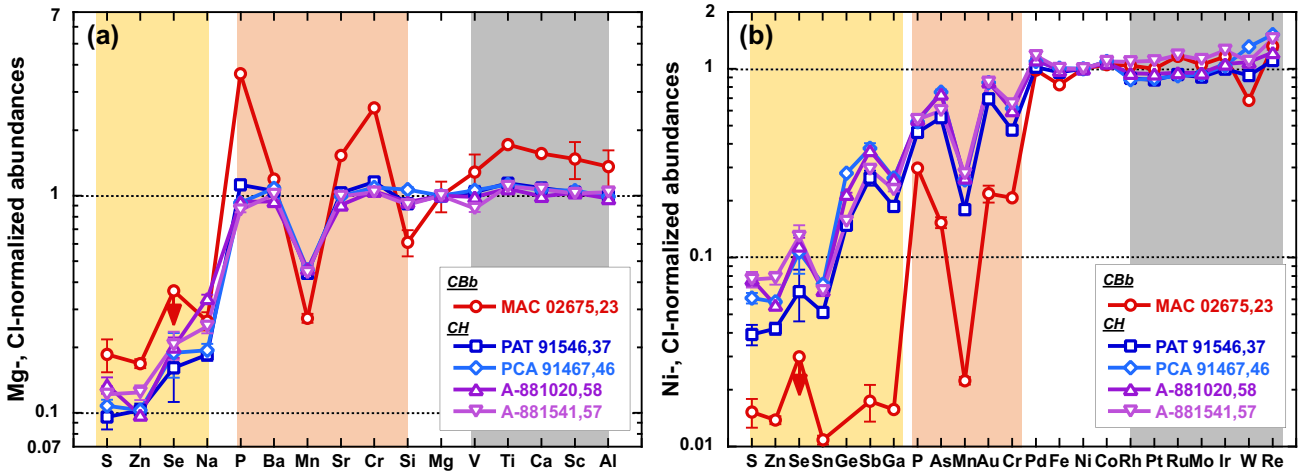

Fig. 1. Bulk chemical compositions of CBb and CH chondrites. (a) Mg- and CI-normalized lithophile element compositions. (b) Ni- and CI-normalized siderophile element compositions. The elements are sorted in decreasing of volatility [9, 10]. Yellow-shaded areas indicate volatile elements. Orange-shaded areas indicate moderately volatile elements. Gray-shaded areas indicate refractory elements. CI chondrite values are from [10].

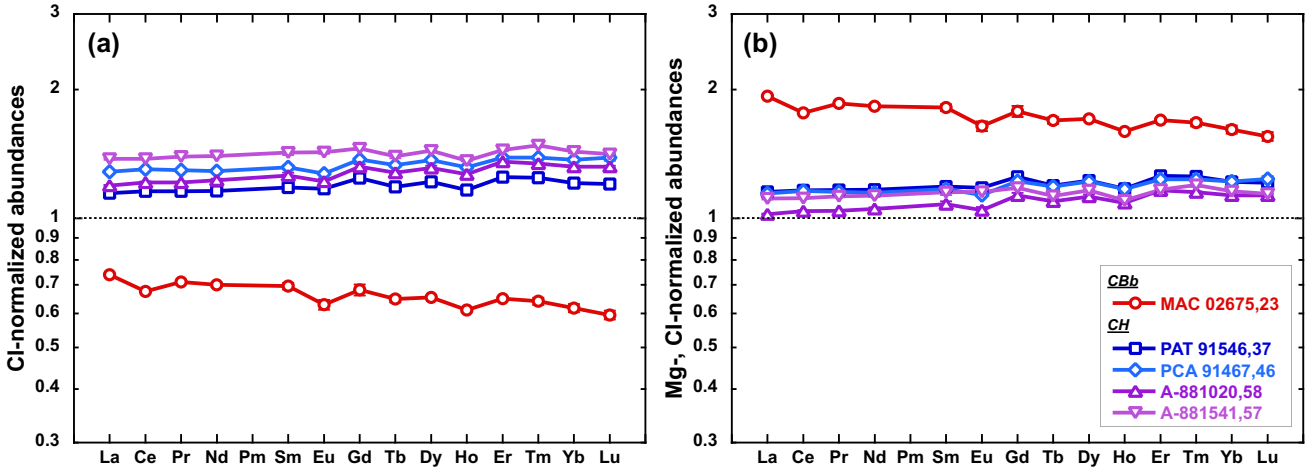

Fig. 2. Bulk REE abundances of CBb and CH chondrites. (a) shows CI-normalized values and (b) shows Mg-, CI-normalized values, respectively. CI chondrite values are from [10].

References: [1] Bischoff A. et al. (1993) *GCA*, 57, 2631-2648. [2] Weisberg M. K. et al. (2001) *Meteoritics & Planet. Sci.*, 36, 401-418. [3] Krot A. N. et al. (2002) *Meteoritics & Planet. Sci.*, 37, 1451-1490. [4] Fedkin A. V. et al. (2015) *GCA*, 164, 236-261. [5] Weyrauch M. et al. (2019) *GCA*, 246, 123-137. [6] Rubin A. E. (2003) GCA, 67, 3283-3298. [7] Scott E. R. D. (1988) EPSL, 91, 1-18. [8] Weisberg M. K. et al. (1988) EPSL, 91, 19-32. [9] Palme H. et al. (2015) EPSL, 411, 11-19. [10] Anders E. and Grevesse N. (1989) GCA, 53, 197-214.

Raman micro-spectroscopic study of carbonates on the surafce of Y-980115

Hiroharu Yui[1,2], Hayato Tsuchiya[1], Shu-hei Urashima[1,2], Keisuke Narahara[1], Aruto Kashima[1], Naoya Imae[3] and Akira Yamaguchi[3]

[1] *Department of Chemistry, Graduate School of Science, Tokyo University of Science*

[2] *Water Frontier Research Center, RIST, Tokyo University of Science*

[3] *National Institute of Polar Research*

Carbonaceous chondrites are among the most pristine extraterrestrial materials available for the study of the chemical evolution occurred at the early stage of solar system. They are classified into at least eight groups based on their mineralogical, bulk-chemical, isotopic properties. However, there are several carbonaceous chondrites recovered from Yamato in Antarctica that does not fit into the traditional eight groups. They are proposed to be categorized as CYs [1] and have been revisited from the viewpoint of the analogues for the rubble-pile asteroid Ryugu [2]. They are extensively aqueously altered, and thermally metamorphosed, but the exact mechanism, timing, and duration of post-hydration heating of them remain poorly constrained. For example, among CY meteorites, Y-980115 has been tentatively categorized into CI1 meteorites, but has several characteristic features not seen in CI1s. Here we studied the micro-crystals of carbonates on the surface of Y-980115 particles by Raman micro-spectroscopy. This is because Raman frequency of ν_1 band and those of lattice modes of the carbonate crystals (T band at ～175 cm^{-1} and L one at ～300 cm^{-1}) sensitively reflect the kind of carbonates [3] and their physical/chemical states. Thus, those Raman spectroscopic features would provide further information on the changes in (and the history of) aqueous environments on the corresponding parent body(ies). Figure 1 compares ν_1 Raman bands of carbonates found on Y-980115 and those on Orgueil (CI1) and Y-791198 (CM2.4, unheated) as references. Among 59 carbonates measured on Y-980115, 46 were assigned to dolomites, showing the excellent agreement with the features observed in CI1 meteorites. However, interestingly, most of them showed the remarkable broadening and the increase in slightly higher component of ν_1 peak (～1100 cm^{-1}). In addition, the disappearance of the T and L lattice modes were observed. Calcite, which is relatively minor carbonate on CIs, also showed the similar features for that on Y-980115. These spectroscopic features indicate that the crystal structures of both dolomite and calcite were extensively decomposed on Y-980115. Interestingly, we also found several aragonite crystals on Y-980115, which is usually found on the CM type meteorites. But in contrast to dolomite, their Raman spectrum had a sharp ν_1 peak and clear T and L bands. Based on the survival of fragmented dolomites and on the coexistence with less-damaged aragonites, we infer that the parent body of Y-980115 experienced extensive aqueous alteration similar to other CIs' at first. Then, its remarkable part was thermally metamorphosed by the collision of other comparable sizes of planetesimal having similar features of CM type meteorites, resulted in the decompositon of the initially formed dolomite. Finally, no further significant hydration ocurred after the collision event. The results observed in carbonates on Y-980115 are in good accordance with the previous studies [1,2], where CY meteorites have mineralogy, textures and elemental compositions often intermediate between the CI and CM chondrites that experienced aqueous alteration and also record a late stage thermal metamorphic event at peak temperatures > 500 °C [1].

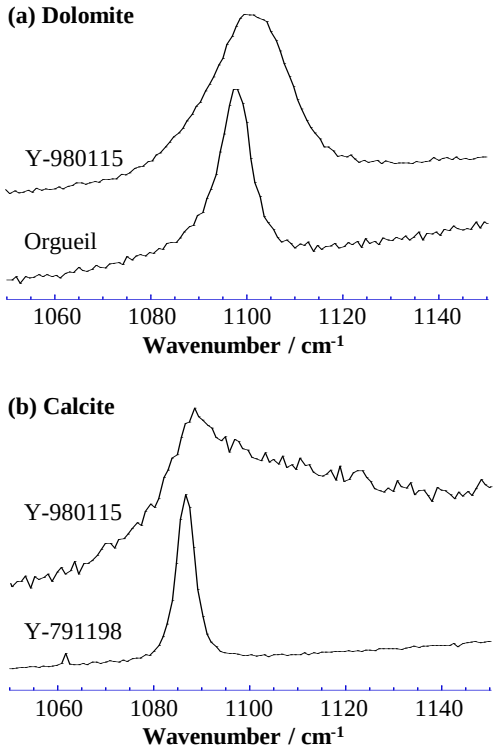

Figure 1 Comparison of the Raman shift and band shape of ν_1 modes of (a) dolomite on Y-980115 (Ref. on Orgueil CI1) and (b) calcite on Y-980115 (Ref. on Y-791198 CM2.4 unheated).

References

[1] Ikeda, Y., An overview of the research consortium "Antarctic carbonaceous chondrites with CI affinities, Yamato-86720, Yamato-82162, and Belgica-7904", Proc. NIPR Symp. Antarct. Meteorites, 5, 49-73, 1992.

[2] A.J. King, H.C. Batesa, D. Krietsch, H. Busemann, P.L. Clay, P.F. Schofield, and S.S. Russell, "The Yamato-type(CY) carbonaceous chondrite group: Analogues for the surafce of asteroid Ryugu", Geochemistry, 79, 125531(1-17), 2019.

[3] Urashima, S., Nishioka, T., and Yui, H., "Micro-Raman spectroscopic analysis on natural carbonates: linear relations found via biaxial plotting of peak frequencies for cation substituted species", Anal. Sci. 38, 921-929, 2022.

Primordial abundance of chondrule in CI chondrite

M. Kimura[1], A. Yamaguchi[1], M. Ito[2], and N. Tomioka[2]
[1]*National Institute of Polar Research, Tokyo, Japan,* [2]*Kochi Institute for Core Sample Research, X-star, Japan Agency for Marine-Earth Science Technology, Kochi, Japan*

CI chondrite is the most significant extraterrestrial sample to estimate the primordial materials in the Solar System. However, CIs lost the primordial features due to heavy aqueous alteration in their parent bodies. Nevertheless, small amounts of anhydrous minerals, such as olivine and pyroxene, have been reported from CIs and CI-related Ryugu samples (e.g., [1]). They are thought to be relicts of chondrule and refractory inclusion. Thus, it is highly probable that CIs had primarily comprised chondrule, refractory inclusion, opaque minerals, and matrix, before aqueous alteration, like other carbonaceous (C) chondrites. Here we estimate the primordial abundance of chondrule in CIs from the calculations based on the bulk chemical compositions of CIs. The parameters for calculations are as follows 1) The chemical compositions of primordial chondrule, refractory inclusion, and opaque minerals were similar to those in C chondrites that were not suffered from the aqueous alteration. 2) The primary matrix composition of CIs was close to the average bulk composition of CIs ([2]) as suggested by [3]. We use the average major elemental compositions of chondrule and refractory inclusion in Y-81020, CO3.05 (Kimura unpublished data), and their variable modal abundances arbitrarily selected for the calculations. Our results are within the range of previously reported CI bulk chemical compositions in case chondrule abundances are < 10 wt. %. If chondrule is more abundantly contained, the bulk composition becomes enriched in volatile elements, such as Na and S, like CM chondrites. The low abundance of chondrule obtained here is consistent with the rare occurrence of anhydrous minerals in CIs and Ryugu. We also calculate the bulk chemical compositions of Tagish Lake, ungrouped C2, which experienced aqueous alteration heavily, and chondrules rarely survived in it (e.g., [4])). Our results show that Tagish Lake primarily had <20 wt. % chondrules before the alteration. The estimated chondrule abundances of CIs and Tagish Lake are much lower than those in the other C chondrites.

The primary low abundance of chondrule in CIs should be closely related to the formation conditions and locations of chondrule. McCain et al. (Nature Astronomy, submitted) suggested that the alteration age of the Ryugu materials was ~1.4 Ma after CAI formation from Mn-Cr dating for carbonate. In this case, the CI chondrite parent body should have formed before chondrule formation, ~1.9 to 4 Ma after CAI formation (e.g., [5]). Almost fine-grained dust (precursor of the matrix) with abundant ice should have accreted to the CI parent body. On the other hand, Mn-Cr ages of carbonates in CI, CM, and Tagish Lake are also estimated to be 4–6 Ma after CAI formation (e.g., [6]). Carbonates in Ryugu formed 3-7 Ma after CAI (e.g.,[7]). In this case, chondrule formed before the accretion and alteration of the CI parent body. Therefore, the CI formation reservoir must have hardly contained chondrules to explain the low primary abundance of chondrules. Desch et al. [8] showed that CIs formed in the outer region of the solar system, >15AU, without chondrule and refractory inclusion, whereas CM and CO formed at 3–4 AU mainly based on the model calculation. Ito et al. [9] showed that Ryugu is partly related to comets. Bryson et al. [10] suggested that Tagish Lake formed at >8–13 AU based on paleomagnetic data. From them, we suggest that almost dust with abundant ice accreted to the CIs and Tagish Lake parent bodies in the outer Solar System. Chondrule had been hardly included in the precursor materials of CIs, whereas it slightly included those of Tagish Lake. On the other hand, chondrule had been primarily abundant for other C chondrite reservoirs in the inner Solar System, and dust and ice were poorer in abundance than those of CIs and Tagish Lake. The primordial chondrule abundance is one of the keys to clarify the physical and chemical conditions and evolution of the early Solar System.

References

[1] Leshin L. A. et al. 1997. Geochimica et Cosmochimica Acta 61: 835-845, [2] Lodders K. 2021. Space Science Reviews 217: 44, [3] van Kooten E. M. M. E., et al. 2019. Proceedings of the National Academy of Sciences 116: 18860, [4] Ushikubo T. and Kimura M. 2021. Geochimica et Cosmochimica Acta 293: 328-343, [5] Fukuda K. et al. 2022. Geochimica et Cosmochimica Acta 322: 194-226, [6] Fujiya W. et al. 2013. Earth and Planetary Science Letters 362: 130-142, [7] Yokoyama T. et al. 2022. Science, 10.1126/science.abn7850, [8] Desch S. J. et al. 2018. The Astrophysical Journal Supplement Series 238, [9] Ito M. et al. 2022. Nature Astronomy. doi.org/10.1038/s41550-022-01745-5, [10] Bryson J. F. J. et al. 2020. The Astrophysical Journal 896: 103